The Interaction Between A Flighted Steel Pipe Pile and Frozen Sand

Prepared by
Robert Cuthbertson-Black, B.Sc. (C.E.)

A Thesis Submitted to
The Faculty of Graduate Studies
In Partial Fulfilment of the Requirements for the Degree of

Master of Science in Civil Engineering

Department of Civil and Geological Engineering
University of Manitoba
Winnipeg, Manitoba

THE UNIVERSITY OF MANITOBA

FACULTY OF GRADUATE STUDIES

*****

COPYRIGHT PERMISSION PAGE

The Interaction Between A Flighted Steel Pipe Pile and Frozen Sand

BY

Robert Cuthbertson-Black

A Thesis/Practicum submitted to the Faculty of Graduate Studies of The University of Manitoba in partial fulfillment of the requirements of the degree of

Master of Science

Abstract

Foundation construction in permafrost regions often make use of "thermopiles" or thermal piles to maintain the permafrost and to transfer load to the soil. Often "thermopiles" are constructed using shafts with continuous helical flighting attached to increase bearing capacity. The behaviour of these flights is essentially unknown as is the associated loss of shaft adfreeze during failure. An experimental study using a flighted instrumented segment pile in frozen sand was undertaken. The pile segment was loaded axially to near-failure.

Load transferred from the pile segment to the surrounding soil consisted primary of two components; direct bearing by flighting and adfreeze/shaft friction. Flighting carried approximately 75% of the applied axial load, while adfreeze/shaft friction tranferred approximately 18% of the load under specific test conditions. At large displacements, yielding at the flighting root resulted in the development of an ultimate axial pile capacity. In general, flighted piles develop significant (1080 kN/m) load transfer capacities.

Acknowledgements

Firstly, I would like to extend my thanks to my thesis advisor, Dr. Len Domaschuk, who provided valuable advice, ongoing patience, insight into many subjects, and moral and financial support.

The Examining Committee consisted of Drs. E. Z. Lajtai. M. Alfaro and R. H. Schilling of the University of Manitoba who provided very constructive criticism and suggestions about my research, which was very much appreciated.

I would like to thank the following groups or individuals for their invaluable assistance or guidance throughout the laboratory, research, and composition phases ;

Mr. Narong Piamsalee, Geotechnical Lab Technician, University of Manitoba

Mr. Ed Lemke, Structures Lab Coordinator, University of Manitoba

Ms. Nancy C. Liston, Librarian, CRREL, Hanover, New Hampshire

Dr. James Graham, University of Manitoba

Dr. Nimal Rajapakse, University of Manitoba

Mr. John Jardine, Arctic Foundations of Canada Limited

I am especially grateful to my parents, Jack and Teenie, and my wife, Crystal for their unconditional support. I would like to dedicate this thesis to them.

Table of Contents

Table of Contents (Continued)

List of Figures

List of Figures (Continued)

List of Figures (Continued)

List of Figures (Continued)

List of Tables

Nomenclature

Symbol	Explanation (Units where applicable)
A_p	Cross-sectional area of pile shaft (mm^2)
b	Element width at strain gage (mm)
c_a	Cohesion intercept (kPa)
d_{HEAD}	Pile segment head displacement (mm)
d_{TOE}	Toe displacement of pile shaft (mm)
D	Outer diameter of pile shaft (mm)
E	Young's Modulus / Modulus of Elasticity (GPa)
h	Element height at strain gage (mm)
I_{z-z}	Moment of inertia (mm^4)
K	Pile compressibility ratio
K_0	Ratio between lateral pressure and overburden pressure
L_c	Standard chord length
L_r	Roughness line length
m	Roughness coefficient
M_B	Bending moment in flighting (kNm)
M_Y	Yield moment in flighting (kNm)
n	Creep rate parameter
p_n	Lateral pressure on pile shaft (kPa)
P	Pitch of flighting (mm)

Nomenclature (Continued)

Symbol	Explanation (Units where applicable)
$P_{APPLIED}$	Applied load on pile (kN)
P_i	Vertical load in pile shaft at gage i (kN)
q_{POINT}	End bearing resistance (kN)
R	Outside radius of pile shaft (mm)
RF	Roughness Factor
S	Penetration rate of pile
t	True thickness of flighting (mm)
t'	Effective thickness of flighting (mm)
T	Ice or soil temperature (°C)
w	Width of flighting (mm)
Z_i	Positive depth from datum to gage i (mm)
Φ	Instantaneous curvature of flighting (mm/mm)
δ	Deflection of flighting (mm)
λ	Soil shear strength or stress (kPa)
λ_{ADF}	Adfreeze shear strength or stress (kPa)
ϕ_a	Effective friction angle (°, Degrees)
ϕ_{lt}	Long term friction angle (°, Degrees)

Nomenclature (Continued)

σ_{C0}	Reference stress at ε_C
σ_i	Vertical stress in pile shaft at gage i (kN)
ε_0	Original strain at gage i (mm/mm)
ε_C	Arbitrary strain
ε_i	Final strain at gage i (mm/mm)
$\varepsilon_{z\text{-}z}$	Measured strain in flighting (mm/mm)

1. Introduction

1.1 Statement of Problem

Exploration and development of Canada's North has been underway for hundreds of years. However, in the past century, development has increased significantly. During this time, coping with frozen soils has been an ongoing challenge for residents, builders and designers alike. Foundations of structures in Canada's North must be designed so as to prevent the thermal degradation of the underlying frozen soil, or else to accommodate the resulting settlement and the potential loss of capacity.

Thermal syphons (heat pipes) were developed in the 1950's as a means of extracting heat from foundation soils under structures. This inhibits the thawing of the permafrost and subsequent settlement. Thermal piles, which are thermal syphons designed to support structures, represent an integration of pile foundations and passive heat extraction systems. The load carrying capacity of these piles is increased by welding a continuous helical strip to the pile shaft to form a continuous "flight". This flighting increases the volume of soil involved in load transfer from the pile to the soil.

Although some research has been undertaken to quantify the behaviour of the flights in frozen sand (the soil type that will be studied here), the subject has received little attention and is essentially unstudied. In addition, the optimum geometry of the flighting is important for efficient use of material and for the construction of reliable foundations. The importance

is underscored by the statement from Ladanyi and Theriault (1989); "...the use in permafrost of corrugated or tapered piles, installed in pre-drilled holes and slurried, seems to offer some clear advantages, because of their more plastic response to short-term loads, and much better possibilities for predicting their long-term behaviour."

1.2 Thesis Objectives

There are two objectives to this thesis project. One is to describe qualitatively the components of load transfer between a flighted steel pipe pile and a frozen sand in which it is embedded. The second, to quantify the transfer mechanisms in terms of applied load, load transfer distribution, pile head displacement and pile geometry where possible.

This thesis document considers the behaviour of rapidly loaded piles in frozen fine-grained sand. Through a review of current literature and a testing program on an instrumented pile segment embedded in a fine-grained sand, a hypothesis on the behaviour of flighted piles will be developed. Optimum dimensions of flighting pitch, thickness and width will also be investigated. Long term behaviour of flighted piles is creep dependant and this will not be considered in this investigation.

1.3 Permafrost

Any soil which remains frozen through more than one summer is, by definition, permafrost or perennially frozen ground (Johnston, 1981). Approximately half of the surface area of Canada is underlain by permafrost. It may be found in two forms: discontinuous, occurring only in patches that are perennially frozen; and continuous, in which the entire region is underlain by frozen soil. Discontinuous permafrost tends to occur where the mean annual air temperature is between -1.1°C and -8.3°C, while continuous permafrost tends to occur where the mean annual air temperature is below -8.3°C. **Figure 1-1** illustrates the approximate boundaries of both zones across Canada (Johnston, 1981).

The depth of permafrost may extend into bedrock for hundreds of metres. For example, the permafrost in the Arctic Archipelago is approximately 460 metres deep (Johnston 1981).

Overlying the continuous permafrost, there is always a soil horizon that experiences annual melting and refreezing. This zone called the 'active zone' and is responsible for annual frost heave. The magnitude of frost heave depends on soil type. The depth of the active layer may range from 100 mm. in the high Arctic, to one or two meters in the discontinuous permafrost region. Common permafrost terms are defined in **Figure 1-2.**

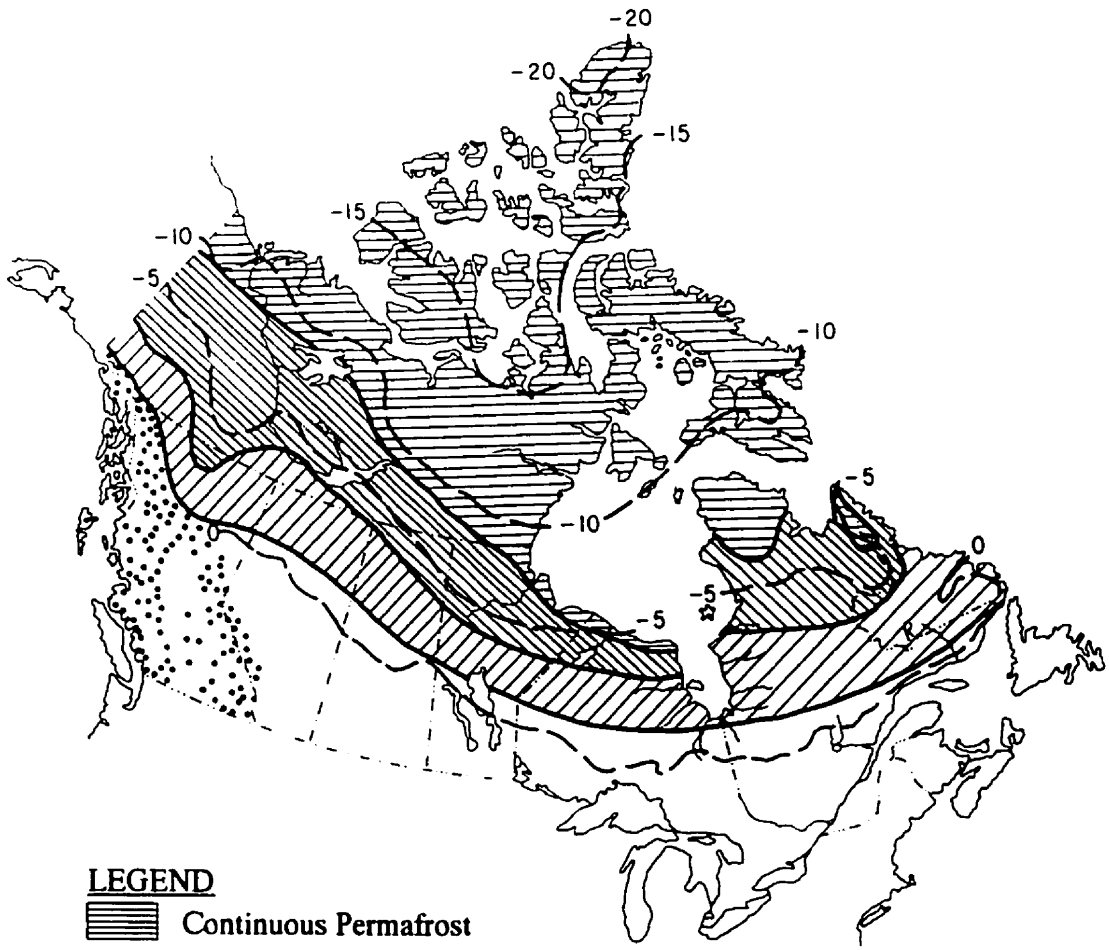

Figure 1-1: The Permafrost Regions of Canada
(Reprinted from Johnston 1981)

The permafrost may consist of any combination of organic soils, mineral soils, and rock that are frozen. The ice content may range from negligible to bulk ice. A granular soil above the groundwater table may be ice free, but have a temperature below freezing. Through gradual freezing, large ice lenses can develop within the soil (Johnston, 1981). Small ponds and lakes can freeze over and become covered with organic soils providing an insulating layer. Over time, the body of water may freeze forming a large amorphous ice mass within the permafrost.

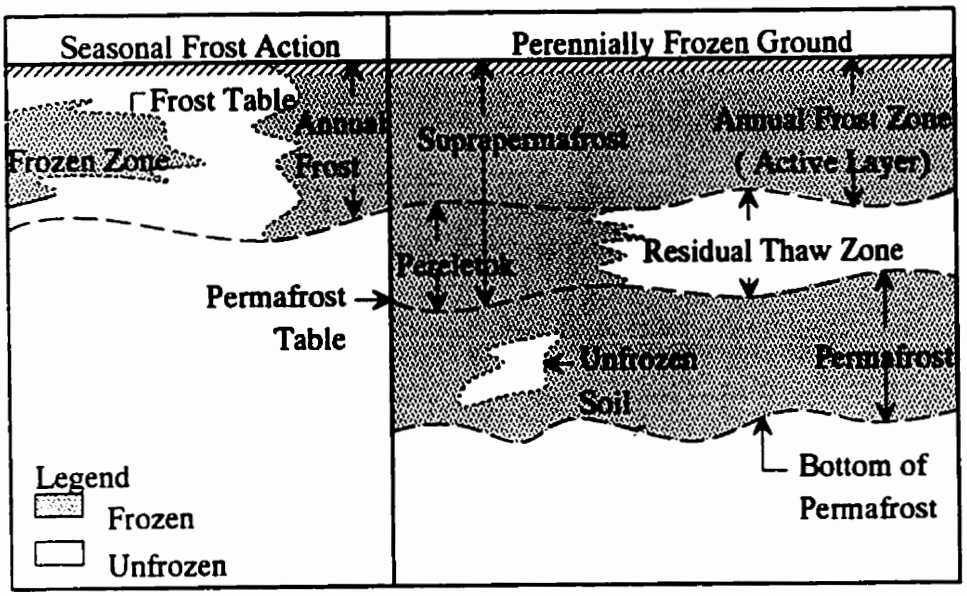

Pereletok : A frozen layer at the bottom of the active layer which remains unthawed for one or two summers.

Figure 1-2: Permafrost Terminology
(From Linell and Kaplar 1963)

Often, the temperature in permafrost is near the melting point of water and is very sensitive to the introduction of heat from man-made structures or the disruption of the insulating ground cover. Most discontinuous permafrost is not colder than -1°C and must be protected against thawing. **Figure 1-3** illustrates the temperature regime which occurs within

permafrost. This figure also illustrates why permafrost may be very sensitive to thermal disturbances. Thawing would result in a significant loss of strength and in large settlements due to thaw-consolidation. The importance of design for permafrost is emphasized by Crawford and Johnston (1971) who stated, "The only certainty in founding structures on permafrost is that the foundation conditions will be variable and generally unpredictable." With this comment in mind, foundation technology on permafrost is improving, though many challenges still remain.

Foundations must support load from the structure above and transfer it into the underlying permafrost. At the same time, they must also avoid disrupting the thermal regime of the permafrost. Permafrost can be disrupted either in the construction phase or during service life of the structure. Preservation of the permafrost is as much a goal of foundation design as is bearing capacity.

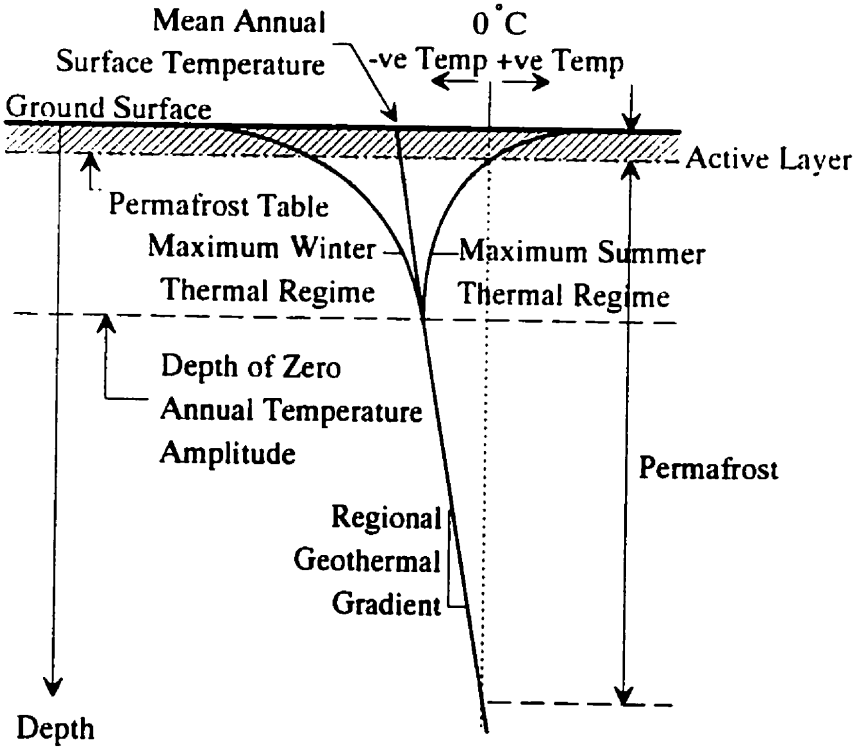

Figure 1-3: Typical Permafrost Temperature Regime
(After Johnston 1981)

1.4 Frozen Soil Constituents

Frozen soil can be considered a highly complex four phase system that consists of solid soil particles, ice inclusions, bound and supercooled liquid water, and air and other gaseous inclusions. **Figure 1-4** illustrates the components of the frozen soil system. The properties of frozen soils depend on the relative proportions of each constituent, their internal properties, and their external interaction with the other components. The composition of soil and ice normally has properties that are not representative of either ice or soil. Although frozen soil

exhibits some behaviour typical of ice, it also shows behaviour such as frictional resistance that depends on the physical properties of the soil skeleton.

To simplify behavioral modelling, the water and gas components are often ignored giving a rheological two-phase material. This assumption is generally valid for coarse-grained granular materials, although fine-grained (clay and silt) soils are significantly affected by unfrozen water. Unfrozen water is very important to the behaviour of all fine-grained frozen soils because it strongly influences strength and creep parameters.

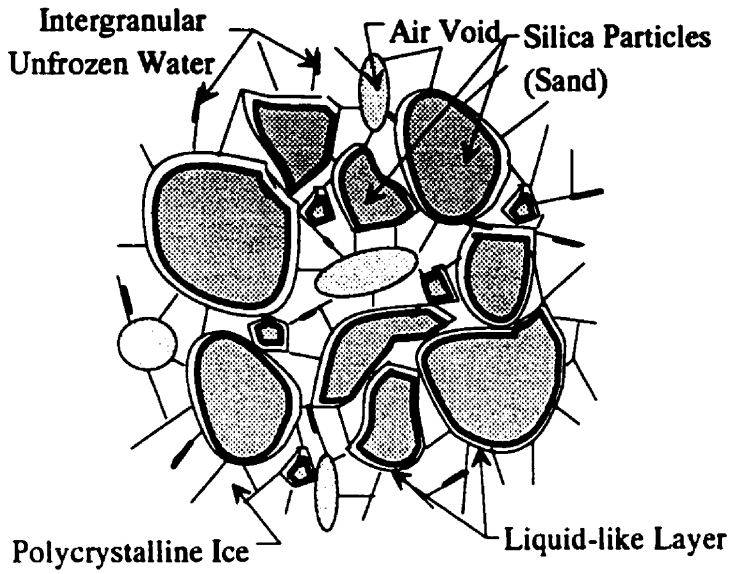

Figure 1-4: Schematic of Frozen Sand System
(Not to Scale)

Most fine-grained soils consist of silicate minerals, usually in the form of small flaky clay particles with high surface area. These minerals have an affinity for the polar water molecule. A layer of oriented bound water molecules is held to the particle surface by the formation of

of successive electrical double layers. Research (Jellinek 1967, Weyl 1951) found that ionic crystal lattices (such as ice) are not fixed, but distorted and polarized. In the case of ice, this results in a liquid-like transition layer on its surface. The two layers of bound water interact and are shared between the ice and silicate particles. The water that is between the bound surface water layers is the site of ice formation (Anderson 1968 quoted in Ting 1981). **Figure 1-5** illustrates the organization of these interfacial layers.

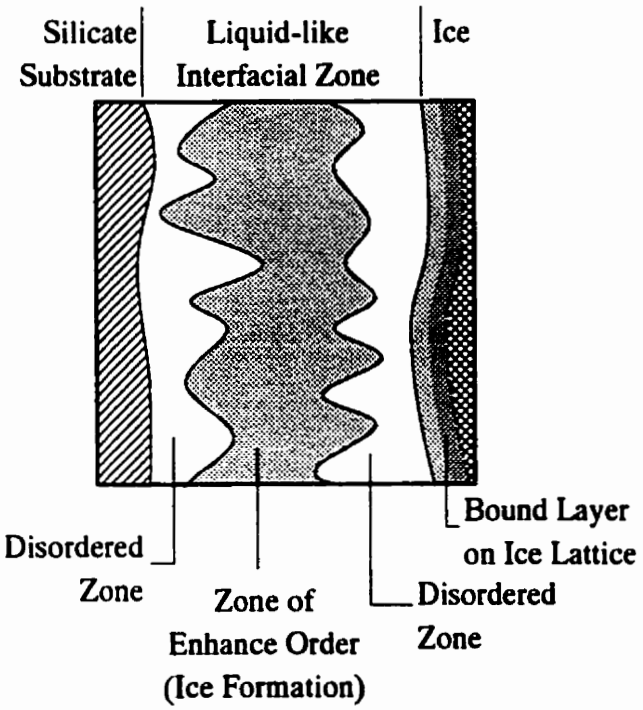

Figure 1-5: Schematic of Silicate-Water-Ice Interface
(After Anderson and Morgenstern 1973)

The liquid-like transition layer is resistant to flow perpendicular to it, but has measurable viscosity parallel to the surface (Jellinek 1967). The water can then flow as stress or temperature dictate. The flow of this water can result in viscous elastic and plastic creep, or strain hardening through crack healing. Its importance can not be overstated. For a detailed

review, the reader is referred to numerous papers listed in the Bibliography.

Gas inclusions in frozen soil can also significantly affect the behaviour of soils. Compression and adsorption of gases can result in additional non-recoverable (plastic) deformations. The bubbles can result in dislocation accumulations which will accelerate the cracking and failure for the ice matrix. It is often observed that "black" ice (slow grown ice without gas inclusions) is much stronger that "white" ice (significant gas inclusions). To the author's knowledge, the effects of gas inclusions in frozen soils have not been studied.

Normal ice known as Ice I (Hobbs, 1974) is an anisotropic, hexagonal crystalline material although it may exist as an amorphous mass. Ice I consists of a planar crystalline structure of hexagonal rings of water molecules. These rings form puckered sheets termed the 'basal plane'. Failure of Ice I is initiated by cracks opening during plastic deformation of individual crystals. The cracks coalesce and concentrate stress at fewer points, causing localized failure. It fractures rapidly when loaded significantly, and creeps at all stresses below failure stresses. The result is failure with limited deformation.

For Ice I, strain parallel to the basal plane is through basal slip in which sheets of water molecules pass over one another. If the strain is in any other axis, basal slip is more difficult and often results in the fracture of the structure. The stress required to induce non-basal slip is more than ten times greater than the stress required to cause basal slip (Higashi, 1969 quoted in Ting, 1981). This results in a preferential creep in monocrystalline (parallel

orientation of ice crystals) ice and reduced strength and higher creep rates for polycrystalline ice (random orientation of ice crystals).

1.5 Strength and Creep Characteristics

Frozen soil can range from ice with some soil particles to soil particles with some ice. The proportion of ice in frozen soil can vary from zero to 100%. The behaviour of the frozen soil depends strongly on the relative magnitudes of each. Minor soil inclusions in ice can increase creep and reduce strength, while pore ice in soils significantly increases strength. The structure and size of ice grains in pore spaces depends on the rate of freezing, the freezing temperature, the porewater chemistry and the soil characteristics (Hobbs, 1974). Generally, all pore ice is polycrystalline and made up of very small grains.

Ice-saturated medium sand has the highest strength of all frozen soils (**Figure 1-6**). Holubec (1990) postulates that the shear strength of frozen sand is higher than that of finer material because of greater interlocking and dilation pressures upon shearing. Gravelly soils tend to experience more particle crushing due to direct contacts and thus lower dilation pressures. This provides less interlocking and lower strength. In frozen saturated sands, another transition in behaviour occurs when the sand volume concentration is approximately 42% by volume. Below 42%, the strength and creep parameters differ from those above 42% sand concentration (Goughnour & Andersland, 1968). At this transition point, sand particles likely interact more directly without interspersed ice crystals. Above 42%, the sand particles are

likely in contact with only a thin bound water layer separating mineral to mineral contact (Anderson & Morgenstern, 1973).

Frozen soils have very complicated creep behaviour that depends on temperature, ice structure, confining pressure, stress level, stress history, soil properties, and pore water salinity (Ting, 1981). Deformations in frozen soil develop through three different straining mechanisms; instantaneous elastic, viscous elastic, and plastic. At low stresses, ice creeps in all three modes: primary (terminating creep), secondary (constant deformation rate) and tertiary (accelerating creep). Creep occurs by a combination of recrystallization, by slip at intergranular and basal planes, and through plastic flow (Hobbs, 1974 and Michel, 1978). Three mechanisms are involved; microcreep or the movement of point and line defects, microcracking resulting from dislocation accumulations and crystal defects, and crystal boundary effects such as pressure melting or migration.

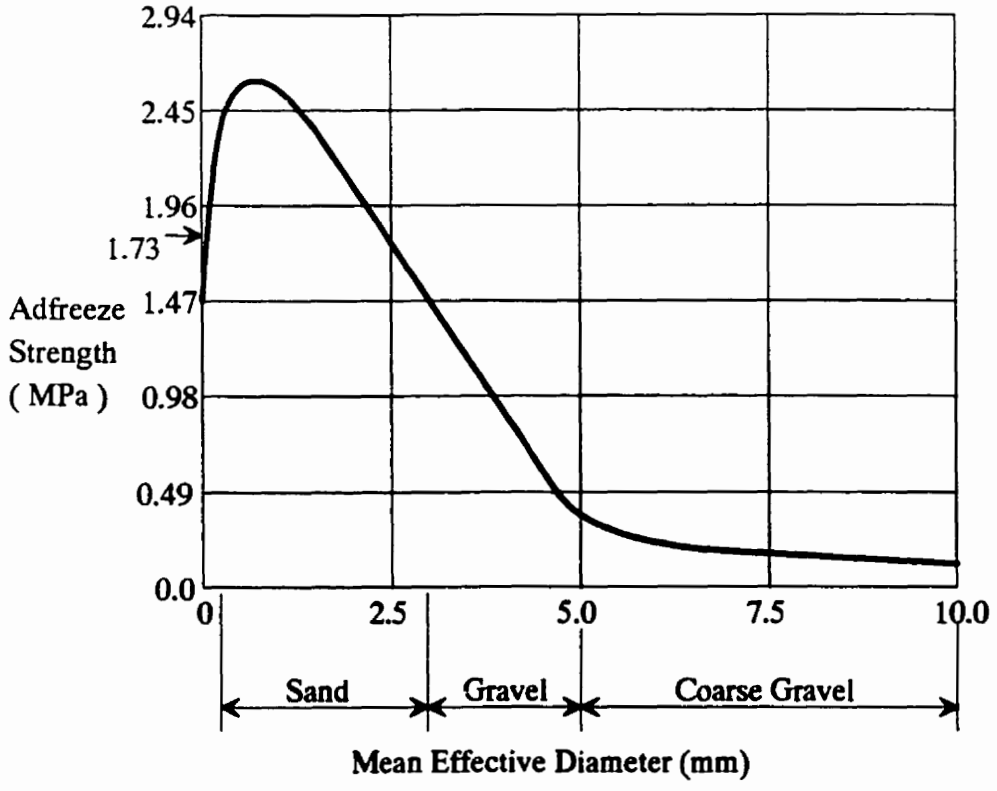

Figure 1-6: Ultimate Strength of Adfreeze to Wood versus Soil Particle Size
(After Tsytovich, 1975)

Frozen soils creep even under low stress levels through the creep component of ice behaviour. During creep, loose granular soils experience densification with a corresponding increase in strength. Frozen clays near melting temperatures (-0.8°C) have exhibited greater creep than that of polycrystalline ice (Roggensack, 1977). This rapid creep is attributed to the presence of a large volume of unfrozen water bound to the clay particles.

1.6 Thermal Syphons and Thermal Piles

Thermal syphons, (commonly known as "thermosyphons",) utilize passive soil refrigeration. They originated with the development of heat pipes. They are used as a heat exchanger between the soil and the atmosphere to preserve permafrost in continuous and discontinuous permafrost zones. As **Figure 1-7** illustrates, a thermal syphon is a long closed pressure vessel charged with a high pressure condensed gas (ammonia, carbon dioxide, propane, etc.). Gas pressures in the order of 500 kPa are used for carbon dioxide. The portion of the pile which is embedded in the soil acts as an evaporator. The segment above the ground surface acts as condenser. The heat from the soil around the embedded portion is absorbed causing the vaporization of the liquified gas. The vapour then rises up the pressure vessel by convection. Once this vapour reaches the portion above the ground, it condenses and the heat of condensation is dissipated to the colder atmosphere. The condensate trickles down and returns to the lower portion to continue the cycle of heat removal from the frozen soil. The convection of high pressure gas occurs only when air temperatures are lower than soil temperatures. Temperature differentials as little as 0.006°C can initiate the convection cycle (Long, 1982). When air temperatures are higher than soil temperature, some heat may be conducted downwards through the vessel walls. The seasonal operation of the thermal syphon in cold regions results in the soil around the thermal syphon being frozen to low temperatures in winter with the soil remaining frozen throughout the summer. For a given size of thermal syphon, the volume of soil frozen and maintained frozen, depends on the soil conditions, the climate and ground cover. Heat migration from the frozen soil directly to the atmosphere

during warm weather can be reduced by using a layer of insulation at ground surface, thereby decreasing the thickness of the active layer in the vicinity of the thermal syphon.

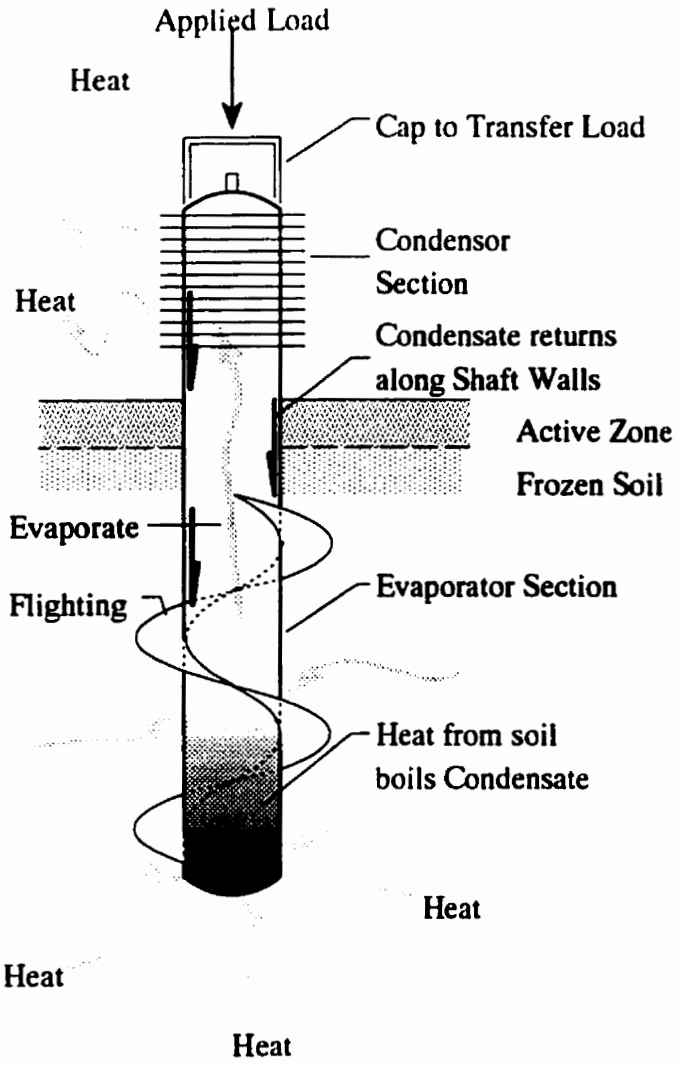

Figure 1-7: Thermal Pile Operation

Foundation engineering in permafrost areas must contend with the variability of soil properties, the potential for significant creep settlements, and thermal degradation. The latter is particularly troublesome if the soil contains extensive ice lenses or ice masses. Frost heave

resulting from the active zone refreezing, can apply significant upward forces to a foundation system necessitating measures to prevent uplift. A foundation must satisfy simultaneously bearing capacity, settlement, frost heave, and permafrost preservation criteria. One such pile, is a thermal pile, which is a thermal syphon designed to carry a structural load. Thermal piles were originally developed by Erwin L. Long over the period of 1956 to 1960. Numerous refinements have been made to their reliability and capacity over time.

Helical flights are welded to the thermal pile shaft to increase the soil/pile interaction thereby increasing the load-carrying capacity. The flights consist of a steel strip rolled into a helical form, similar in appearance to a coil spring. Flighting is omitted from the portion of the thermal pile to be located within the active layer. A bond-inhibiting coating may be applied to that portion of shaft segment to further reduce frost heave forces on the pile.

For flighted steel pipe piles embedded in frozen soil, the basic mechanisms for transfer of load from the pile shaft to the soil mass are;

- bonding between the pile shaft and the soil
- mechanical interaction and friction along the shaft
- end bearing
- bonding, direct bearing and ultimately shear by the flights

Bonding occurs through the direct electro-chemical bond between the foundation structure and pore ice. Generally, chemical bonding between the structure and the soil skeleton is rare.

Mechanical interaction and friction depend both on the nature of the surface of the pile and on the structure of the soil particles. It represents the interaction between the two surfaces moving parallel to each other. End-bearing is a complicated phenomenon that depends on soil strength, creep and flow behaviours, and on the stiffness of the foundation and of the soil.

The method of thermal pile installation involves placing the pile into a oversized, prebored hole and backfilling the annular space with a sand slurry. Holubec (1990) recommended that boreholes be large enough to provide a fifty millimetre (50 mm.) annulus beyond the flighting tip to permit sand slurry placement. Slurry is placed in lifts and vibrated to reduce the likelihood of void formation and to assure higher densities. In permafrost, preboring may be replaced with steam thawing. Generally attempting to directly install thermal piles by driving has either been impractical or unsuccessful. If construction takes place during winter, the thermal pile and low air temperatures will quickly freeze the slurry and refreeze any surrounding soil that has thawed. Construction of the structure can then follow. If pile installation takes place in summer, building or superstructure construction is commonly delayed until winter temperatures can adequately refreeze the soil. If construction is not delayed, loads on the thermal piles must remain below the capacity of the pile in unfrozen soil.

Thermal piles fabricated off-site are generally less than 300 mm. in diameter. Thermal piles larger than 300 mm. in diameter have been fabricated and installed on-site. (Personal communication with Arctic Foundations of Canada).

Flighted piles have been used as anchors for transmission towers and poles, and for supporting building structures in permafrost. For example, Manitoba Hydro has used thermal piles to replace grillage foundations for monopod transmission towers. Thermal piles have also been used to support nursing stations, communications towers, pipelines (notably the TransAlaskan Pipeline System), and warehouses. Despite frequent use of flighted thermopiles, the mechanisms of load transfer are not fully understood. Design is a partially based on a program of pile load testing and empirical information. This provides justification for the work undertaken in this thesis.

2. Literature Review

2.1 Straight Shaft Piles

2.1.1 Introduction

Straight-shafted piles can be broadly grouped into either end-bearing piles or friction piles. End-bearing piles transfer load down through the pile shaft to the pile tip and then transfer load by shearing in the underlying soil strata. Friction piles transfer load over a portion of the pile shaft length by surface shear or adhesion to the surrounding soil strata. These two groups of piles have distinctly different load transfer behaviour, and this is reflected in the design methods that are used.

The relationship between the elasticity of the soil and the pile is important to the mechanics of the pile shaft and load transfer. Friction piles are often assumed to have a linear load transfer from the top of the shaft to the bottom of the shaft with a small (often negligible) end-bearing contribution. This idealization results from the assumption that the pile is perfectly rigid in relation to the soil.

Pile end-bearing resistance depends on many factors, including the pile length-to-diameter ratio, load history, soil properties, and the temperature history. To establish an end-bearing capacity for a given pile, these factors must be conservatively accounted for.

2.1.2 Piles in Frozen Soil

Friction piles placed in frozen soil transfer their loads to the soil principally through adfreeze. Adfreeze is a shear bond between the pile shaft and the adjacent frozen soil skeleton. Generally, adfreeze is considered a combination of the ice-to-surface bonding (adhesion), mechanical interaction, and friction. The proportions of each are related to the soil temperature, strain rate, and ice, water and particle contents. Generally, piles placed in permafrost regions are designed as friction piles, making use of the available adfreeze between the frozen soil and shaft.

Theriault and Ladanyi (1988) used a numerical model to describe the load transfer in a friction pile in permafrost. For a given applied load, the progression of the failure of the shaft bond was described. This is illustrated in **Figure 2-1**. A minimum shear strength (often called 'residual' shear strength in the literature) was included to describe the effects of confining pressure around the pile, caused by freezeback or dilatancy in the soil during failure. Complete failure of the pile resulted in a uniform 'residual' shear resistance along its length. Similarly, loads below the failure load would redistribute with time. As **Figure 2-1** illustrates, the point of adfreeze failure progresses over time down the length of the pile. This model is similar to Mattes and Poules' model (1969) with the exception that a yield criterion is included in Theriault and Ladanyi's model.

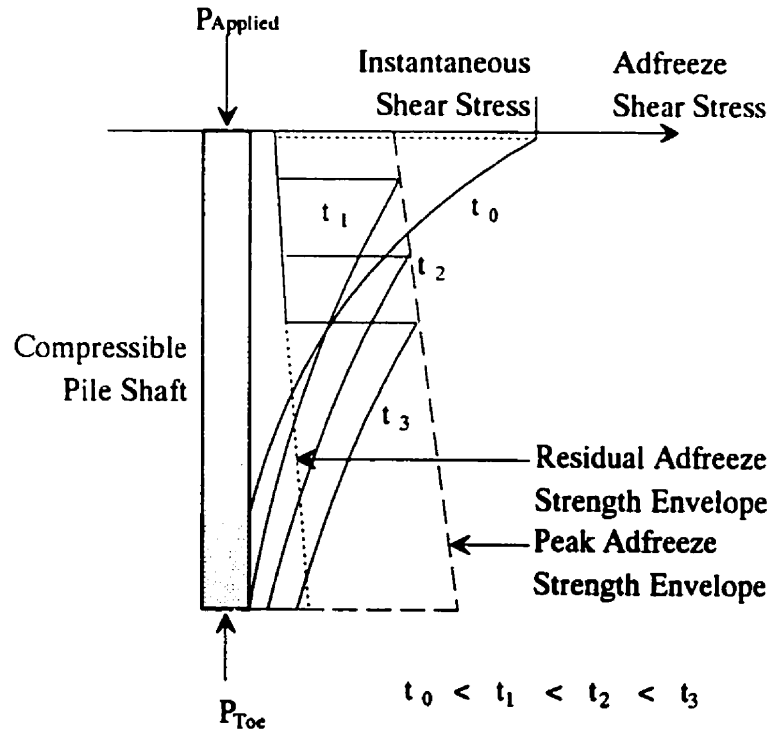

Figure 2-1: Distribution of Adfreeze Shear Stress versus Time
(Modified from Theriault and Ladanyi, 1988)

As most unfrozen soils exhibit limited creep in comparison to frozen soils, long pile behaviour varies significantly. Short term creep of the frozen soil along the shaft allows large shear strains to occur without reaching failure. Therefore, an applied load can be transferred further down the pile because of the relative straining along the pile shaft. This can result in the pile end-bearing becoming significant. Other research has found end-bearing loads ranging from a few percent to 24% of the applied pile load.

Vialov (1988) undertook an investigation of model steel pipe piles. He found the end-bearing load to be 8% of the applied load in hard-frozen loams at -4°C. For plastic loams, the end-bearing loads were 19% of the applied load. The end-bearing resistance may double when the

bearing loads were 19% of the applied load. The end-bearing resistance may double when the pile is part of a cluster, while for plastic-frozen soils, the tip load reached 61% of the pile load. These experimental results are very different from other research quoted in this section. Vialov undertook tests in which the pile length was ten times the shaft diameter. The testing of short piles identified the importance of the structural elastic compression of the pile shaft in the development of shaft resistance, especially within plastic frozen soils. Stubby, relatively rigid piles distribute the load more uniformly to the soil, resulting in creep along the entire shaft and the development of significant end-bearing loads. This is quite different from the behaviour of long, slender piles. This observation is supported by the model pile analysis conducted by Mattes and Poules (1969) who found that end-bearing was a function of the length-to-diameter ratio and the relative pile shaft compressibility.

Allowable end-bearing stresses are from 5.3 to 7.9 times the adfreeze stresses at time of failure as determined from combined friction and end-bearing, and friction only laboratory pile tests (Long, 1973). If the pile settlement rate is very low, the result is a very low point resistance. Alternately, large short term loads can result in rapid penetration rates which in turn will generate significant point resistance.

As the modulus of elasticity of frozen soil is very high in relation to unfrozen soil, the effect of pile stiffness is accentuated. As the modulus of elasticity of the soil increases, the ability for the soil to strain in response to the shear stress from the pile reduces. The frozen soil is then subject to higher shear stresses. The result is a very high load transfer rate near the

ground surface. This load transfer rate would rapidly decline with depth, resulting in the lower portions of the pile shaft transferring negligible load while the adfreeze strength may be fully mobilized near the surface.

Parameswaran (1981) demonstrated a significant effect on the total adfreeze strength resulting from the surface character of the piles. **Figure 2-2** illustrates the relationship which was found for a B.C. fir pile and a steel H-section. The H-section is not representative of the true behaviour of steel because of its numerous corners causing stress concentrations, reducing the strength potential of the bond. **Figure 2-2** also demonstrates the contribution of friction and interlock on total adfreeze strength. For all rates of displacement of a wood pile, a constant value separates the total adfreeze strength curve for ice and for frozen sand.

Parameswaran speculated that adfreeze strength increased as a consequence of increased porosity of the surface (B.C. Fir vs. Concrete vs. Steel), thereby allowing water to enter the pores of the timber and concrete piles and possibly increasing the bond area. The effect of the small pores in a surface may be a function of individual ice crystals extending across the potential failure surface. In rapidly frozen soil, the crystals are small, likely significantly smaller than the pores, while under normal freezing rates, the ice crystals would otherwise be large in relation to the pores. At some transition point in the relative porosity of the pile surface, direct interaction between soil asperities and the pores adjacent to them begins to occur. Honeycombed concrete would be an example. This effect is macroscopic where surface roughness is greater than several hundred microns.

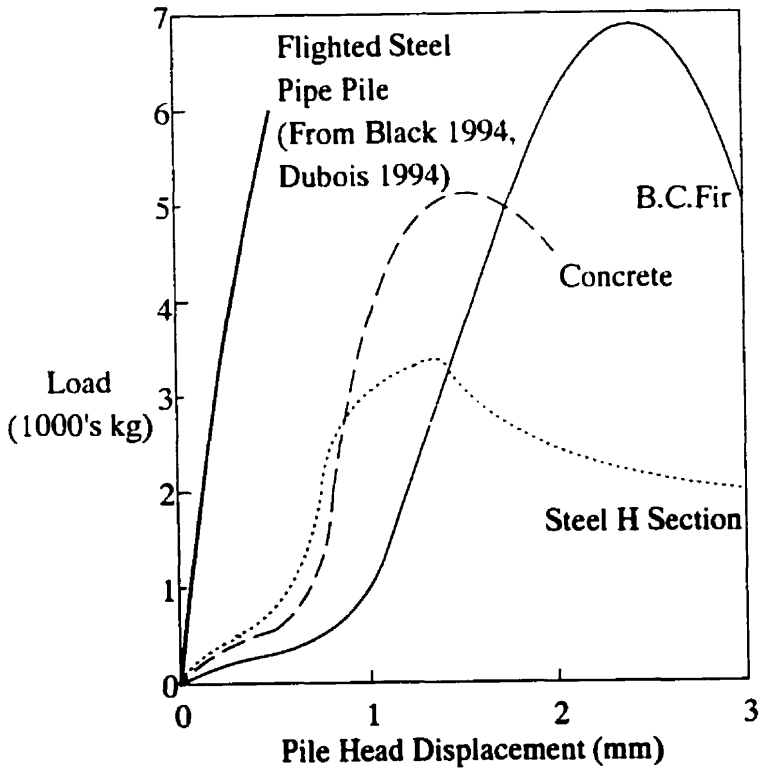

Figure 2-2: Typical Load-Displacement Curves
(Modified from Parameswaran, 1981)

Research by Jellinek (1958, 1959, 1962) demonstrated that adhesion strength was a function of temperature. From 0°C to -13°C, shear failures were at the interface between steel and ice. Below this temperature, Jellinek found that the failures were within the ice (ie. a cohesive shear failure in the ice). The experiments found adhesion was temperature dependant above -13°C, and independent below. The modulus of elasticity of frozen soil also varies with temperature, increasing with decreases in temperature.

Sego and Smith (1989) demonstrated that the surface finish of the pile was very important to the development of surface shear strength. They stated "sandblasting *of* (sic) the pile surface

doubled the adfreeze strength at the pipe-backfill interface". Not only did the peak strength increase, but the tests indicated that the bond was more ductile. The peak strength was reached at a much larger displacement (greater than three times). Residual strengths appear to be comparable to strengths determined from other tests irrespective of the surface treatment. The material to which the ice is bonded, is a significant factor in the bond strength. Coatings, rust, metal composition and the contamination of water may degrade the strength, or change the behaviour of the adfreeze bond. Tests conducted by Parameswaran (1978) suggest that the exposure of metal is not the important factor. The bond is readily affected by the overall surface roughness which is increased by the sandblasting. Sego stated that the presence of a thin layer of enamel is insignificant provided that the surface roughness is not coated over.

In addition to short term load capacity, the long term capacity of a friction pile is also important. The long term adfreeze strength of frozen soils is currently unknown due to the duration and complexity of conducting such tests. The limited long term strength of adfreeze, if it exists, is likely based on the slow rate at which the liquid-like layer of water within the soil reacts to stress (through its intrinsic viscosity). For projects with a finite life expectancy, the long term strength can be more easily defined as the stress level which does not result in excessive settlement within the foundation's lifetime.

Adfreeze depends on normal stress in cohesionless granular soils whose strength is essentially frictional in nature (Heydinger 1987). Alternately, in fine grained soils, adfreeze is largely

cohesive in nature. In cohesionless soils, it also varies with density. As the volume of ice increases, the frictional contribution reduces.

The adfreeze bond strength between the pile surface and soil is controlled by the degree of contact. This degree of contact is controlled by four factors; the difference between thermal expansion coefficients of the engineering material and the soil-ice system, the compressibility of the pile shaft and its lateral strain under compression, arching of the soil-ice system at the pile interface, and the existing lateral pressure applied by the overburden.

Two important conclusions are drawn from Ladanyi and Morel (1988) regarding the importance of dilatancy (volumetric expansion during shear). For dense sand with a fixed density and confining pressure, the dilatancy is much greater for frozen saturated sand than unfrozen sand. For frozen Ottawa fine sand, Ladanyi and Morel found that unconfined dilation at failure was approximately four times greater than when it is unfrozen. Frozen sand also demonstrates ice-cavitation below the critical confining pressure at failure. With dilatancy during failure, frozen soil experiences strain hardening (also known as dilatancy hardening).

Weaver and Morgenstern (1981, quoted from Ladanyi 1991) found that adfreeze shear strength is inversely related to ice content and directly related to pile roughness. For rough piles, the strength is determined away from the immediate contact surface between the pile and soil, and involves the interaction between the frozen soil and asperities. As a result, the limiting case involves the long term adfreeze strength equalling the long term shear strength.

Roggensack and Morgenstern (1978) found that the apparent friction angle of frozen soils was very close to that of unfrozen soils. The frictional component of shear strength is provided by the soil skeleton and depends on particle size distribution, particle shape, orientation or arrangement, and relative density. The difference in behaviour is a much higher cohesion intercept during initial failure. Vyalov (1963) speculated that this is due to the ice matrix cementation within the skeleton. It may also be the result of surface tension within the liquid-like layer of water between silicate particles in clay-rich soils. This behaviour is similar to that found in artificially cemented aggregate soils. The cohesion intercept is time and temperature dependant. With increasing time to failure, the intercept decreases, while with decreasing temperature, it increases. For cohesionless frozen soils, the overall long term strength is greater than the long term strength of the unfrozen soil under identical conditions (Ting, 1981).

The behaviour of friction piles in frozen soils is significantly more complex than similar piles in unfrozen soil. This is due to the unique properties of frozen soils. Frozen soils are more sensitive than thawed soils to temperature, strain rates, time, and material interaction. The result is adfreeze bond strength and load transfer distribution that are interdependent and also separately dependant on numerous variables.

2.2 Piles with Shaft Protrusions

2.2.1 Introduction

The surface of friction piles is often shaped to modify the load transfer process in an attempt to increase the load resistance capacity. The pile shaft may have a continuous helix, concentric rings, lugs, and other modifications for this purpose. Lugs, rings, helical flights, and other protrusions serve to increase the volume of soil involved in a shear failure, and tend to move the failure plane from the soil-shaft surface to within the adjacent soil mass.

The behaviour of such shaped piles is complicated by their relative stiffness, the size of the protrusions, and the effect the protrusion geometry has on the force equilibrium near the pile shaft surface. Also, the strain deformation of those protrusions changes with displacement of the pile, thus modifying the load transfer mechanism with displacement. A combination of these factors results in a wide range of potential load transfer mechanisms.

A separate discussion of research on shaped piles in soil, rock, and frozen soil will review the field study and theoretical basis of ongoing work.

2.2.2 Shaped Piles in Unfrozen Soil

Research into shaped piles in unfrozen soil has centred around the behaviour of expanded

base, tapered, and corrugated piles, and tension anchors. Piles are shaped to increase the effective rate of load transfer. The shear surface or slip surface is extended away from the pile shaft to increase the volume of soil involved in load transfer. Shaped piles are manufactured in the following types; expanded base, belled base, ringed, spiral or helical, tapered, corrugated, and stepped.

Corrugated shaft piles are also described as having peak strengths 2 to 3.5 times higher than smooth piles regardless of displacement rate. Ladanyi and Guichaoua (1985) also concluded that corrugated piles were the most efficient of smooth surface and straight shaft, smooth surface and tapered shaft, and corrugated surface and straight shaft configurations. **Figure 2-3** illustrates the varying displacement behaviour of those pile types. Extending the surface of the pile to such a point that the shear failure occurs away from the adhesion surface permits a more ductile failure. This failure tends to mobilize the residual (large strain) strength of the soil, which is approximately 50% of the peak strength (Ladanyi and Guichaoua, 1985).

Full scale testing of piles with flat-corrugations (two flat faces, and two wedge shaped faces, each with secondary wedges) found that the corrugations increased bearing resistance of the piles by factors of 1.4 to 1.7 over square piles, and by a factor of 1.2 to 1.4 over wedge shaped piles. The flat-corrugated piles tests resulted in gradually increasing settlement with each load increment towards a maximum sustainable load (Abbasov and Kovalevskii, 1984).

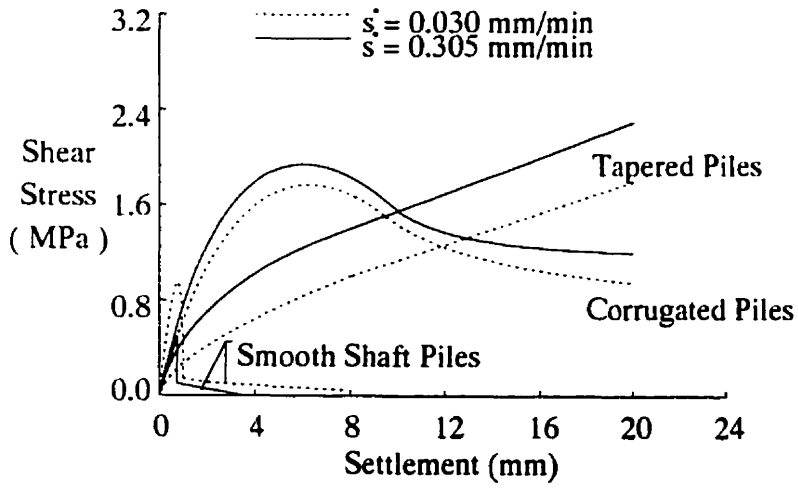

Figure 2-3: Shear Stress versus Settlement for Three Pile Types
(After Ladanyi and Guichaoua, 1985)

One of the earliest studies of the bearing resistance of flighted cylinders was by Wilson (1950). The research included a model pile study, full size load tests, and a theoretical investigation. The theoretical study investigated the assumption that the screw pile was a rigid body within an elastic isotropic mass. The screw piles consisted of a cylindrical shaft with an acute angled conical point. Just above the pile tip, a single pair of half-revolution flights were attached. The tests were performed in a variety of cohesive and granular soils by "screwing" the pile into the soil to its bearing depth. Wilson also reprinted the load-settlement curves of four concrete screw piles tests using different number of flights performed by H.D. Morgan (1944). Those curves are reprinted as **Figure 2-4**. Wilson's study concluded that the bearing capacity of the "screwcrete" piles corresponds well to the sum of the bearing capacity of a flat circular plate bearing at depth, and the shaft friction developed by the soil along the shaft. Wilson (1950) discussed the impact of the reduction of shaft resistance due to the presense

of the flighting, and the effect of pile installation on the soil properties by disturbance.

A model pile study was performed by Clemence and Pepe (1984) to identify the effect of lateral stress around multihelix tension anchors. The study found that the lateral stress in the soil increased from its static value to a value approaching the passive pressure limit of the soil (Kp). The lateral pressure (K_f) at failure was found to be 30 to 40% lower than those proposed by Meyerhof and Adams (1968), although the lateral stress during failure did increase up to 90% in medium dense sand.

An extensive test program of approximately 200 screw piles was reported by Trofimenkov and Mariupolskii (Undated). The tests consisted of piles with diameters from 0.25 metres to 1.0 metres, in soils ranging from soft to hard clays, and medium dense and loose sand, using a variety of loading methods, including continuously increasing, stepwise increasing, and pulsating methods. Several conclusions were drawn from this comprehensive study. Trofimenkov and Mariupolskii found that a critical depth to diameter ratio exists during pull out tests which determines if the performance of the anchors is governed by the free boundary surface. This finding was confirmed by Ghaly, Hanna, and Hanna (1991). Also, during both tension or compression tests, a compacted zone of soil was formed on the advancing face of the screw plate, which had an inclined surface at 45° to the pile axis.

Rao et al (1991) tested a series of eleven model piles having helical plates with varying geometry. Tests were done in compression and tension in three different types of cohesive

soil. The intent of the study was to determine a basis for design of screw piles in cohesive soils. The helical plates did not consist of continuous flighting, but instead were separate helical plates with the pitch intended for convenient installation purposes. The spacing of helical plates was a function of design. In all cases, the helical plates were two, to three times the diameter of the pile shaft. All model piles were slowly rotated (screwed) into the prepared soil mass, which consisted of remoulded clay. Their analytical model for determining theoretical capacity assumed that in compression, a cylindrical failure surface develops from helical tip to helical tip, with the lower helix behaving as an end-bearing pile tip. In comparing the model with tests, the results corresponded very well at a helix spacing ratio (spacing between helix versus helix diameters) approaching unity to 1.5. However, as the helix spacing ratio increased, the accuracy of the model declined proportionately. This suggests that the model of the pile load transfer behaviour is not fully representative of broadly-spaced helical plates and can not be extended to all pile geometries.

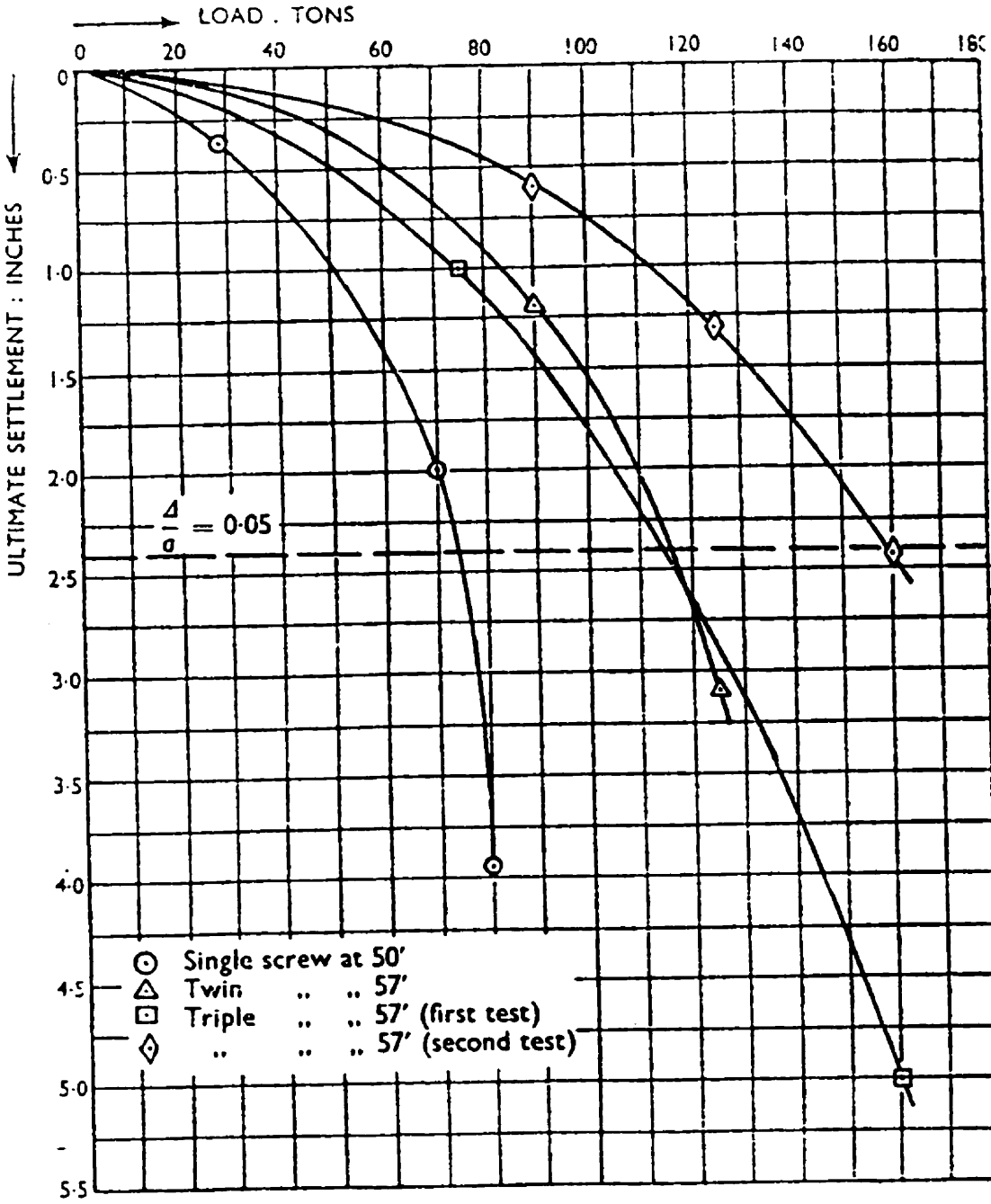

Figure 2-4: Load versus Settlement for Cylinders with One, Two, and Three 8 Foot Diameter Screws
(Morgan, 1944)

A theoretical analysis and laboratory study of load transfer between ribbed inclusions and non-cohesive soil was performed by Irsyam and Hryciw (1991) to identify factors affecting load transfer in various geotechnical reinforcement systems. The laboratory study used a carbowax technique to identify the failure surface developed by shear failures within a direct shear box mechanism. For small rib spacings, the shear failure surface was approximately a straight line parallel to the plane of displacement. Large rib spacings developed a failure surface with three distinct regions (**Figure 2-5**), consisting of a zone of soil arching, a transition zone, and a passive resistance zone.

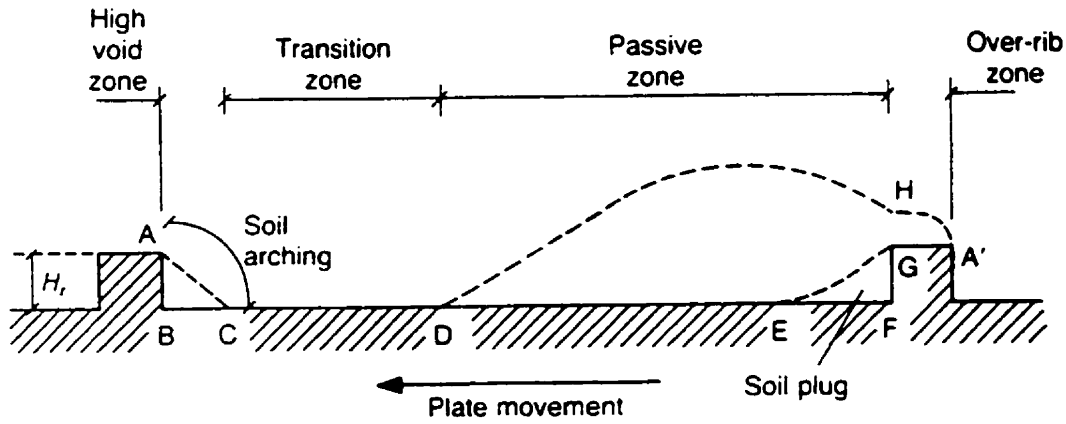

Figure 2-5: Intrarib Zones for Large Rib Spacing
(Modified from Irsyam and Hryciw, 1991)

A theoretical analysis was performed to develop a pullout resistance model for a large spacing between ribs, which included the contribution of the transition zone and the passive zone. An analytic plasticity model solution developed by Sokolovski (1965, 1960), was adapted for determining the pullout resistance provided by the passive zone (**Figure 2-6**). The model provides computed values for the frictional component, and the passive pressures developed on the rib and base plate. Comparision with the test results found that the model's predicted behaviour and failure shape agreed very well for dense sand, and well for loose sand. The method of velocity characteristics was also applied to the test results, but the agreement was relatively poor.

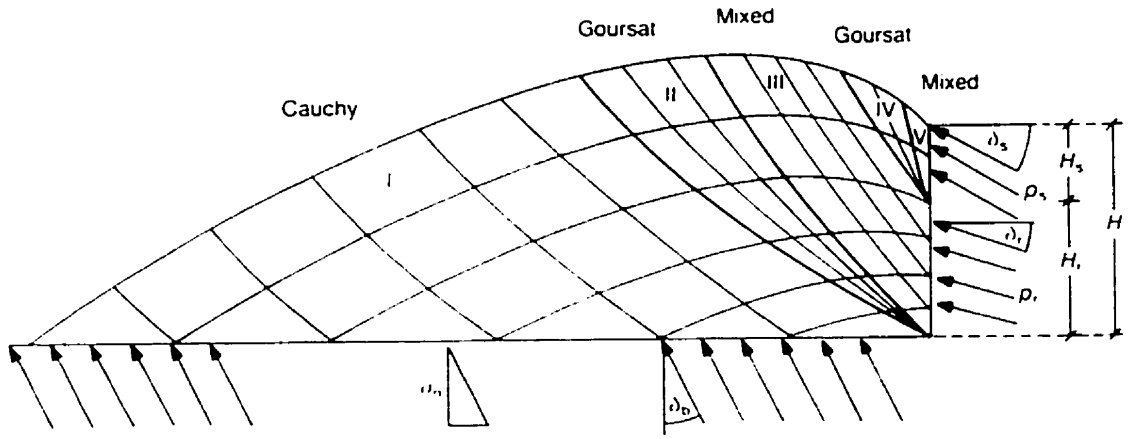

Figure 2-6: Plasticity Model for Passive Resistance Against Ribs
(Irsyam and Hryciw, 1991)

Having developed an analytic model that agreed well with test results, an optimum rib could be determined. It represents the maximum number of passive resistance zones per unit length of reinforcement, which in turn requires that the length of the transition zone is minimized. Within this study, the optimum rib spacing was ten times the rib height for loose Ottawa sand,

and thirteen times the rib height for dense Ottawa sand. For spacings approaching twice the height of the rib, the zone of passive resistance disappears and shear resistance becomes a function of a planar soil to soil friction surface.

Hryciw and Irsyam (1993) undertook a direct shear box study of rigid ribbed inclusions in dry sand to improve the understanding of shear transfer at peak loads through the observation of zones of dilation, contraction, and steady state shear zone development. The study found that shear resistance was a function of sand particle properties, sand density, and surface roughness. The tests were performed with a direct shear box with plexiglass sides using a normal stress of 50 kPa., video recording equipment, and the use of a carbowax solidification technique to identify the developed shear surfaces. Video monitoring of individual particles noted that in dense sand, "the sand particles move not only tangentially to the plate, but also in the upward normal direction. A zone of relatively high dilation occurs above the inclusion surface." **Figures 2-7 and 2-8** show the direction of the grain movements gradually varies from 0 degrees from the horizontal at the interface to 50 degrees from the horizontal at about 6 mm. above the rib. Gradual movements of the shear zone coalesced into a distinct narrow shear zone at large displacements. For a large rib spacing (>10 x rib height), a curved failure surface initiated above the top of the rib, touched the base plate, and continued to the next rib. Full development of a shear zone with residual shear stresses provided for a maximum sustainable load. Hryciw and Irsyam (1993) anticipated and confirmed that a critical void ratio zone developed ahead of the ribs, while a low density soil fabric developed behind the ribs. The varying failure surfaces for different types of sand, and density are shown in **Figure 2-9.**

Earlier research by Irsyam and Hryciw (1991) identified the optimum rib spacing which develops a full passive resistance zone, a minimized transition zone, and a small zone of soil arching behind the rib **(Figure 2-10)**. For rib spacings smaller than optimum, the passive region progressively reduces until the spacing is approximately twice the rib height. At this spacing, the shear resistance is developed from soil to soil friction, and a small contribution of soil to rib tip friction.

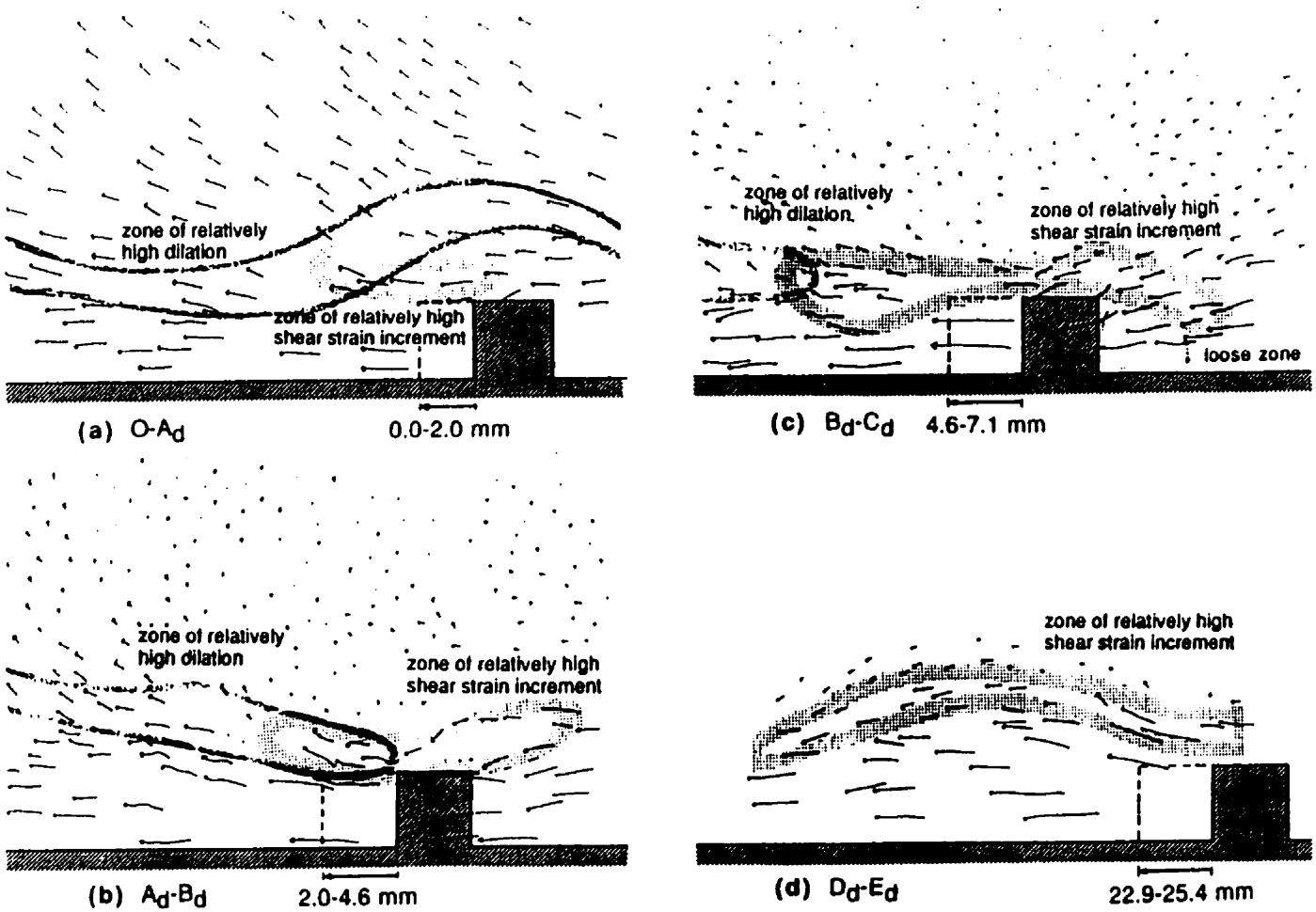

Figure 2-7: Displacements of Select Grains and Behaviour Zones (Ottawa 20-30, e=0.52, σ_n = 50.0 kPa, a = 2.5 mm, s=33.0 mm)
(Hryciw and Irsyam, 1993)

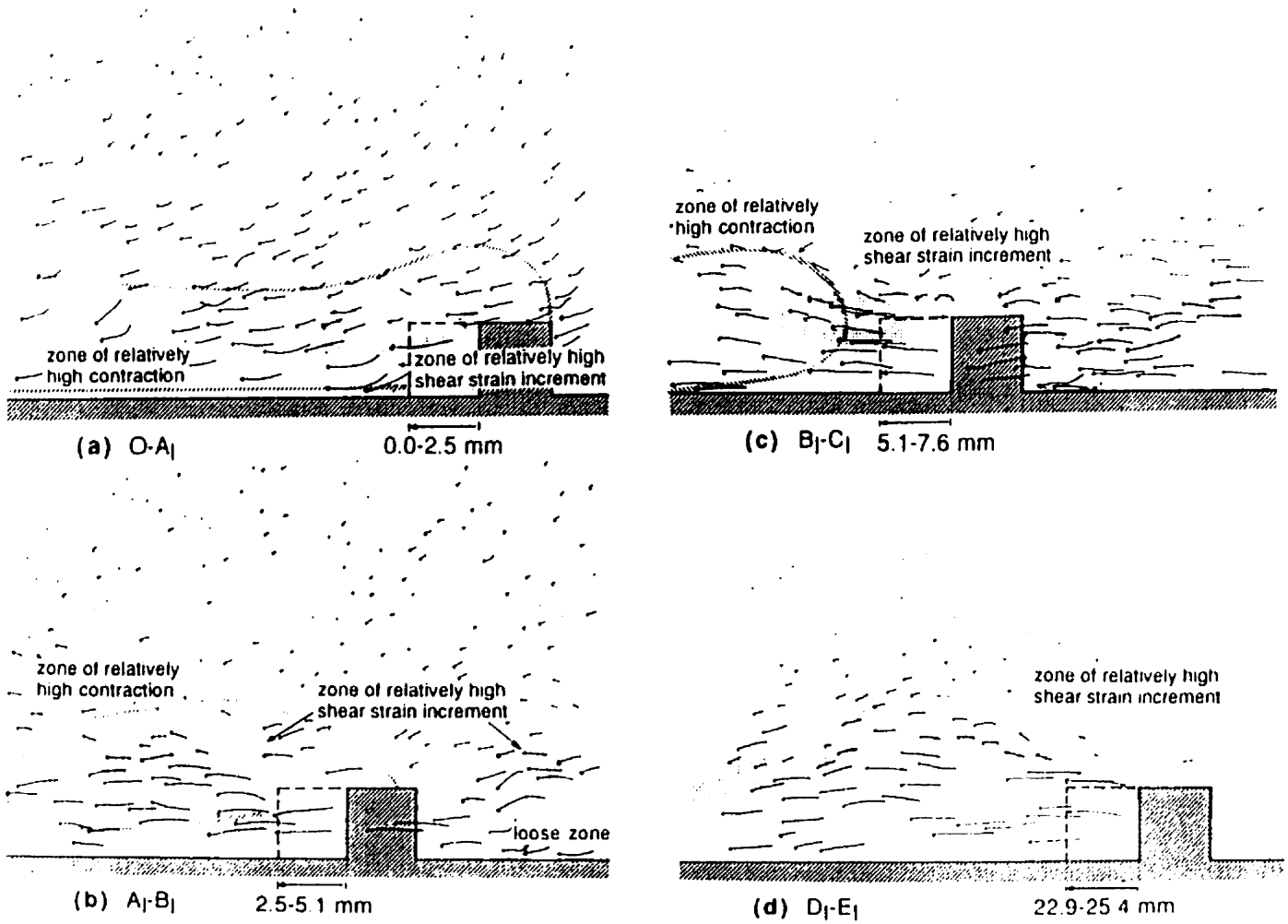

Figure 2-8: Displacements of Select Grains and Behaviour Zones (Ottawa 20-30, e=0.63, σ_n=15.5 kPa, a=2.5 mm, s=33.0 mm)
Hryciw and Irsyam, 1993)

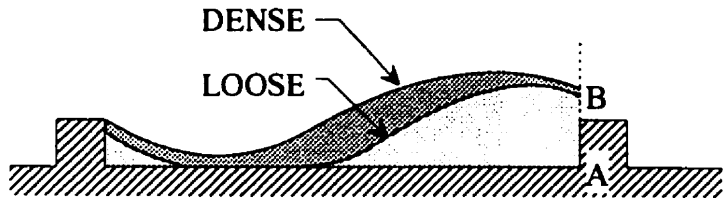

Ottawa 20-30

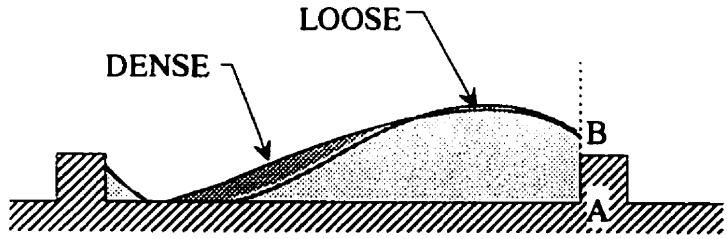

Ottawa 40 - 50

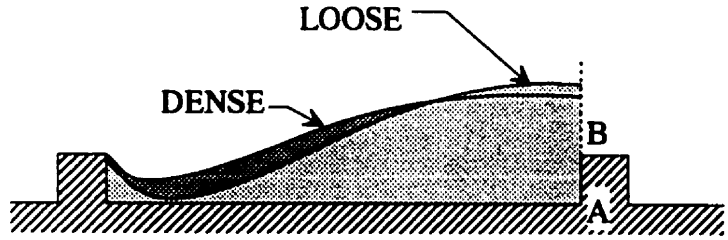

Glazier Way 20 - 30

Figure 2-9: Density Effects Observed from Carbowax Solidification (Ottawa 20-30, a=2.5 mm, s=33.0 mm)
(Modified from Hryciw and Irsyam, 1993)

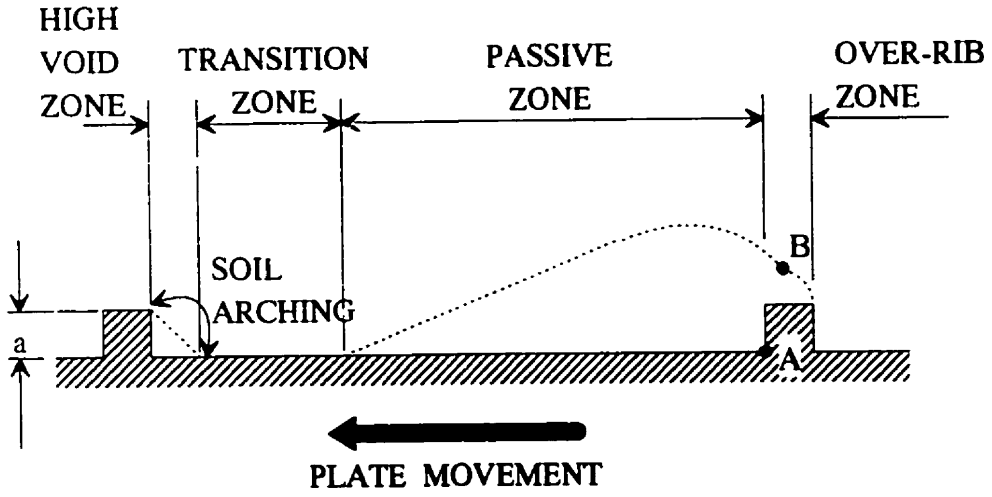

Figure 2-10: Intrarib Zones for Large Rib Spacings
(Hryciw and Irsyam, 1993)

Some testing was performed with trapezoidal ribs (similar to those found on reinforcing steel) to determine the effect of rib geometry. The study found that no passive zone developed, and sand grains flowed over the ribs from front to back, resulting in a shear resistance purely from surface roughness and friction. The shear zone thickness was reduced.

2.2.3 Shaped Piles in Rock

There is limited published literature on the use of shaped piles in rock. Most literature focusses on tensile rock anchors and their transfer of load from the anchor shaft to the rock mass. There is limited literature on modified rock sockets.

Under-reaming and belling of compression pile bases has not been used significantly due to the difficulties in assuring competent contact between the pile shaft and the rock. In a situation where piles were constructed with belled bases, it was to increase the end-bearing area. Generally, in design, where the bases are belled, a portion of shaft load transfer is neglected. This is due to the effects of reduced confinement near the top of the bell. The remainder of the shaft is assumed to behave as smooth-shaft piles in rock.

Horvath and Kenney (1979) summarized research on rock-socketed caissons from Canada, Australia, U.K., and U.S.A. They noted that there was a lack of information on socket shaft wall roughness. However, a general relationship between qualitative roughness to developed shaft resistance was proposed as shown in **Figure 2-11**. Generally, these piles were understood to carry their loads principally through modified shaft friction.

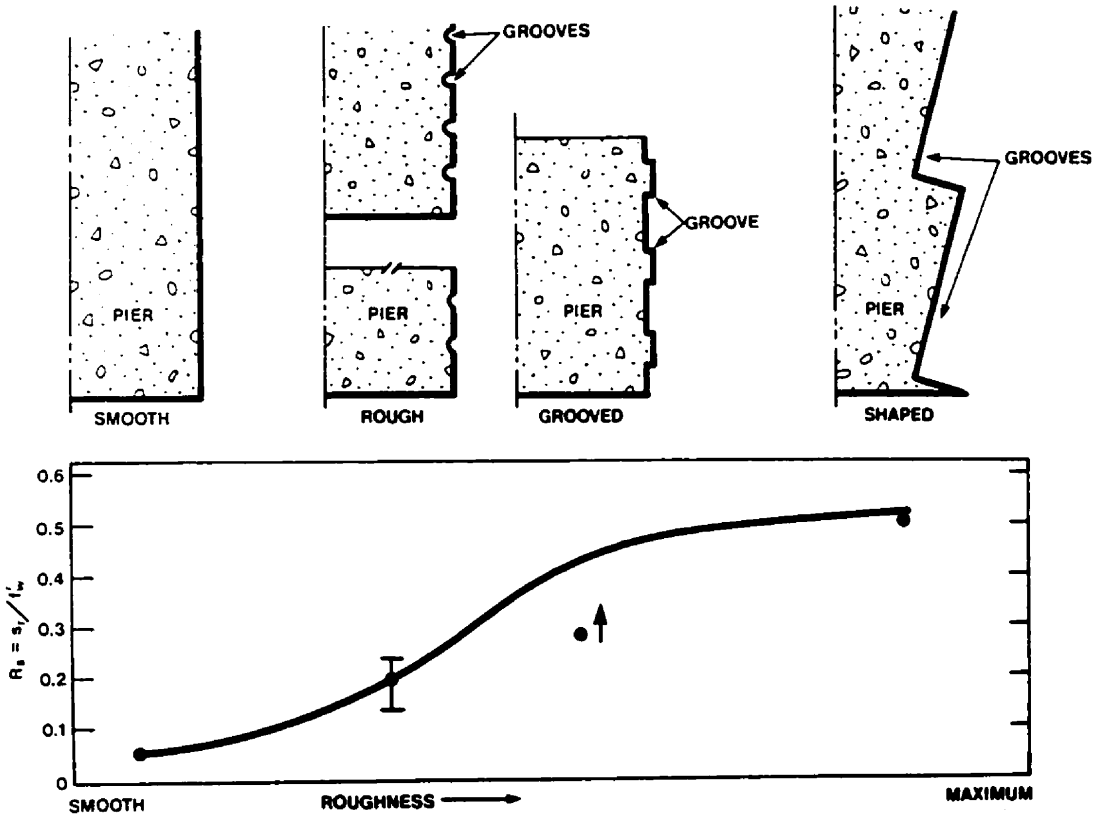

Figure 2-11: Shaft Resistance versus Roughness of Socket Wall
(Horvath and Kenney, 1979)

Glos and Briggs (1983) performed two instrumented rock-socketed caission load tests in shaley sandstone (soft rock). The rock sockets consisted of 600 millimetre diameter shaft with two sets of grooves cut into the rock socket walls. Each groove was four inches high and three inches deep and placed 450 millimetres apart. Strain gages within the socket found that load transfer was non-linear and generally confirmed the predictions by Pells and Turner (1979). High rates of load transfer occurred near the top of the socket, and decreased to a uniform amount after two socket diameters, consistent with predictions from elastic theory. The effect of the grooves was not determined. However it was speculated that they increased the effective diameter of the socket.

2.2.4 Shaped Piles in Frozen Soil

Surface Roughness of Piles in Frozen Soil

A much larger literature base exists for the behaviour of piles in permafrost and the various results of model pile investigations in frozen soils. However, for flighted steel pipe piles, the literature base is limited. No investigation of flighted anchors or piles appears to have been completed, although related research had been conducted. The behaviour of smooth, lugged and threaded bars, and the properties of the bond between frozen soil and steel have been investigated. Those investigations now provide background material for the research program undertaken by the author.

Model steel pile testing in frozen sand by Alwahhab et al (1984) determined a relationship between the load transfer coefficient (m) and the surface roughness (RF). The load transfer coefficient was defined as the ratio between the adfreeze bond strength and the long term soil internal cohesive strength. A dimensionless surface roughness coefficient was defined as the actual surface length in relation to its chord length. Testing included lugged piles which produced results that correlated well with the relationship. This permits the prediction of adfreeze bond strength if both the pile surface properties and the soil cohesion properties are known. The relationship is illustrated in **Figure 2-12**.

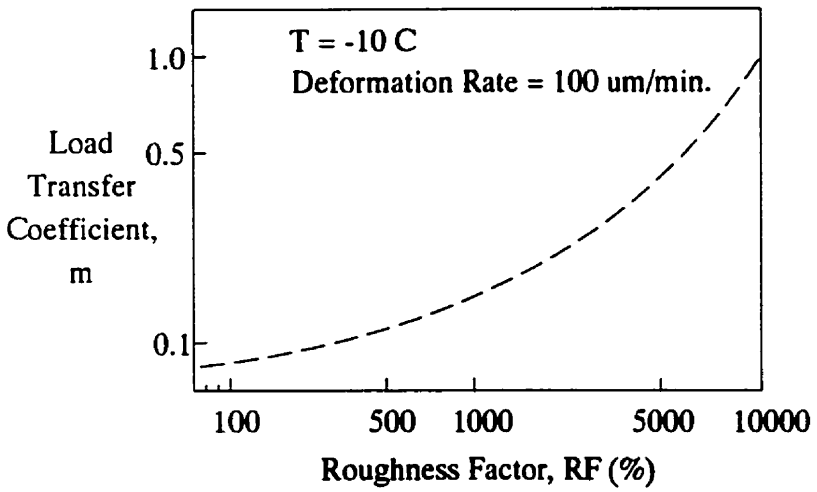

Figure 2-12: Empirical Relationship Between "m" and "RF"
(Modified from Alwahhab and Anderson, 1984)

Holubec (1990) conducted five model tests in frozen soil using 43 millimetre diameter rod and a pipe pile, two metres long. The tests included two threaded rod piles grouted with Set-45 grout, two threaded rods placed in oversize holes and filled with gravelly sand slurry and a slurry of air track cuttings, and one 140 mm. diameter pipe pile. The results of the tests suggested that the sand-backfilled threaded rod had twice the ultimate compressive resistance of the plain pipe pile, while the grouted threaded rod had over three times the pipe pile's ultimate compressive resistance. This reinforced the importance of pile surface roughness in increasing the load capacity and creep resistance. The gravelly sand resulted in a substantially stronger bond than the air track cuttings, demonstrating the importance of backfill properties. Holubec postulated that the gravelly sand developed greater interlocking and shear dilation. Holubec also speculated that the ideal pile for frozen soils would have a continuous spiral, which "will transfer the shear stress from the steel to the backfill/soil uniformly, as opposed

to horizontal rings which concentrate the stress, and allow easier flow of the granular soil in the annulus during backfilling". The rotation of the stress field below the flight results in a more uniform loading of the soil than the incremental change that occured below each successive ring on a ringed or lugged pile.

Sego (1989) undertook adfreeze tests using various types of backfill and steel pipe piles. In the series of tests described, the piles consisted of 33 mm. O.D. steel pipe piles which were installed in 51 mm. O.D. holes. These sizes were selected so that the ratio of diameters "was the same as that commonly encountered in the field". A comparison of the four pile test results underscores the importance of backfill soil properties (**Figure 2-13**). Native soil properties did not appreciably affect the pile capacity (**Figure 2-14**). This suggests that the failure surfaces occur near the pile and did not involve large volumes of adjacent soil.

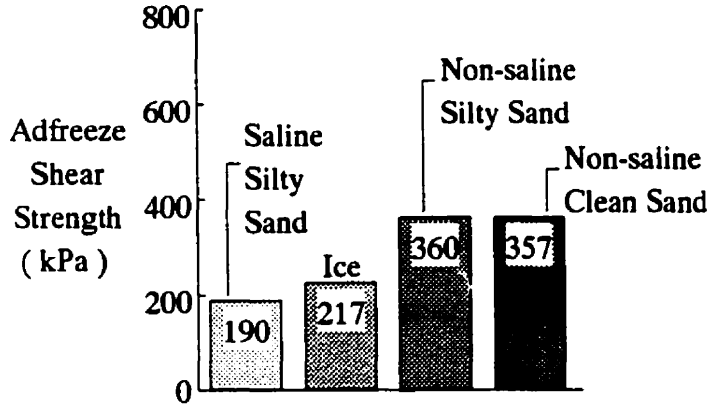

Figure 2-13: Backfill Properties versus Adfreeze Strength
(After Sego, 1989)

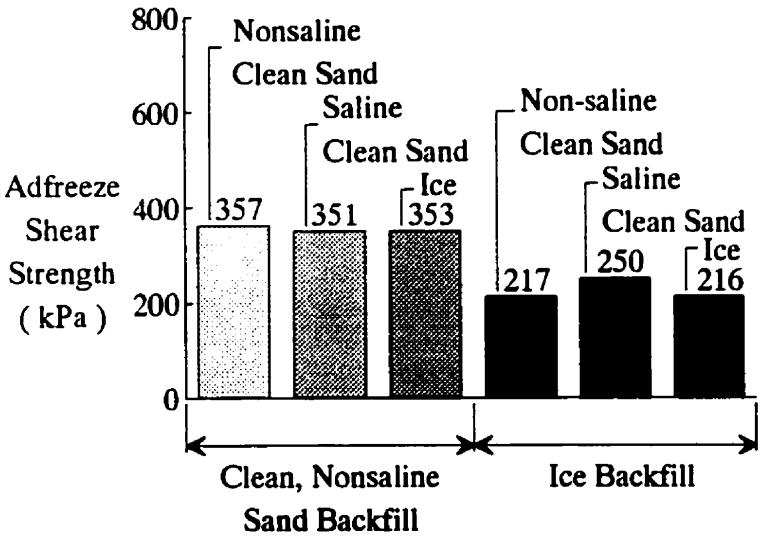

Figure 2-14: Native Soil Properties versus Adfreeze Strength
(After Sego, 1989)

A number of researchers have identified variations in shear strength as a function of pile size or cross-sectional area. Tsytovich (1975) and Inoue and Frederking (1986) discussed this issue. In part, this variation is a function of lateral pressure exerted by a diametric expansion of the pile while loaded. Inoue and Frederking (1986) tested wood piles in a saline ice sheet. The results indicated that the adhesion strength was inversely proportional to the square root of the diameter of the piles. An investigation conducted by Saeki (1981) found similar results using freshwater ice. The dependency of adfreeze strength on pile diameter is the result of pile shaft compressibility. If two piles of equal cross-sectional area, but different outside diameters are restrained by a rigid soil, the pile with a least diameter applies a much larger lateral pressure to the soil. This is based on elastic mechanics of solids, in which a thin walled cylinder will expand diametrically when loaded axially. As most engineering materials exhibit elastic properties and expand perpendicular to compressive strains (effect of Poisson's Ratio),

lateral pressures between pile and soil will occur. The compressibility of pile shafts has been recognized as the controlling parameter of load transfer distribution in piles, especially long piles. This is especially true in frozen soils which have very high modulus of elasticity.

A model pile analysis was undertaken by Mattes and Poules (1969), who considered the behaviour of compressible piles in an ideal elastic soil. They found that the compressibility, K, (ratio of $E_{PILE}A_{PILE}$ vs. $E_{SOIL}A_{SOIL}$) of a pile dictates the shear stress distribution along the pile shaft. The importance of this pile compressibility factor can be illustrated in **Figure 2-15** where shear stress is plotted against unit depth. Pile compressibility is both a function of material elastic modulus and relative cross-sectional areas.

The Young's Modulus for frozen soil can be based on experimental data or empirical equations developed by Tsytovich (1975). Using Tsytovich's relationships for E_{SOIL}, and the common range of dimensions for pipe pile, the pile compressibility (ratio of $E_{PILE}A_{PILE}$ vs. $E_{SOIL}A_{SOIL}$) is often less than K = 10 (at -5°C). Mattes and Poules (1969) state, "Piles having a value of K less than about 100 may be classified as very compressible, and for the case K = 1, the compressibility of the pile is identical to that of the surrounding soil."

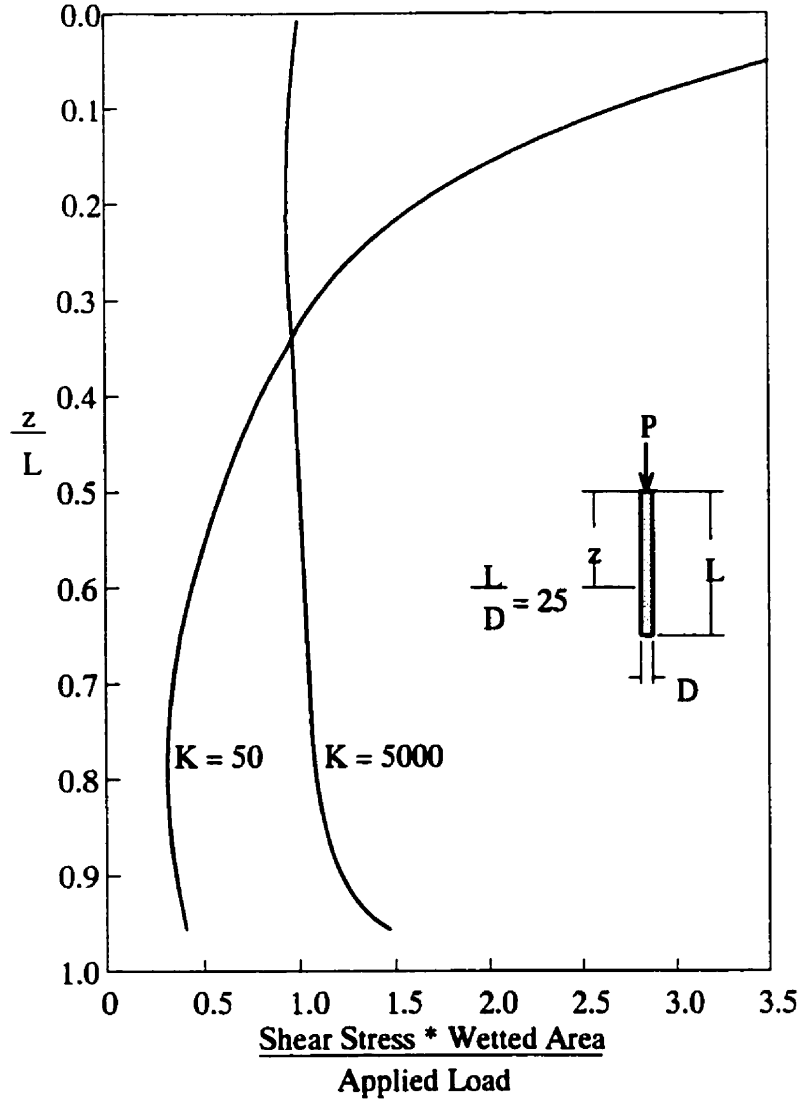

Figure 2-15: Distribution of Shear Stress versus Pile Compressibility
(After Mattes and Poules, 1969)

Lugs and Rings on Piles in Frozen Soil

Small scale model pile tests were performed in frozen sand with varying lug or annular ring dimensions, and varying number of rings (Andersland and Alwahhab, 1981). The testing

confirmed that load transfer was a combination of ice adhesion, friction between frozen sand and the pile, and mechanical interaction between the pile and the sand mass. Ice adhesion was mobilized at small displacements, followed by the mobilization of friction and mechanical interaction. Ultimate load transfer increased in direct relation to the number of lugs. As ultimate capacity was governed by friction and mechanical interaction, Andersland and Alwahhab (1981) speculated that optimum lug spacing was a function of the overlap of pressure bulbs. Model pile testing with different frozen sand densities also confirmed that load transfer increased as the volumetric proportion of sand particles involved increased.

Andersland and Alwahhab (1983) also conducted small scale model pile tests in which model piles with lugs were pulled from a block of frozen sand. The tests were constant displacement and constant load tests, and were used to determine the strength and creep behaviour. The sand (classified as fine sand) was frozen to -10°C. The pile lugs were found to "increase the volume of ice matrix and soil particles involved in the initial bond rupture." The use of lugs also greatly improved the creep resistance of the pile, with larger lugs being more resistant. The spacing of lugs on the model piles was apparently "dependant on pressure bulb overlap for consecutive lugs and formation of a void space behind the lugs." The paper identified several important aspects of lugged bars and piles that can be extrapolated to flighted piles.

Ladanyi and Guichaoua (1985) performed a series of thirty-three model pile tests in frozen saturated sand to assess the improvement in shaft resistance provided by corrugations or slight tapers over straight shafted piles. The tests demonstrated a clear difference in load-

displacement behaviour between the three pile types. Smooth-shaft pile adfreeeze tests failed in a brittle manner, reaching a peak strength with limited displacement, followed by a low residual strength and higher rates of settlement. Corrugated pile tests had a more ductile behaviour, reaching a peak strength followed by a gradual decline in resistance at large settlements. Corrugated piles show a non-brittle behaviour due to the mobilization of soil to soil shear resistance rather than adfreeze strength. The tapered piles generally showed a small peak strength corresponding to failure of the adfreeze bond, followed by a gradual and steady increase in resistance with no evidence of strength loss. The study concluded that for corrugated for piles "at any given penetration rate, their peak strength is from two to 3.5 times higher than that of smooth piles. They are the most efficient of the three *pile types tested (sic)*".

Biggar and Sego (1993) undertook a series of pile tests in saline permafrost to assess various pile surface treatments and backfill materials. They found that pipe piles with four 12 mm. lugs (rings) carried twice the load of a smooth pipe pile, while a sandblasted pipe pile carried four times as much. This emphasizes the importance of surface roughness on the development of pile capacity. The load-displacement behaviour of the piles also varied. As the roughness of the piles increased, the ductility increased. Load transfer behaviour of smooth piles was brittle, or strain weakening, while the lugged piles failed plastically, or by strain hardening. The tests conducted by Biggar and Sego suggest that lugged piles experience an adfreeze bond failure below the ultimate capacity. The remaining capacity is through the soil shear resistance developed by the lugs. Biggar and Sego stated that the increase in capacity of

lugged or flighted piles is approximately linear until the failure of the adfreeze bond. After the failure of the adfreeze bond, flight flexibility and shaft compressibility become significant. The load transfer then becomes more complex. Flexibility of flights and shaft compressibility is significant because the elastic modulus of rapidly loaded frozen soil is greater than the elasticity of thawed soils. During loading of lugged piles, surface adhesion failed at small strains, followed by load transfer by lug interaction. Biggar and Sego (1993) noted that grouted and lugged piles do not develop uniform stress distributions due to the load transfer occuring within the backfill. It was also noted that pile capacity increased approximately linearly with the increase in lug projection into the backfill.

A model pile study of steel cylindrical piles with lugs in frozen sand by Stelzer and Andersland (1986) examined the effect of various lug spacings and sizes. The model pile consisted of a 9.5 mm diameter steel pile with a single steel lug varying in projection from 0.79 mm to 3.18 mm and 12.7 mm thick. All lugs would perform rigidly in relation to the frozen sand. A void was formed in the frozen sand at some distance ahead of the lug to simulate the presense of an adjacent lug ahead of the model pile lug. The lug spacing was assumed to vary from 10.2 mm to 25.4 mm. Inspection of test specimens after testing found a dense zone of sand ahead of the pile lug height, and a probable zone of flow encompassing the densified zone. Behind the lug, a void nearly equal in height to the pile displacement was formed as shown in **Figure 2-16**. Stelzer and Andersland presented a potential chronology of the model piles displacement, which described the changes to the soil mass as the pile displaced. At small displacements, the adfreeze bond fails and the pile moves rapidly. As a zone of compacted and

crushed sand develops ahead of the lug, the model pile resistance increases due to mechanical interaction of the lug and the soil mass. At large displacements, a shear failure surface develops between adjacent lug tips. Linear relationships between the lug spacing and the displacement at the start of failure were identified for two lug heights (1.59 mm and 3.18 mm). The relationship is well defined for the larger lug, and less so for the smaller lug. This may be due to the effect of the sand particle size (0.42 mm to 0.60 mm) relative to the lug heights. Also, the investigation identified the need for a minimum lug spacing to fully develop the mechanical interaction between the lugs and soil. The lug spacing also affected the load capacity at a critical displacement (identified as onset of failure).

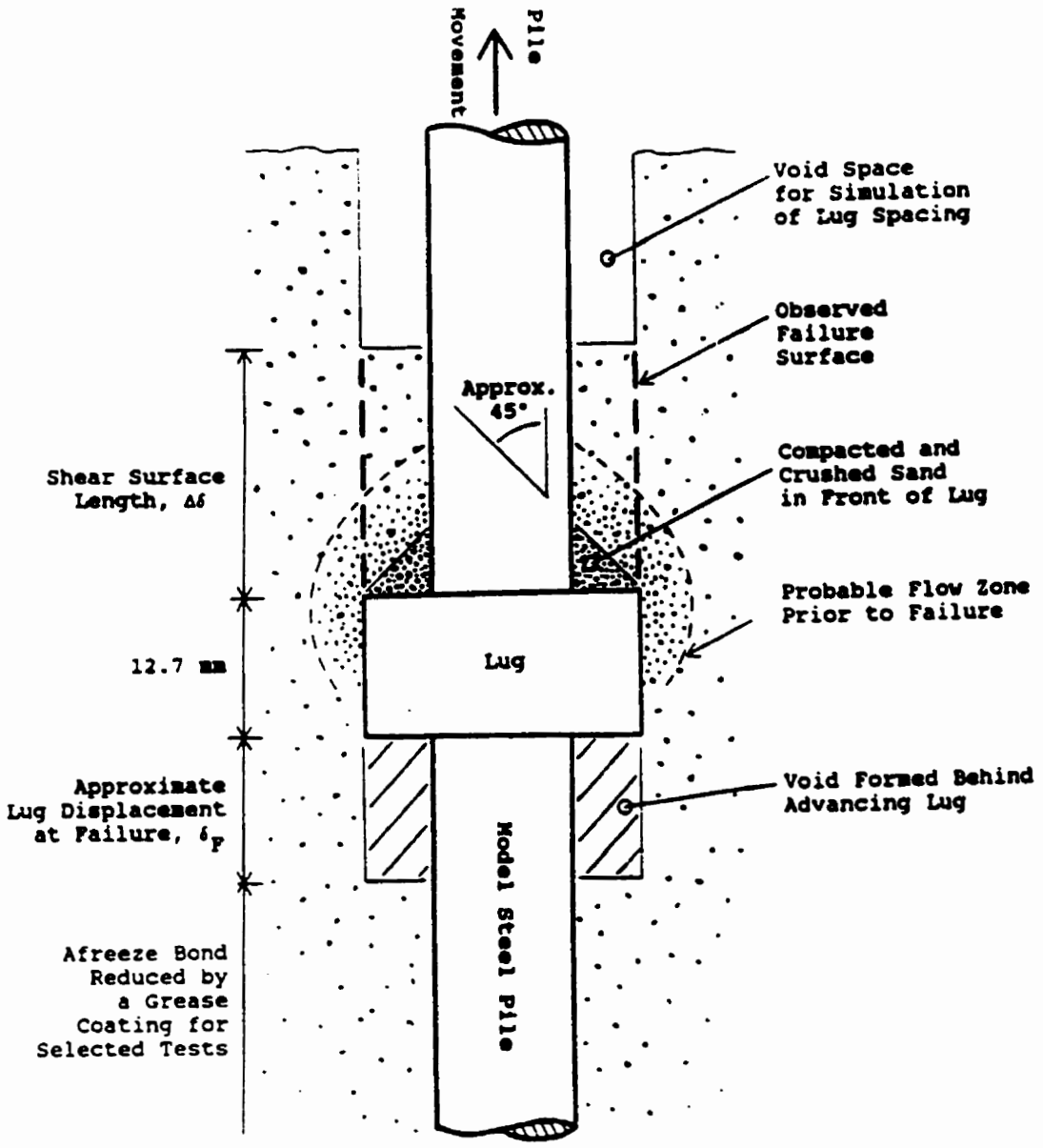

Figure 2-16: Interaction Between the Model Pile and Frozen Sand at the Start of Pile Failure
(Stelzer, 1988)

For those soils that experience plastic flow during extended loading, "larger lugs (more than 2 x maximum particle size) compressed frozen sand at their leading edge and densified the adjacent frozen soil. Particle crushing occurred along with formation of a zone of material flow and/or slippage in front of and around the lugs", (Stelzer and Andersland, 1986). Significant strength increase can then develop through the densified sand. Densification occurs only when sufficient time is permitted for the sand to behave in a drained manner.

A load transfer chronology put forth by Stelzer and Andersland (1986) suggests that most adfreeze forces are lost by the time lugs or flights carry significant loads. A small zone above the lug remained to contribute to adfreeze forces. The zone ahead of the lugs is influenced by the pressures developed by the lugs, and may have high mechanical interaction forces due to dilatancy effects increasing the confining force. "At lug spacings that fully develop mechanical interaction, the pile displacement-time behaviour is relatively unaffected by variations of lug spacing until reaching a critical displacement (start of pile failure)" (Stelzer and Andersland, 1986). The relationship between this critical failure displacement and lug spacing for two lug heights is shown in **Figure 2-17**.

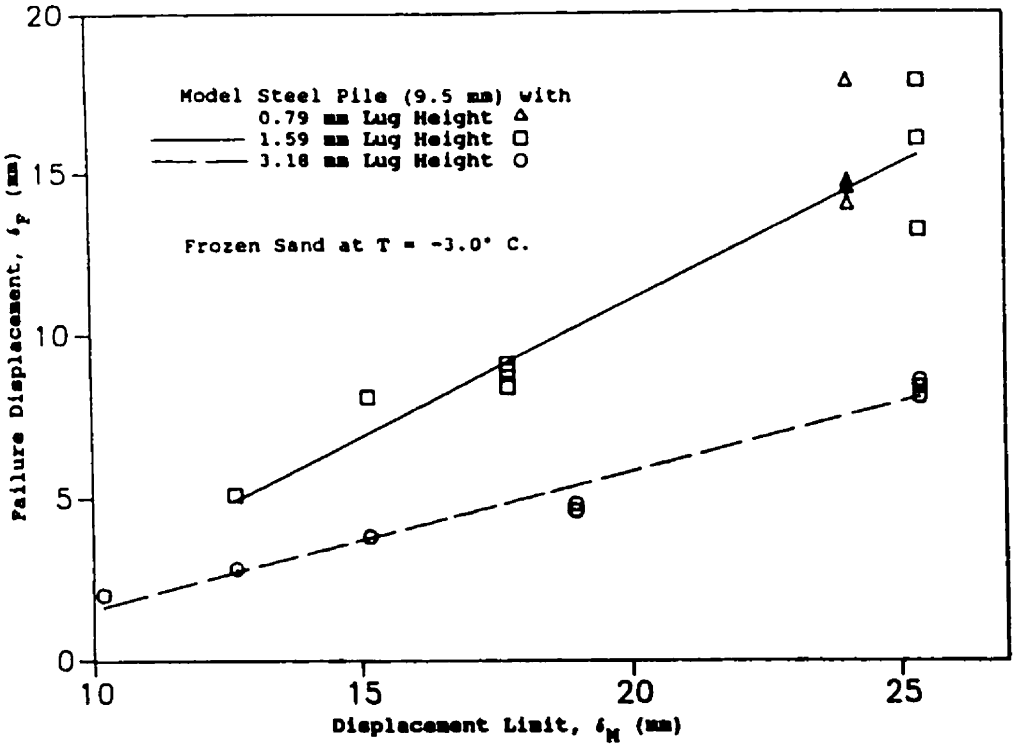

Figure 2-17: Relationship Between Lug Displacement and Pile Displacement at Failure (Stelzer and Andersland, 1986)

Continuous Flights on Piles in Frozen Soil

Dubois (1994) conducted full-scale testing of two thermal piles in the in-ground freezing pit at the University of Manitoba. Each pile was instrumented to determine the load transfer per segment of pile. One pile with flighting, and one pile without flighting were tested. Several conclusions were drawn from the experiment, notably, that the flighted pipe pile was stiffer, required much smaller displacements to transfer load to soil, and was less susceptible to creep. Unfortunately, the precise mode of load transfer from the flighted pile to the soil was not identified. The behaviour of the pile appeared to follow the load transfer distribution

described by Linnel and Lobacz (1980).

A preliminary investigation by the author (Black, 1994) involved loading three short segments of geometrically similar pile shafts with variations in load transfer. One pile segment consisted of a shaft with flighting and adfreeze permitted, the second pile segment consisted of a shaft with flighting and adfreeze prevented, and thirdly, a pile segment with no flighting and adfreeze permitted. The segments were loaded to failure. The testing identified a difference in the behaviour of flighted piles with shaft adfreeze and flighted piles without shaft adfreeze. The adfreeze contribution was not more than 12% of the ultimate capacity. An analysis of the results speculated on a failure surface beginning at the pile shaft and progressing to an ultimate cylindrical failure surface defined by the tips of the flighting. Thus, initially the capacity of the pile is dictated by the adfreeze bond and the ultimate capacity is dictated by the shear strength of the soil as illustrated in **Figure 2-18**. Using indirectly measured adfreeze and shear strengths in the laboratory, the failure surfaces for various displacements were generated. These failure surfaces appeared to coincide with the proposed load transfer hypothesis.

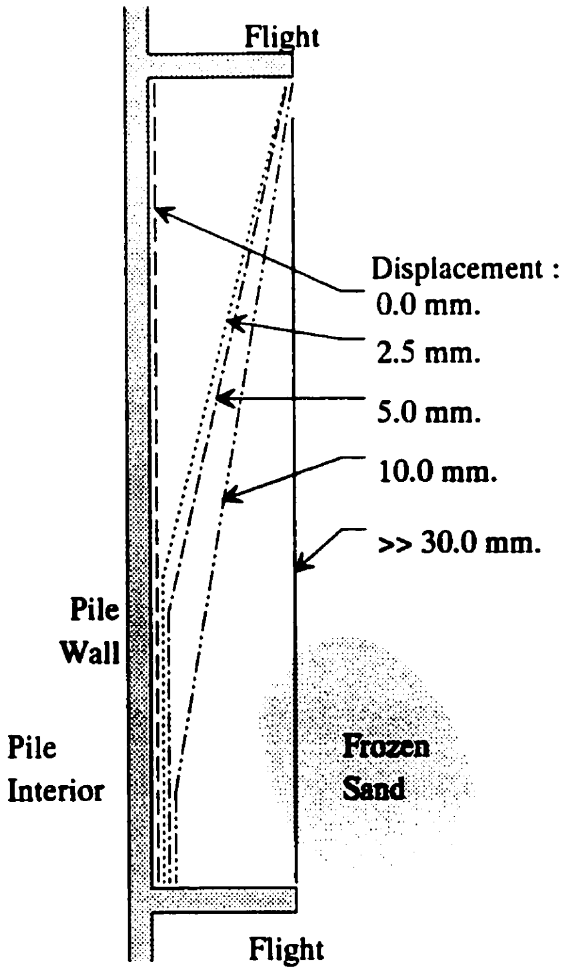

Figure 2-18: Failure Surfaces Corresponding to Selected Displacements (Black, 1994)

Long (1973) discusses the merit of using rings or helixes on piles in leiu of smooth shaft surfaces to avoid the limitations of adfreeze load transfer. Adfreeze load tranfer is brittle, strain limited, and sensitive to many environmental conditions, such as pile surface condition, temperatures, etc. Frozen soil tends to be stronger in shear, more ductile, and less sensitive to installation conditions. This suggests distinct benefits of relying on frozen soil shear strength with pile flighting over the more brittle behaviour of smooth-surface pile shafts. The

use of rings or helixes moves the failure surface away from the pile surface into the soil mass and utilizes the shear strength of the soil. Long stated that "Blades *(helical flights)* are designed to permit some *deflection* of the blades before the underlying soil reaches its ultimate shear strength, thus distributing the stresses further along the pile without soil shear occurring." On a loaded flighted pile, the flights undergo progressively less deformation with depth. This is because generally the load transfer decreases with depth. The compressibility of the pile shaft compared to the surrounding soil affects the load transfer rate, usually resulting in a non-uniform rate.

Load Transfer of Flighted Piles in Frozen Soil

For long slender piles in permafrost, the distribution of load transfer along the pile shaft is time-dependant. Initially the load is carried by the upper portion of the pile. After a period of time as creep occurs in the highly stressed region, the load transfer at the lower portions of the shaft will increase. After a very long period of time, the load transfer may become linear as the soil around the pile shaft becomes equally stressed. As Linnel and Lobacz (1980) suggested, the transfer of load may become linear with the exception of the lower portion of the pile that may still have a non-uniform stress distribution. This is illustrated in **Figure 2-19**.

Principally, there are three possible modes of failure for a flighted steel pipe pile. They consist of; (i) a shear failure surface extending cylindrically from flighting tip to flighting tip as described by Black (1994) and Dubois (1994), (ii) a structural failure of the flighting resulting in a behaviour similar to a conventional pipe pile, and (iii) a rotational failure in which the pile

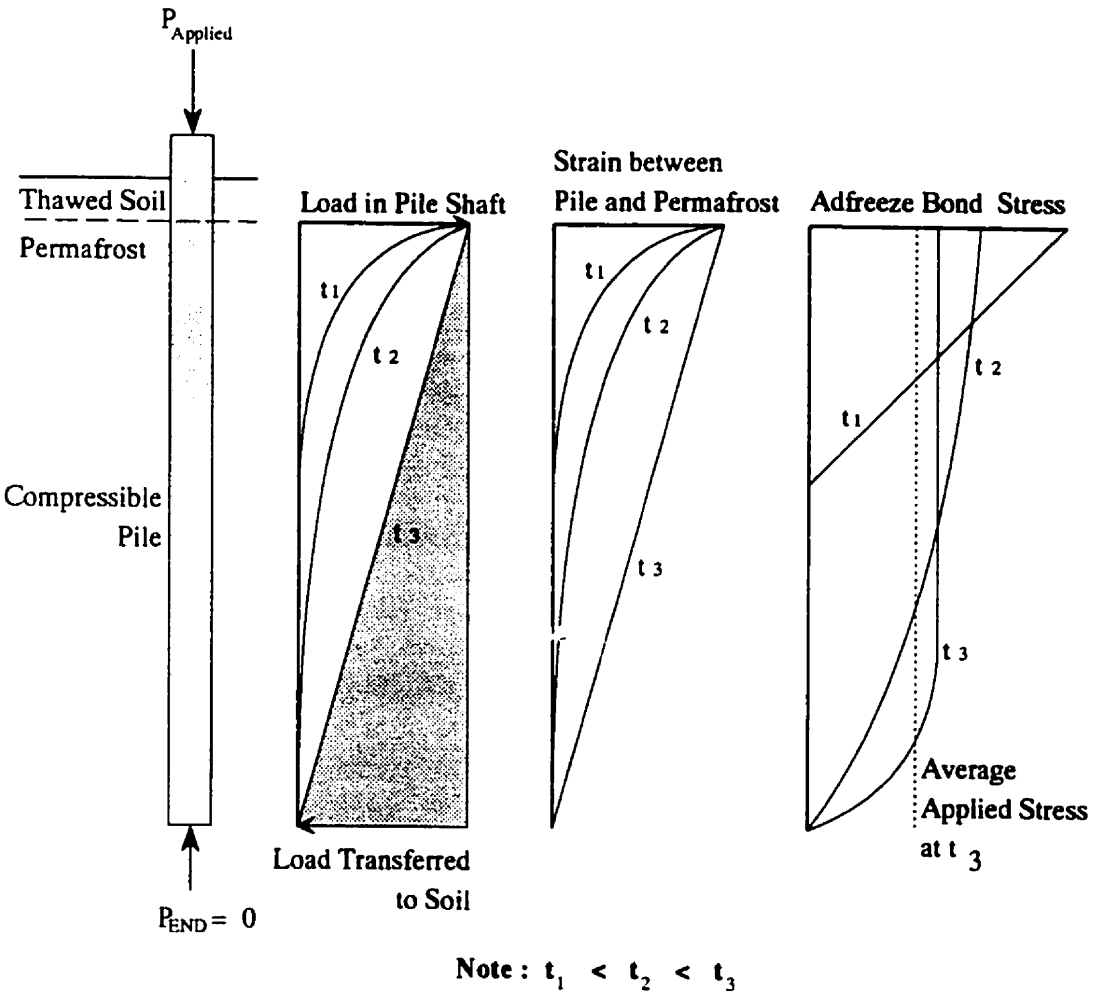

Figure 2-19: Typical Distribution of Load and Stress Along Pile Shaft
(Modified from Linnel and Lobacz, 1980)

rotates after an adfreeze failure on all surfaces. All of these failure modes are illustrated in **Figure 2-20.**

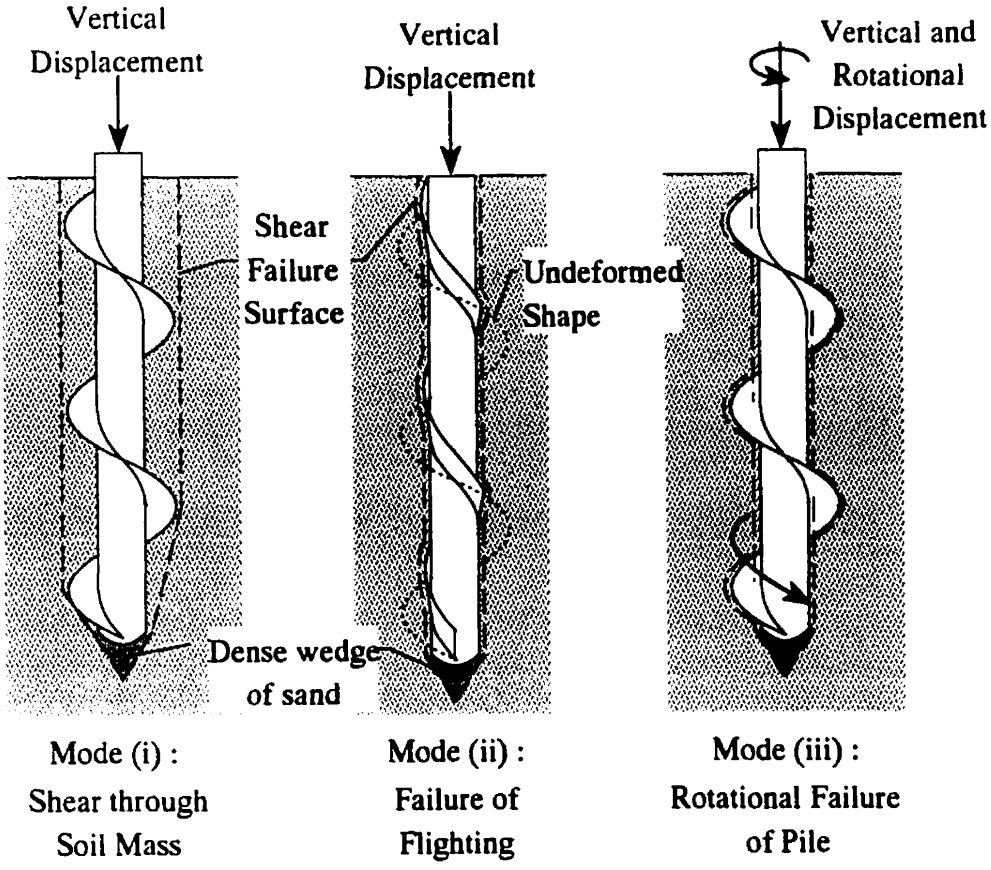

Figure 2-20: Conceptual Pile Failure Modes
(Based on Dubois, 1994)

During the rapid loading of a flighted steel pile in frozen soil, there is a rapid increase in shear stress near the top of the pile. Initially, load transfer is through a combination of adfreeze and to a limited extent on the flights bearing on the surrounding soil mass. As strain increases at a given point on the shaft, the adfreeze bond fails and load transfer occurs through mechanical

interaction and friction only. Since most of the load is being carried by the upper portion of the pile, the failure of the adfreeze bond occurs almost instantaneously at a small displacement. As pile displacement increases, the adfreeze bond fails progressively along the pile length. The failure of the adfreeze may be either cohesive (failure of the ice) or adhesive (failure of ice-pile bond), depending on pile surface smoothness and soil temperatures. As soon as the adfreeze fails in the vicinity of a flight, the flight itself deflects somewhat after the loading on the flight increases. Increasingly, the load is transferred through bearing of the flights, while displacement of the pile shaft causes a progressive adfreeze failure down the pile. The load transfer mechanism described above is supported by results reported by other research (Stelzer and Andersland, 1986, Biggar and Sego, 1993, etc.) which indicates a transition from one mechanism to another mechanism.

Dubois (1994) conducted an analysis of a flighted pipe pile undergoing each of the failure modes and calculated the average stress exerted on the frozen sand. Of the three modes that were considered in that paper, the mode with the lowest load transfer per unit area was the mode (iii), adfreeze only (CASE 3 in Dubois 1994). The highest load transfer per unit area was a composite failure surface comprising both shaft adfreeze and soil shear. Obviously, the highest load transfer per unit area represents the most likely mode of failure of a pile which has maintained its structural integrity, but as Black (1994) described, the composite failure is an intermediate failure surface that occurs prior to the ultimate failure surface. Failure occurs first where the stresses are highest.

2.3 Hypothesis

Under rapid axial loading, helically flighted steel pipe piles embedded in frozen sand exhibit progressive failure of load transfer mechanisms. This progression begins with failure of the surficial adfreeze shear bond and ultimately develops as cylindrical shear failure surface extending the flighting tip to adjacent flighting tip. The ultimate load carrying capacity of a helically flighted steel pipe pile is governed by the residual shear strength of the backfill material.

It is hypothesized that the helical flighting transfers a portion of the applied load at small displacements, and at the ultimate load capacity, the flighting transfers a maximum proportion of the applied load, while adfreeze/shaft friction carries the remainder. The portion of each is to be determined by the pile segment geometry and soil properties.

3. Experimental Study

3.1 Test Setup

3.1.1 Introduction

The objective of the test program was to separate the load transfer into that proportion carried by the pile shaft, and that proportion carried by the flighting. The deflection of the flight would be used to determine the portion of the applied load transferred by the flighting, while measurements of strain along the shaft would be used to determine the load carried by the shaft along its length.

This Chapter reviews the test facilities, the model pile segment, the test setup and procedures, summarizes the results of the loading tests, and any observations relevant to the analysis of the problem.

As noted by Ladanyi (1991), testing a short segment of pile can provide load transfer information without the complication of dealing with pile compressibility. With a short pile segment, the effects of shaft compressibility are minimized and the behaviour of a single unit length can be used. This permits the determination of local effects without making the effects of shaft elasticity significant. For this reason, a short model pile segment was used for testing.

3.1.2 Cold Room Test Pit

The pit in which the test was carried out was 2.5 metres square, 2.235 metres deep, and was enclosed in an insulated, refrigerated cold room. The in-ground test pit consisted of a 200 mm. thick reinforced concrete box insulated with 200 mm. rigid insulation on the exterior, and 100 mm. rigid insulation on the interior. The interior of the pit was lined with a waterproof liner. The cold room was 5.0 metres square, 3.0 metres high, and had an operating temperature range of +35°C to -35°C.

Over the test pit, there was a large reaction frame consisting of two W460 x 82 cross-beams supported at their ends by W460 x 82 beams, which were attached to four W150 x 22 rigidly fixed columns. All structural connections were bolted to allow changes to the cross-beam placement. The cold room was also equipped with a 1000 kg. capacity overhead chain hoist. The hoist permitted reconfiguration of the reaction frame or installation and removal of test specimens from the test pit.

The test pit had a drain located in the middle of the pit floor which was connected to a tube that came up through the pit floor to the corner of the test pit, and which extended to the top of the test pit at the level of the cold room floor. This was used to introduce water into the bottom of the pit and permit complete saturation of the sand by exclusion of air pockets, which might occur from adding water rapidly from the test pit surface.

The configuration of the cold room and test pit are illustrated in **Figure 3-1**.

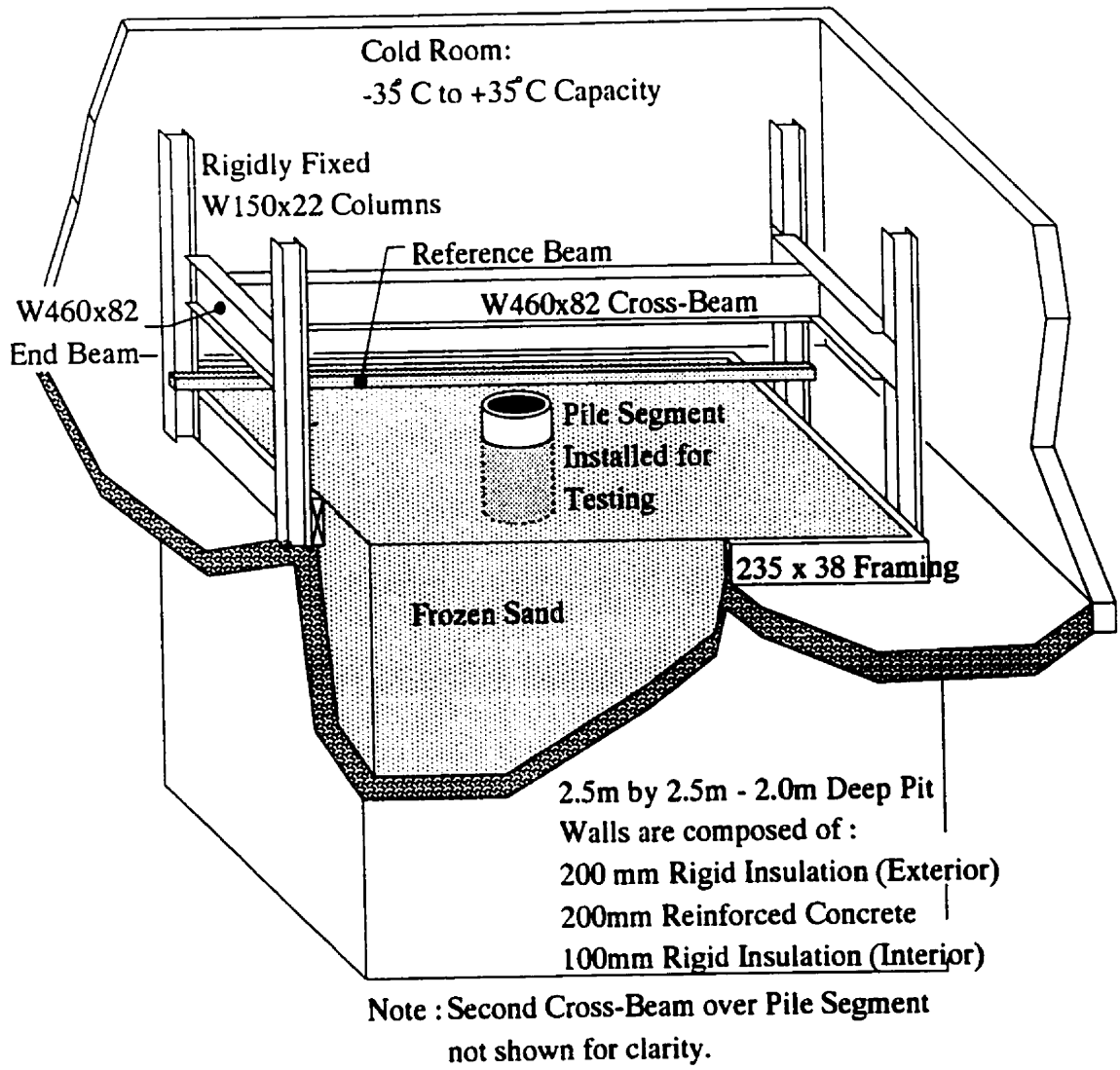

Figure 3-1: Cold Room and Test Pit Configuration

The cold room and test pit were also equipped with an array of thermocouples (Constantan and copper, Type T) for temperature monitoring. Thermocouples were installed at the cold room ceiling, at the test pit surface, and in an extensive three-dimensional array throughout the in-ground test pit. The array permitted the regular monitoring of the frost front both

vertically and horizontally.

3.1.3 Test Pit Sand

The pit was filled with a beach sand which was a fine, quartz sand with 4% fines. The grain size distribution is shown in **Figure 3-2**. The effective size (D_{10}) was 0.10 mm., the coefficient of uniformity (C_U) of 2.20, and the coefficient of curvature (C_C) was 1.31. The sand was classified as poorly graded and has a U.S.C.S. classification of SP.

Unconfined compression tests were carried out to determine the strength parameters of the sand in a frozen state. Three, 38.7 mm. diameter by 112.8 mm. long cylindrical specimens were prepared in molds at the same dry density (1500 kg/m^3) and bulk density (1850 kg/m^3) as the backfill sand. The specimens were then frozen at -25°C and then allowed to warm to -5°C before testing. The unconfined compression tests were conducted in a manner similar to those used in concrete strength testing. The results are found in **Table 1**.

Table 1 : Unconfined Compression Test Results

	Peak Load (kN)	Peak Stress (MPa)	Surface Temp. (°C)
Specimen 1	14.06	11.97	-5.6
Specimen 2	14.24	12.12	-5.2
Specimen 3	14.84	12.63	-4.9

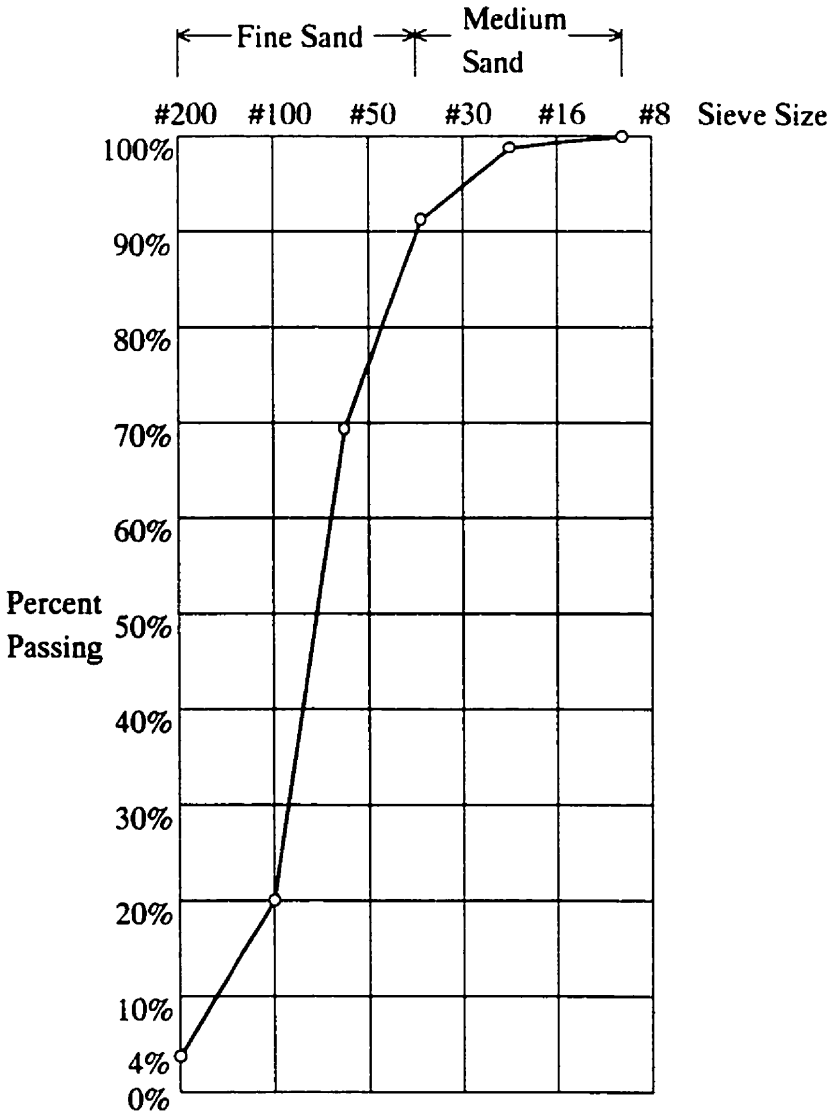

Figure 3-2: Test Sand Grain Size Distribution

Failure occurred at the ends of the specimens likely because of warming of the specimen ends due to heat conduction through the end caps. The failure modes consisted initially of compression followed by development of several shear surfaces near the ends. The unconfined

compression strength of the frozen sand ranged from 11.97 MPa to 12.63 MPa.

3.1.4 Pile Segment

A segment of flighted steel pipe pile was provided by Arctic Foundations of Canada Inc. of Winnipeg. The central pile shaft segment consisted of a 423 mm. long, 168.9 mm. outside diameter, 7.7 mm. thick (Schedule 40) seamless steel pipe. The flighting was manufactured by Uniflyte Co. Ltd. of Winnipeg and was made of 40 mm. wide by 4.54 mm. thick mild steel flat stock. The steel was rolled into a helix form and then welded (full penetration fillet weld, top and bottom of flighting) to the pipe shaft. The pitch of the flighting was 242 mm. One complete pitch was installed on the upper part of the pile segment. The lower part of the segment was used to examine adfreeze forces only. The pile segment was sandblasted (termed a "near-white metal" blast) to provide a smooth uniform surface to ensure uniform behaviour unaffected by the variation and extent of mill scale or lacquer on the pipe segment or flighting plate.

Two vertical strings of strain gages were attached to the pile at 90° to each other. The arrangement and spacing of the strain gages are illustrated in **Figures 3-3** and **3-4**. Both strings of strain gages also included three strain gages attached to the top surface of the flighting. These gages were used to measure the strains at the top surface of the flighting. The strain gages used on the pile segment consisted of six 5 mm. long 120 Ohm general purpose aluminum foil strain gages manufactured by Showa Measuring Instruments Co., Ltd., supplied

by InterTechnology Inc. and designated N11-FA-5-120-11. The remaining 31 strain gages were 10 mm. long 120 Ohm general purpose strain gages also manufactured by Showa Measuring Co., Ltd. and designated N11-FA-10-120-11. In both cases, prior to attaching the gages the surface of the pile was filed smooth, sanded to a uniform finish, cleaned and prepared as recommended by InterTechnology. The strain gages were then waterproofed and the lead wires fixed to the pile shaft with high strength epoxy. The exposed strain gage lead wires were carefully packed in white petroleum jelly to prevent bonding to the frozen sand.

The leads from the strain gages were then attached to a 120 Ohm strain gage Wheatstone bridge adaptor board to convert the changes in strain gage resistance to measurable voltage changes. This board was custom-built for this test program.

Two constantan and copper thermocouples (Type T) were installed on the pile segment. One thermocouple was installed at the top of the pile, and the other at the bottom. This permitted monitoring of shaft surface temperatures.

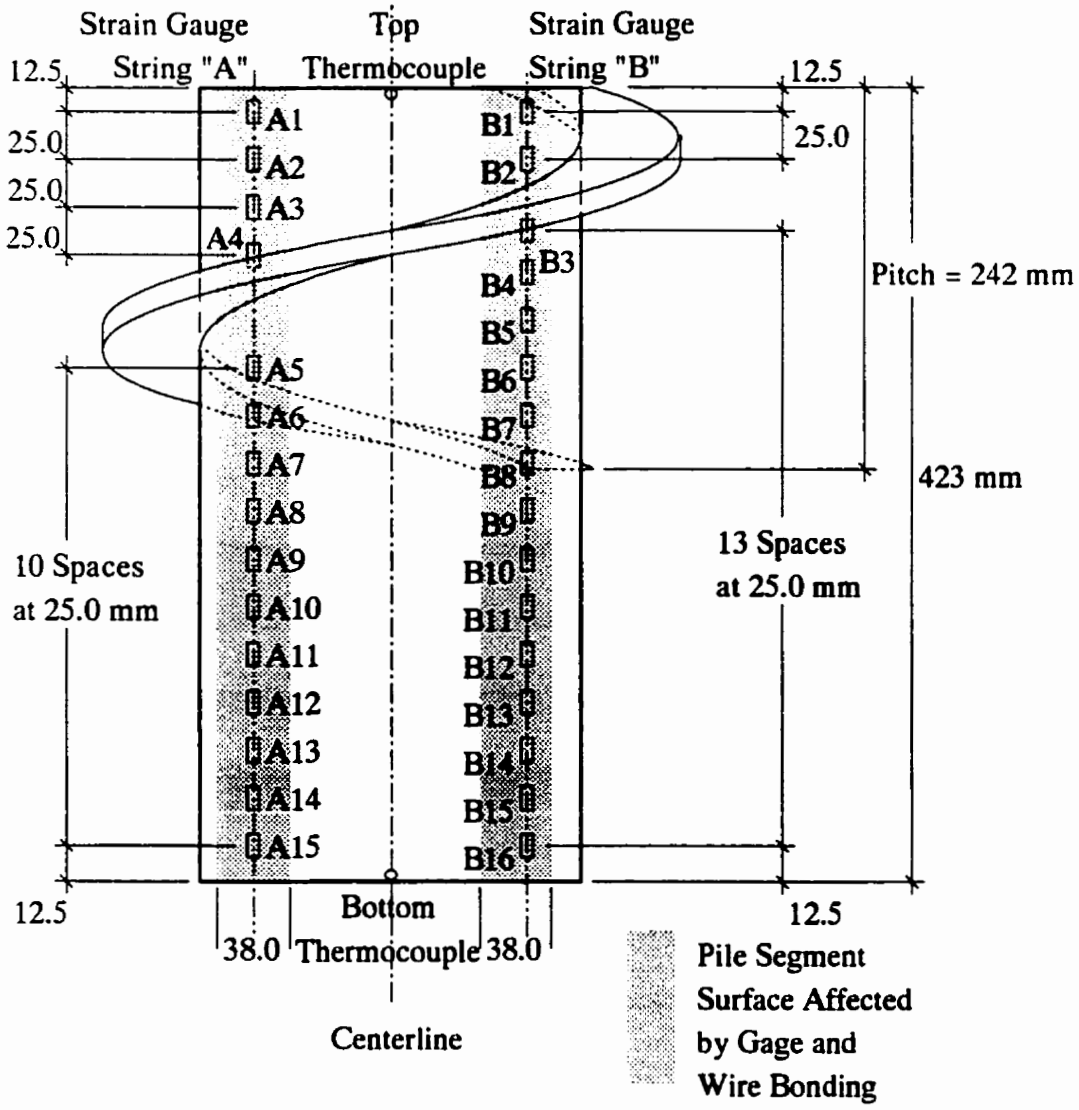

Figure 3-3: Side View of Pile Segment Strain Gage Placement

All of the electronic instrumentation was connected to a FLUKE HELIOS I 60 Channel Data Acquisition System (DAQ). The HELIOS I DAQ was then connected via a RS-232 serial interface to a PC compatible computer to provide data recording. The software used on the PC was called FLUKEH2 which was written in Microsoft BASIC. This software provided communications and operating instructions to the DAQ. The entire system of instruments is

shown schematically in **Figure 3-5.**

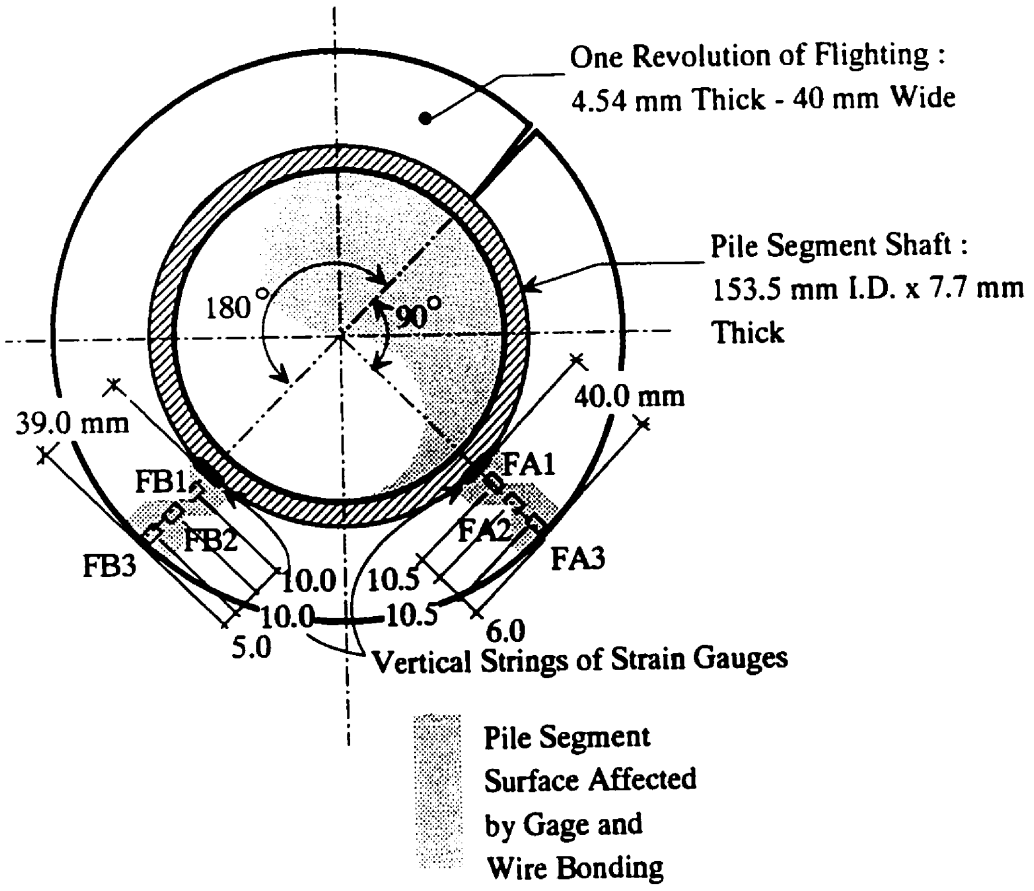

Figure 3-4: Plan View of Pile Segment Strain Gage Placement

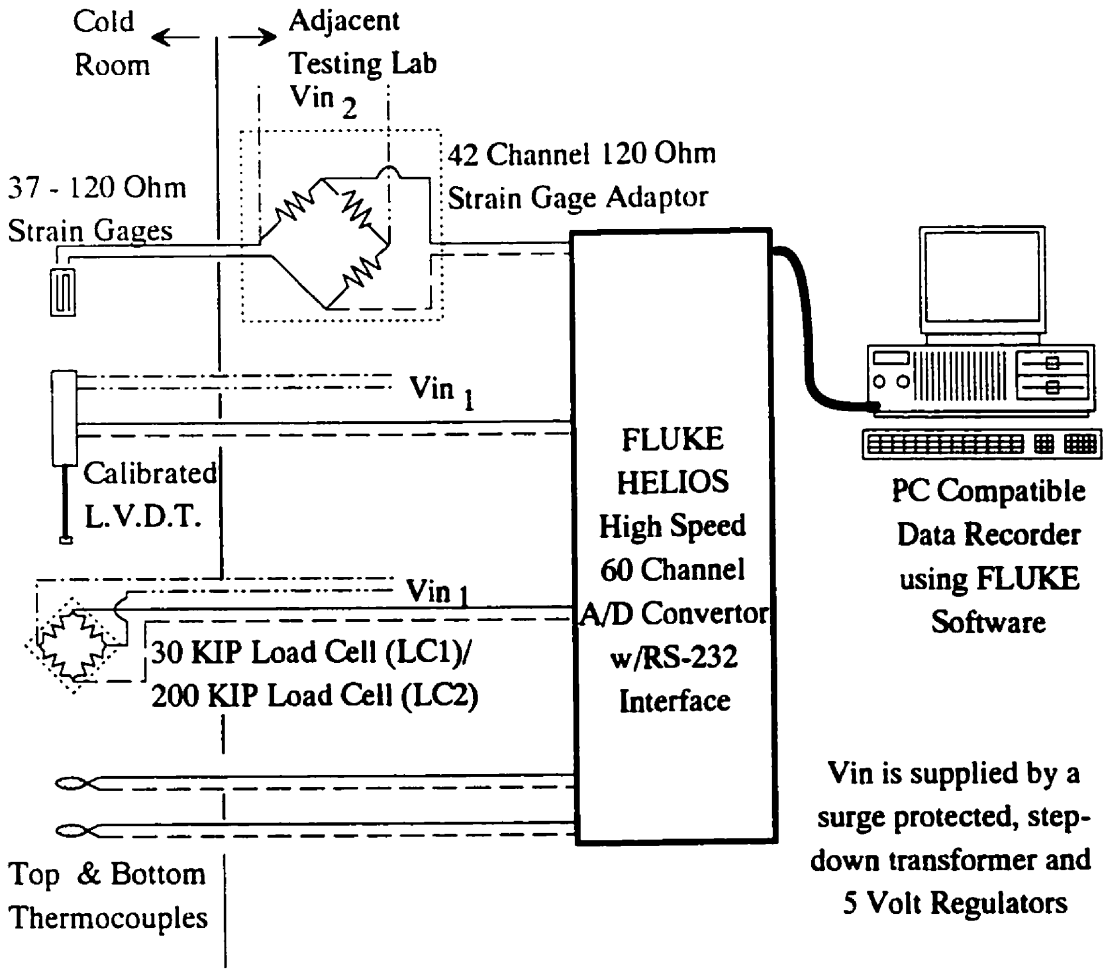

Figure 3-5: Instrumentation Schematic

3.1.5 Pile Installation

The test pit sand was saturated from the bottom up by adding water through the aforementioned tube and drain system. This procedure forced air upwards out of the sand as the ground water level rose. Flooding took place slowly over a period of two days to facilitate saturation.

The pile segment was installed in a pre-formed hole 450 mm. in diameter and 650 mm. deep. The pile segment was installed on top of two layers of 38 mm.-thick low-density polystyrene foam to prevent any significant end-bearing from developing. The installation is shown in **Figure 3-6**.

The pile segment was centred in the preformed hole discussed in Section 3.2.1, and the hole was backfilled with dry sieved sand to remove detritis and large stone. The thin layers (25 - 50 mm) were then saturated with prechilled (<+5°C) water. Manual compaction was used to ensure that the sand was placed in full contact with the underside of the flighting and compacted to a nominal dry density of 1.5 Mg/m^3. Due to the small annulus around the pile segment, mechanical compaction could not be used around the pile. Compaction was performed by hand packing using a 25 millimetre diameter steel bar.

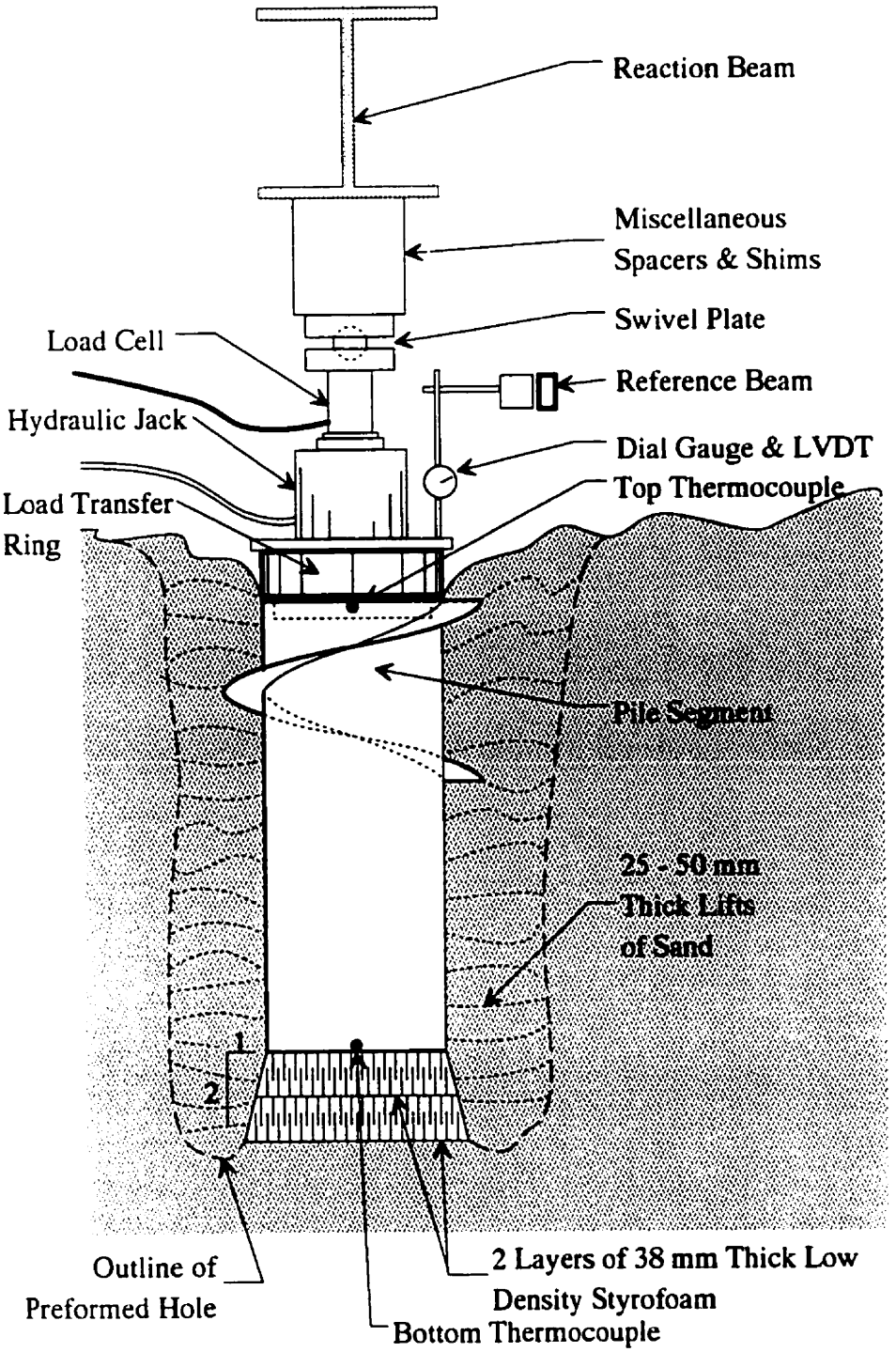

Figure 3-6: Pile Segment Installation and Testing Setup

A 168.9 mm diameter load-transfer ring was placed on top of the pile and the backfilling continued until the saturated sand was 25 mm. above the pile segment. This avoided ablation of pore ice near the top of the flighting and ensured saturation of all sand encompassing the pile segment. Vertical alignment of the pile was checked repeatedly during backfilling.

Care was taken during backfilling to ensure that the strain gage wires were not separated from the pile segment shaft. The lead wires from the lower thermocouple, and the lower 16 strain gages were run through the interior of the shaft. This was done to reduce the volume of wires running up the exterior of the shaft, which might have affected the adfreeze bond. In all cases, the lead wires were bonded with epoxy at intervals of 75 mm. Lead wires and the thermocouple wires were passed through a notch in the shoulder of the load transfer ring to the exterior of the shaft.

Following installation of the pile segment and its instrumentation, the temperature in the cold room was maintained at -30°C to allow thorough freezing of the soil around the pile segment. It was then raised to -10°C for 21 days to permit relaxation of any freezeback pressure. At the end of the freezing period, the temperatures in the Cold Room were raised to bring the pile surface temperatures to -5°C as closely as practical for testing.

3.1.6 Load-Test Apparatus

Applied loads were measured with strain gage load cells. The load cells were calibrated prior

to use, and the calibration was checked again after the load tests.

Pile head displacements were measured with a linearly varying differential transformer (LVDT) with a 25 mm operating range. The LVDT was calibrated prior to use. A dial micrometer was also used to manually record the displacements, and to provide a visual indication of displacement rate, and total head displacement. Both the LVDT and the dial micrometer were mounted to a 50 mm. by 25 mm. rigid tubular steel beam which spanned the test pit. This beam acted as a reference beam and was used to isolate the measuring equipment from the vibration and deflection of the reaction cross-beam. Both reaction and reference beams are shown in **Figures 3-1 and 3-6**.

Hydraulic rams which were used to apply the load to the pile segment were commercially built ENERPAC RCS-502 222.5 kN. hydraulic rams. Hydraulic power was provided by a hydraulic pump driven by compressed air. The pump was regulated by a feedback pressure gauge which allowed the system to maintain constant loads on the pile. Load magnitudes were selected and marked on the controlling air pressure gauge.

Vertical loading of the pile segment was assured by using a swivel plate between the hydraulic ram and the reaction beam. The load was distributed to the pile walls by a load transfer ring consisting of a 10 mm. thick steel plate on top of a short segment of 168.9 mm. O.D., 11.0 mm. thick (Schedule 80) pipe. The top of the pipe was machined flat to support the 10 mm. plate, while the bottom of the pipe had a shoulder machined into it to match the inside

diameter of the pile segment. This arrangement provided a uniform transfer of the applied load from the hydraulic ram to the pile segment walls. The arrangement of all the instruments and components of the test apparatus is shown in **Figure 3-6**.

The soil temperature at which the test was to be conducted was selected as -5.0° C plus or minus 0.5°C. A soil temperature of -5°C was selected as a compromise between several factors.

At very low temperatures (<-10°C), the soil is in a condition similar to the state it would be in if the thermal pile were operating properly. At very warm temperatures (>-3°C), the soil is in a condition much like its natural state near the melting point and assumes the thermal pile is not functioning.

Also, the compressibility of the pile varies with soil temperature. At very low temperatures, the frozen soil is very rigid, making the pile relatively compressible (K approaches 1), while near-melting temperatures result in more compressible soil, resulting in a less compressible pile (K >> 10). For the experiment to reflect some of the behaviour from both extremes, an intermediate temperature (-5°C) was selected.

3.2 Procedure

3.2.1 Procedures for Freezing the Sand

Air temperatures within the cold room were reduced to -30°C to accelerate soil freezing, and to minimize segregation during freezing. The Type T (Constantan and copper) thermocouples in the test pit were monitored daily to record the progress of the freezing front through the in-ground test pit, the temperature gradient within the frozen soil, and the impact of air temperature changes on the soil mass.

It was anticipated that a long period of extremely cold air temperatures would be required to freeze the entire test pit. Consequently, an open pre-formed hole was formed in the saturated sand to allow preparation of the pile segment and instrumentation in conjunction with freezing of the sand in the test pit. The pre-formed hole was formed by burying a five gallon capacity plastic pail into the saturated sand. Once the sand had frozen to a depth below the pail, the pail was cut into segments from the interior and removed, leaving a smooth cylindrical hole in the saturated sand. The hole was then covered to prevent ablation of the pore ice at the void surface. The installation is illustrated in **Figure 3-6**.

At the end of the 21 day period of extremely low air temperatures, the air temperatures were raised to allow the sand to reach -10°C to provide a relaxation period for any freezeback pressures which had developed in the sand. At the end of this period, the air temperature in the Cold Room was raised to -2°C. This allowed the soil temperature to increase from below

and above to achieve a uniform temperature distribution along the pile shaft length. Soil temperatures increased more rapidly from below due to higher heat conductivity through the test pit walls from the adjacent soil than the insulated test room enclosure. When the near-ground surface temperature rose to -6°C, the air temperature was adjusted to -6°C and was held at this temperature for the duration of the test.

3.2.2 Loading Procedure

Once uniform soil temperatures were achieved, the loading system was put into place. The test was conducted in accordance with ASTM D1143 - 81 (Re-approved 1987). This Standard is titled *Standard Test Methods for Piles Under Static Axial Compressive Load*. It details the procedures to be used in conducting full-size pile loading tests. Section 5.6 titled *Quick Load Test Method for Individual Piles* was considered appropriate for this investigation.

Prior to the first load increment being applied, the data acquisition system was set to record data from the pile segment for five minutes without an applied load. This allowed an initial average zero to be recorded, and the power supplies to be stabilized.

Loading was conducted in increments of approximately 4 kN every five minutes. At the end of each load increment, the pressure in the hydraulic system and the head displacement were recorded manually. The LVDT, load cell, thermocouples, and strain gages were recorded

every 30 seconds by the data acquisition system. It became apparent that the capacity of the loading apparatus would be reached before the pile failed. Loading was continued until the capacity of the load cell, (133.5 kN) was reached. At this point, the pile segment was unloaded and allowed to rebound. Rebound data was recorded.

The loading system was modified by adding a second hydraulic ram and replacing the load cell with a higher capacity, (445.0 kN), load cell, (LC2). The testing was resumed after an elapsed time of seven days ensuring that the soil temperatures were approximately the same as when the testing was interrupted. First, the pile was loaded rapidly to a load equal to that load at which the initial loading sequence was stopped. The loading procedure previously described was then resumed. Once the maximum sustainable load was reached, the hydraulic system was stopped, and the data acquisition system was allowed to record data for an additional five minutes. Pile failure was taken to be the onset of accelerating creep (Neukirchner, 1991).

3.2.3 Unloading Procedure

The pile was unloaded in accordance with ASTM D 1143 - 81. The hydraulic pressure was reduced to zero through five equal decrements. Each of these decrements was maintained for five minutes, with the pressure being controlled manually by a release valve on the hydraulic system. At the end of the unloading procedure, data were recorded for ten (10) minutes to monitor the behaviour of the pile segment under the weight of the loading apparatus alone.

3.3 Results

3.3.1 Pile Load Application No. 1

A large amount of data were recorded during this experiment. The data will not be presented in all possible forms because of the volume. The most significant data sets are presented below.

The maximum, minimum, and average temperatures recorded during Load Application No. 1 are shown in **Figure 3-7**. The mean temperature at the top of the pile was -4.2 °C, and the mean temperature at the bottom of the pile was -4.9 °C.

Several strain gages (9 of 37 installed) did not respond properly during the course of the experiment. There are potentially several causes of this :

i.) Loss of strain gage bonding due to improper pile segment surface preparation

ii.) Infiltration of water causing a short of the strain gage circuit

iii.) Defective gages or insulation on conductors

iv.) Lead wires breaking during displacement of pile segment

v.) Induced electrical noise in strain gage circuits due to poor shielding.

vi.) Faulty bridge circuits and/or data acquisition channels

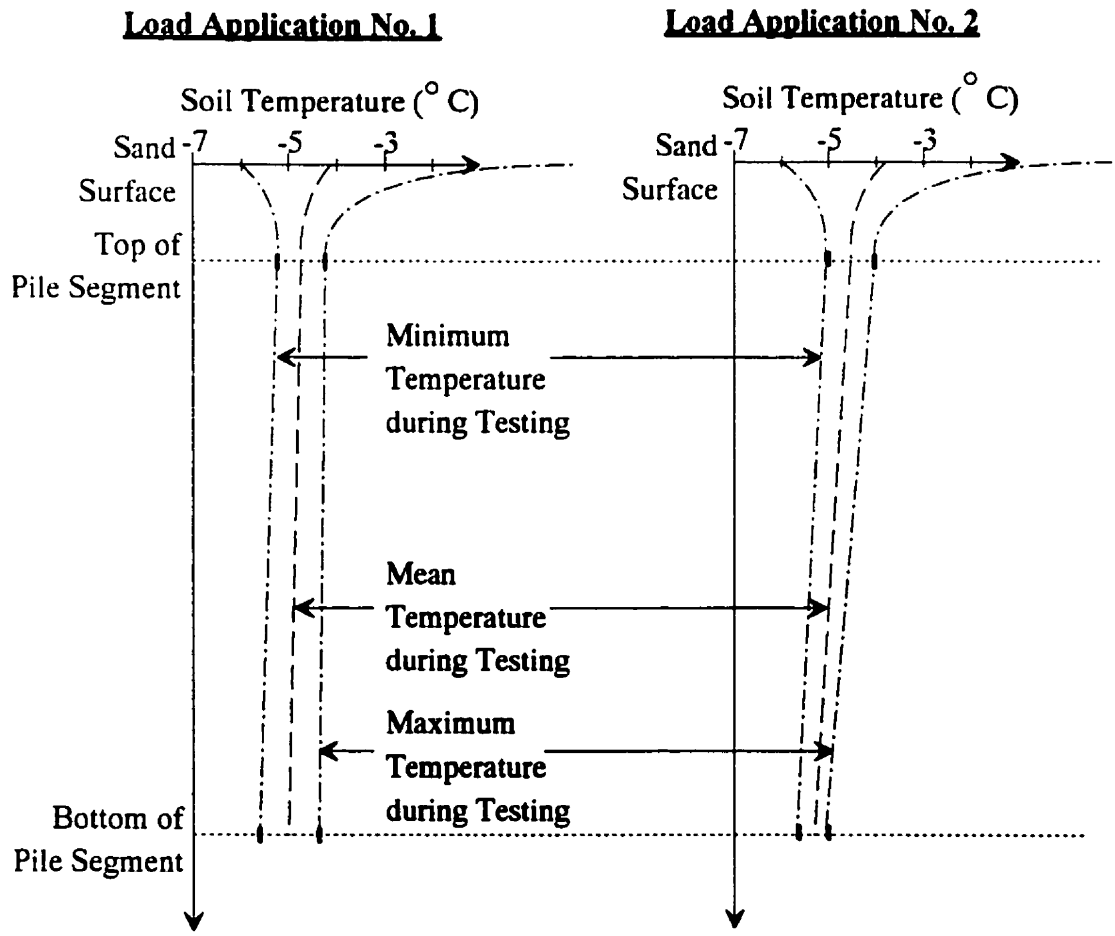

Figure 3-7: Temperature Ranges during Load Application No. 1 and No. 2

Measures were taken prior to the experiment to prevent, as much as possible, these faults from developing. The failure or problems with the data will be addressed individually during the Analysis of Results in Chapter 4.0. The thermocouples, load cell (LC1), and the LVDT functioned properly during the test. Physically, the pile segment displayed no unusual behaviour. The sand surface remained undisturbed during the test. The pile segment appeared to displace vertically without any lateral or angular displacement.

The principal results of Load Application No. 1 are summarized in **Figures 3-8** (Applied Load

versus Time), **3-9** (Head Displacement versus Time), **3-10** (Head Displacement versus Applied Load), and **3-11** (Temperatures versus Time). Results of strain gage measurements are in the Appendices.

Figure 3-8 illustrates the step-wise load application rate of approximately 40 kN per hour. At the end of the load application, the applied load was reduced in six approximately equal increments resulting in an equivalent unloading rate of 550 kN per hour.

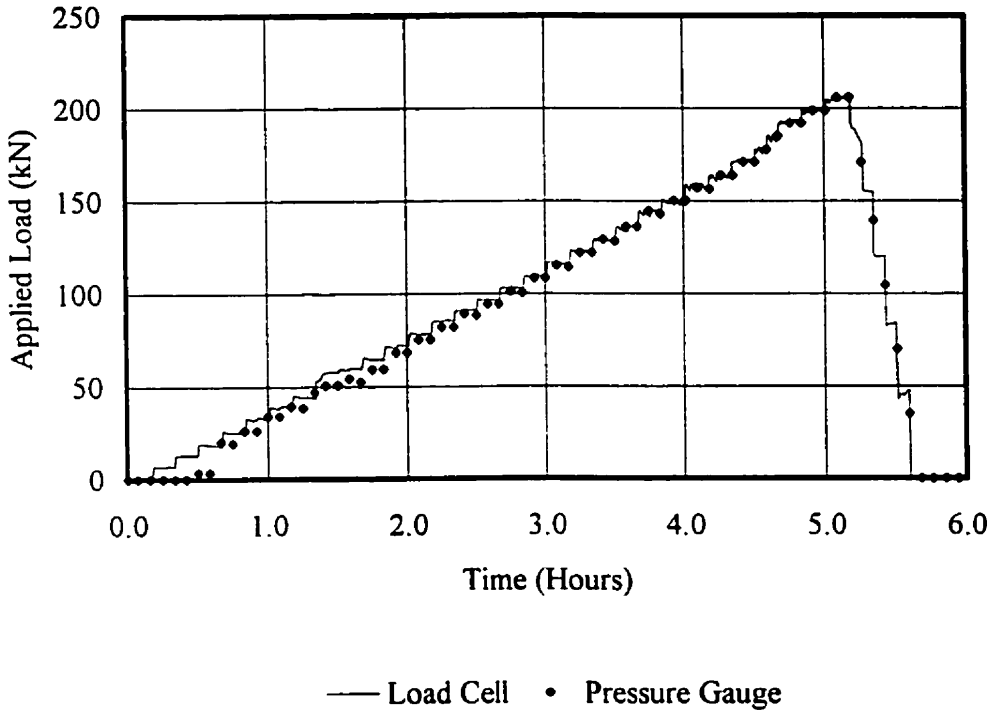

Figure 3-8: Applied Load versus Time - Load Application No. 1

Figure 3-9 illustrates a fairly uniform rate of displacement of 0.825 millimetres per hour until a significant step-like increase in displacement at 3.75 hours, followed by another period of displacement at a rate of 3.67 millimetres per hour until unloading began.

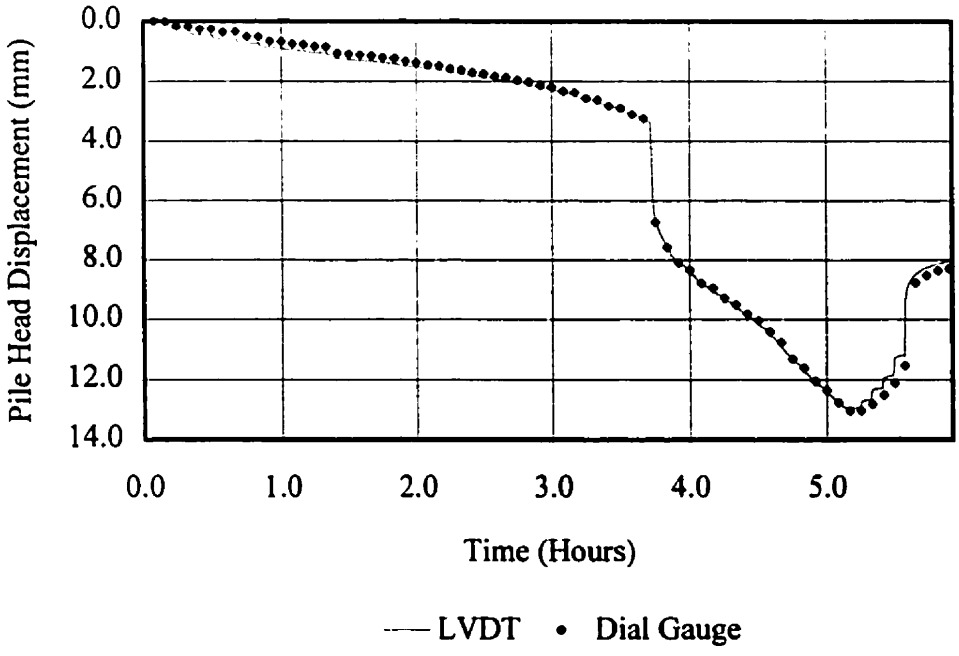

Figure 3-9: Head Displacement versus Time - Load Application No. 1

Displacement versus applied load is illustrated in **Figure 3-10** in which the pile undergoes a fairly uniform rate of displacement of 0.0229 millimetres of displacement per kN of applied load. At approximately 140 kN, a rapid displacement of approximately 3.0 millimetres occurred, followed by fairly uniform displacement at a rate of 0.080 millimetres per kN of applied load. Rebound of the unloaded pile segment appears to have included 1.5 millimetres of elastic recovery after all load was removed from the pile segment.

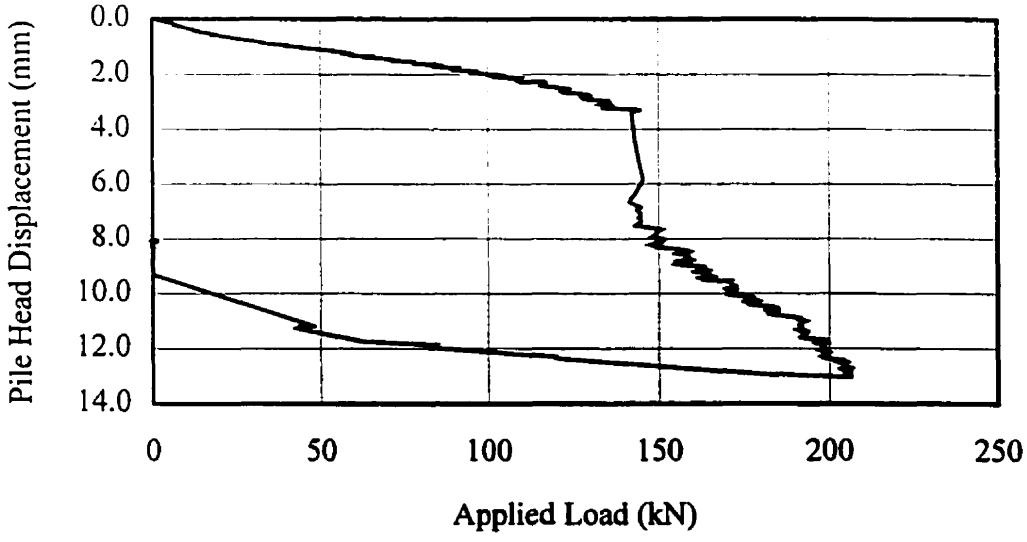

Figure 3-10: Head Displacement versus Applied Load - Load Application No.1

Soil and air temperatures are recorded in **Figure 3-11**, where room air temperature cycled frequently with the operation of cold room air conditioning. The Figure also illustrates the steady warming of the soil below the pile segment during the experiment, and also the response of soil temperatures at the top of the pile segment to cold room air temperatures.

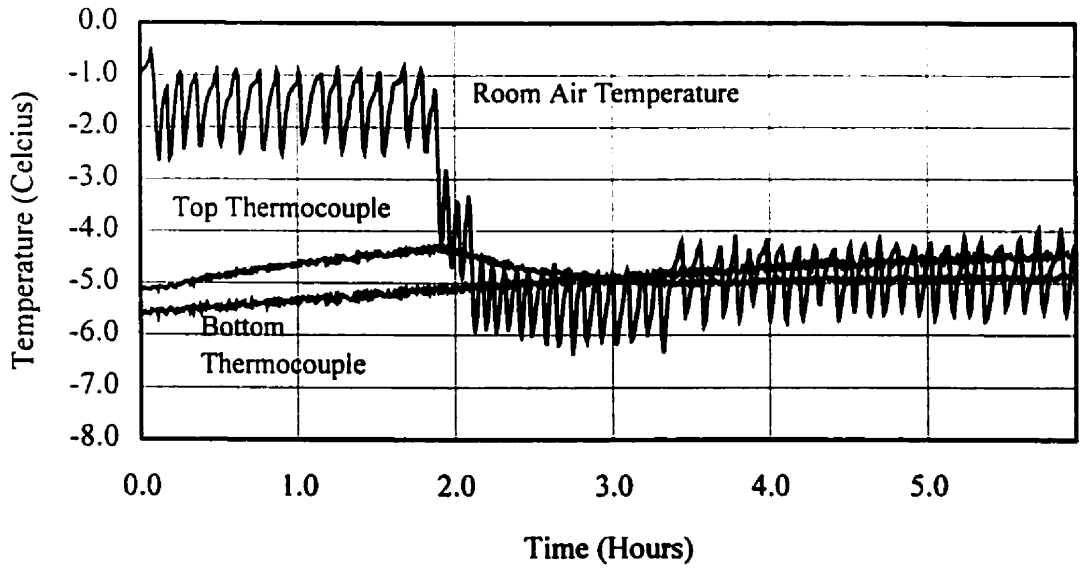

Figure 3-11: Temperatures versus Time - Load Application No. 1

3.3.2 Pile Load Application No. 2

The temperature ranges recorded during Load Application No. 2 are shown in **Figure 3-7**. The mean temperature at the top of the pile was -5.35 °C, while the mean temperature at the bottom of the pile was -4.26 °C.

Instrumentation problems which occurred during Load Application No. 2 are similar to those encountered in Load Application No. 1 (18 of 37 strain gages were unreliable). The thermocouples, load cell (LC2), and the L.V.D.T. functioned properly during the test.

As before, the pile segment displayed no unique or unusual behaviour. The sand surface remained undisturbed during the test. The pile appeared to displace vertically without any lateral or angular displacement.

The principle results of Load Application No. 2 are summarized in **Figures 3-12** (Applied Load versus Time), **3-13** (Head Displacement versus Time), **3-14** (Head Displacement versus Applied Load), and **3-15** (Temperatures versus Time). Results of strain gage measurements are in the Appendices.

Figure 3-12 illustrates the step-wise load application rate of approximately 50 kN per hour starting from the same applied load (200 kN) as Load Application No. 1 ended at. At the end of the load application, the applied load was reduced in five approximately equal increments resulting in an equivalent unloading rate of 750 kN per hour.

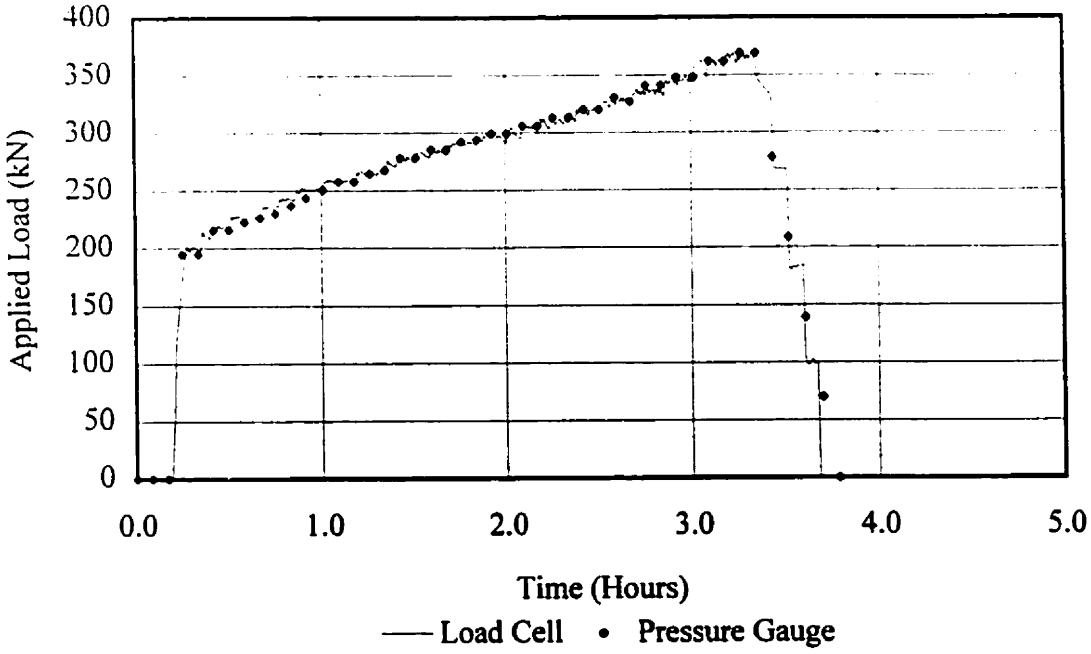

Figure 3-12: Applied Load versus Time - Load Application No. 2

Figure 3-13 illustrates an increasing rate of displacement initially starting at 3.5 millimetres per hour increasing to a rate of 11.0 millimetres per hour until unloading began. Approximately 5.0 millimetres of rebound occurred during unloading.

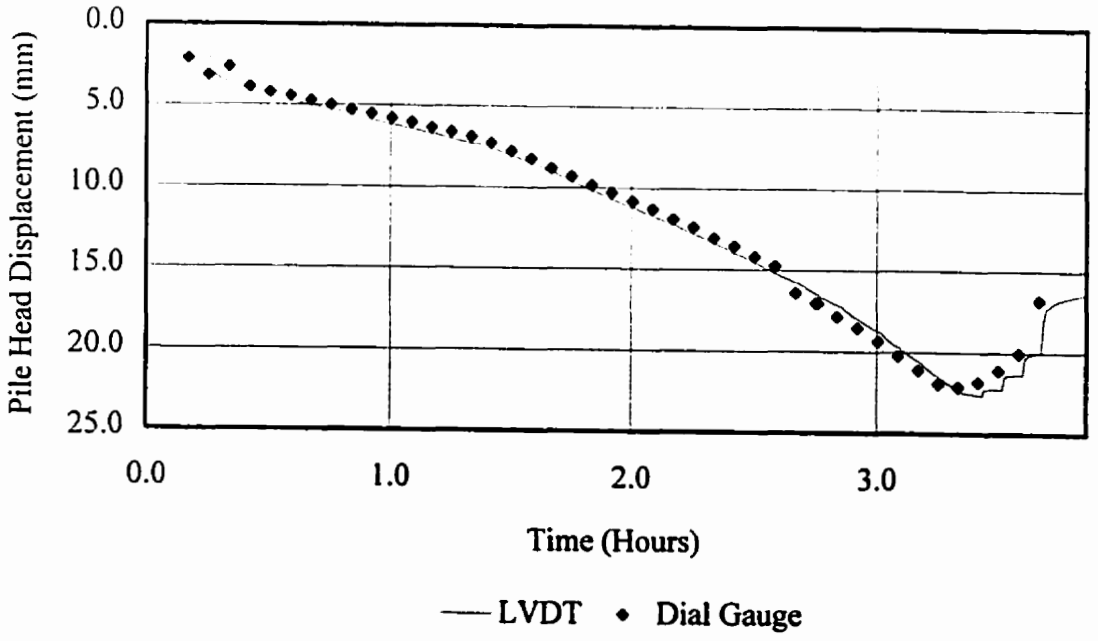

Figure 3-13: Head Displacement versus Time - Load Application No. 2

Displacement versus applied load is illustrated in **Figure 3-14** in which the pile undergoes approximately 3.0 millimetres of displacement during the initial loading. This was followed by a second phase of uniform rate of displacement of 0.0630 millimetres of displacement per kiloNewton of applied load. At approximately 275 kN, a third phase of fairly uniform displacement occurred at a rate of 0.123 millimetres per kN of applied load. Rebound of the unloaded pile segment appears to have included 5.0 millimetres of elastic recovery as all load was removed from the pile segment.

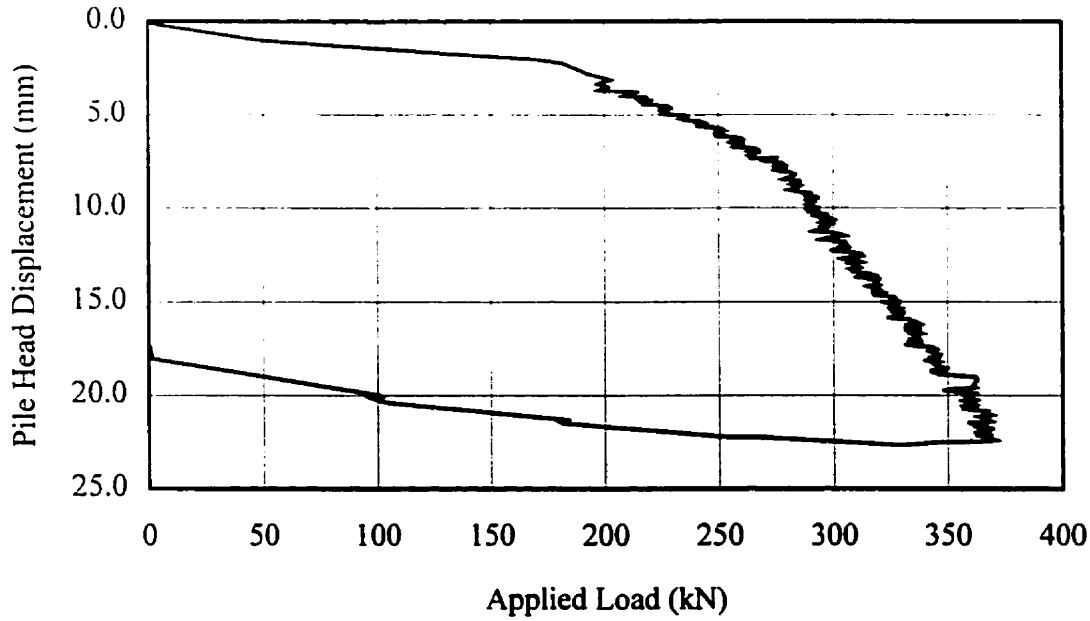

Figure 3-14: Head Displacement versus Applied Load - Load Application No. 2

Soil and air temperatures are recorded in **Figure 3-15**, where room air temperature cycled frequently with the operation of the cold room refrigeration system. The Figure also illustrates the steady warming of the soil below the pile segment during the experiment, and also the response of soil temperatures at the top of the pile segment to cold room air temperatures similar to those illustrated in **Figure 3-11**.

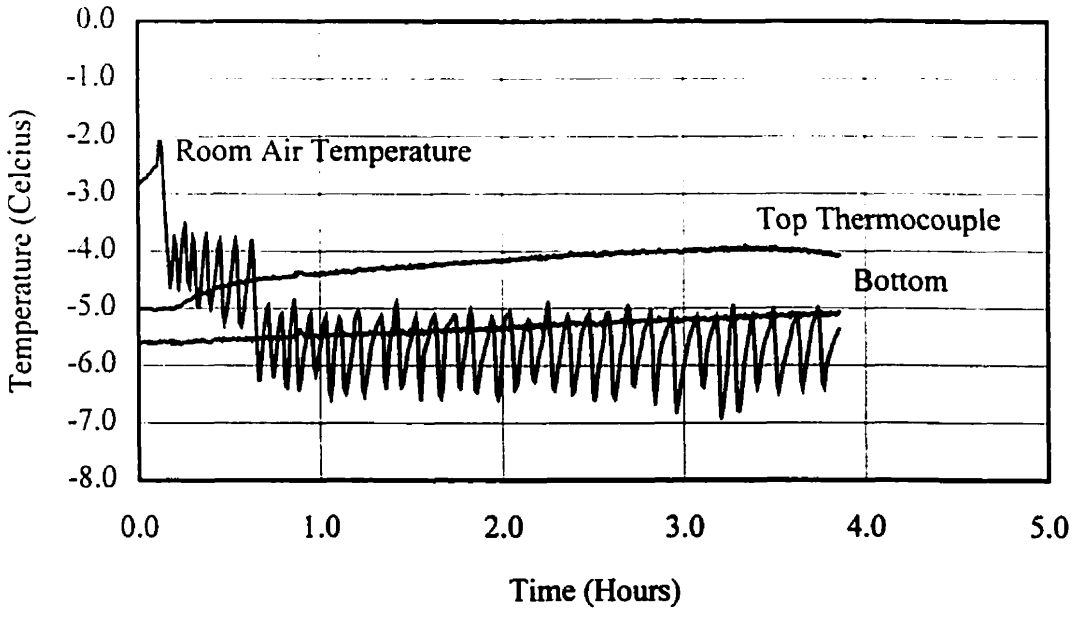

Figure 3-15: Temperatures versus Time - Load Application No. 2

3.3.3 Frozen Soil Properties

At completion of the pile segment testing, samples of the in-situ frozen sand were removed to allow determination of soil properties by using a 75 mm. O.D. hollow stem auger of a design proposed by the University of Alberta (by Biggar and Sego). The core was nominally 38 millimetres in diameter. The borehole was drilled 200 millimetres away from the side of the pile shaft without difficulty. One meter of core was recovered.

Five segments of the recovered core were used to calculate the bulk density, dry density,

moisture content, degree of saturation, and void ratio of the frozen sand. The results are plotted in **Figure 3-16**. Dry densities ranged between 1600 and 1450 kg/m^3 . Degree of saturation ranged from 77% to 65%. Over the height of the pile segment, the soil properties were fairly uniform. Near the test pit surface, some ablation likely occurred during test setup reducing the sample moisture content and the degree of saturation. The soil layer below the pile segment was more densely packed, likely due to the history of tests performed in the test pit prior to this test program.

3.3.4 Examination of Pile Segment

The pile was checked for deviation from the vertical, and the appearance of the surrounding soil surface was noted at the end of the load tests. There was no visible evidence of surface changes or soil being displaced laterally.

A plug of ice had formed in the bottom of the pile segment and above the void form. It formed during the refreezing of the pile segment after a five day, unplanned shut-down of the cold room refrigeration system. The plug of ice was approximately 100 mm. thick and consisted of clear ice. It likely formed by the percolation of melt water from the test pit surface down through the pile interior through gaps between the load transfer ring and the pile segment.

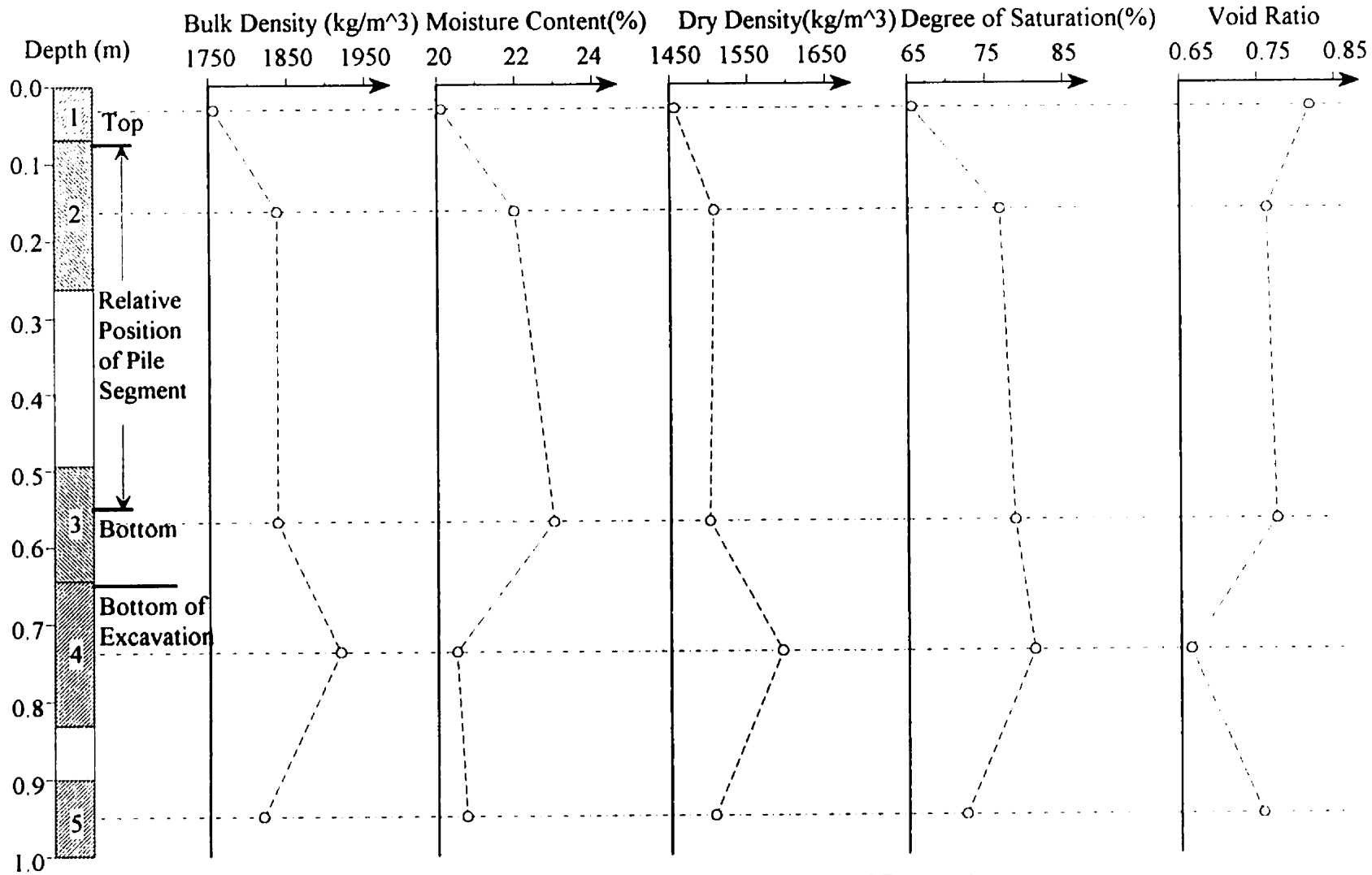

Figure 3-16: In-situ Frozen Sand Physical Properties

Once sampling of the in-situ frozen sand was completed, the frozen soil within the pit was allowed to thaw. As the thaw front progressed, a 0.5 metre square by 0.75 metre deep pit was dug adjacent to the pile segment, without exposing the pile segment. Dewatering was necessary as the pit was dug. Once the 0.75 metre depth had been reached, the sand was slowly and carefully excavated away from the side of the pile segment, exposing half of its diameter at the pile/soil interface. There were no visible indications of slip planes or cracks observed during this examination.

The thawed sand above the pile segment flight was loose and easily compressed, however the sand below the flight was much denser and resisted indentation. A void projecting into the sand approximately one millimetre wide and four millimetre high occurred along the tip of the flights. This was observed prior to removing the pile segment.

The pile segment was then carefully removed from the thawed soil by pulling it sideways into the excavated pit, leaving behind a cast of its shape in the undisturbed sand.

Once the pile segment was removed, the sand cast along the pile segment shaft provided evidence that some of the sand may have displaced downward with the pile segment. Small zones of sand (< 10 mm. high x 30 mm wide) had lower margins of densified sand, while the upper margins had small voids (< 2 mm). This pattern occurred sporadically over a large area. The pattern suggested that some sand displaced with the pile segment, densifying sand below

the bonded area, and developing a void above the bonded sand. There was no evidence of shear or slip planes below the flights and careful excavation into the pile segment cast revealed no obvious indication of internal planes of movement.

The void form below the pile segment was intact, although compressed 15 to 17 millimetres where the foam contacted the wall of the pile segment. The void form was permanently compressed an average of seven millimetres overall, likely due the compressive force resulting from the formation of a plug of ice within the pile segment during failure of the refrigeration system. The pile segment shaft wall was imbedded into the void form approximately a further ten millimetres for a total of 15 to 17 millimetres. Due to the low compressive strength of the low-density polystyrene foam, it is expected that the plug of ice within the pile segment did not contribute significantly to pile segment end-bearing.

Examination of the pile segment noted that the walls of the pile segment showed no signs of yielding or buckling. However, there was permanent deformation of the flighting. The flights which were originally perpendicular to the pile segment shaft were deformed upwards. The deformation of the flights appeared to be concentrated in the region just beyond the upper and lower fillet weld, and immediately adjacent to the pile shaft wall. Table 2 lists the deformation of the flights measured at 30° increments around the shaft beginning at the top of the pile segment, while **Figure 3-17** illustrates the measurement locations.

Table 2 : Deformations of Flights

Position from Top Edge	Deformation at Flighting Tip, δ_d (mm)	Width of Flighting, w (mm)	Calculated Angle of Deformation, θ_d (Degrees)
Top (0°)	5.89	40.0	8.38°
30°	7.30	40.0	10.34°
60°	4.61	39.5	6.66°
90°	5.10	39.5	7.36°
120°	5.22	39.0	7.62°
150°	4.41	40	6.29°
180°	4.97	39.5	7.17°
210°	3.61	39.0	5.29°
240°	3.71	40.0	5.30°
270°	4.01	39.5	5.80°
300°	2.91	40	4.16°
330°	5.51	40.5	7.75°
Bottom 360°(=0°)	7.31	41.5	9.99°

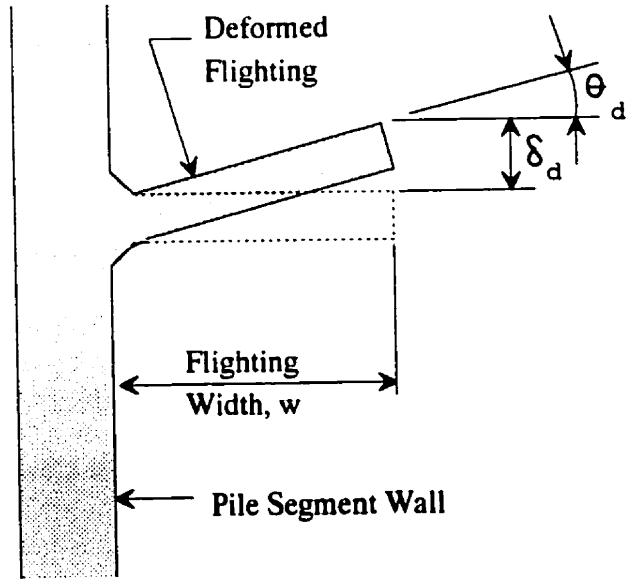

Figure 3-17: Notation for the Deformation of Flighting

The largest flighting tip deformation was 7.31 millimetres, the smallest was 2.91 millimetres, and the average flighting tip deformation was 5.0 millimetres upwards. The flighting at the top and bottom of the pile segment was permanently deflected the most.

4. Analysis of Results

4.1 Introduction

Using the data derived from the experiment, the flighting strain gage results were converted to equivalent internal bending moments. This allowed determination of the net equivalent pressures acting on the flighting, as a function of best fit equations of the internal bending moment calculations. The flighting and shaft strain gage data were used to separate the relative proportions of load transfer through adfreeze and through flighting bearing. This permitted analyses of the flighting segment behaviour in relation to the applied load and pile head displacement.

4.2 Moment Distribution on Flighting

The bending moments within the flighting can provide information about the behaviour of the flighting segment during displacement. The bending moments were calculated from the recorded strains using the principles of mechanics of solids. If a small vertical slice of the pile flighting is to be considered an axisymetric element, the bending moment within the flighting at a selected strain gage location can be calculated by :

$$M_{BENDING} \approx \frac{\epsilon_{z\text{-}z}\, E_{STEEL}\, I_{z\text{-}z}}{0.5\, t'} \qquad \text{...Eq. (1)}$$

Where:	E_{STEEL} =	Young's Modulus = 200 GPa (Assumed)
	I_{Z-Z} =	Moment of Inertia at strain gage (mm^4)
	t' =	effective thickness of flighting (mm)
	ϵ_{Z-Z} =	Recorded strains (mm/mm)

The moment of inertia, I_{Z-Z} and the effective thickness are derived from the geometry of the element, which is illustrated in **Figure 4-1**. Element properties are tabulated in Table 3. Data from Strain Gages **FB1, FB2, and FB3 (Position of gages are identified in Figure 3-4)** were used for all flighting analysis since the data contained fewer instrument-associated problems and provided a cleaner data set for analysis.

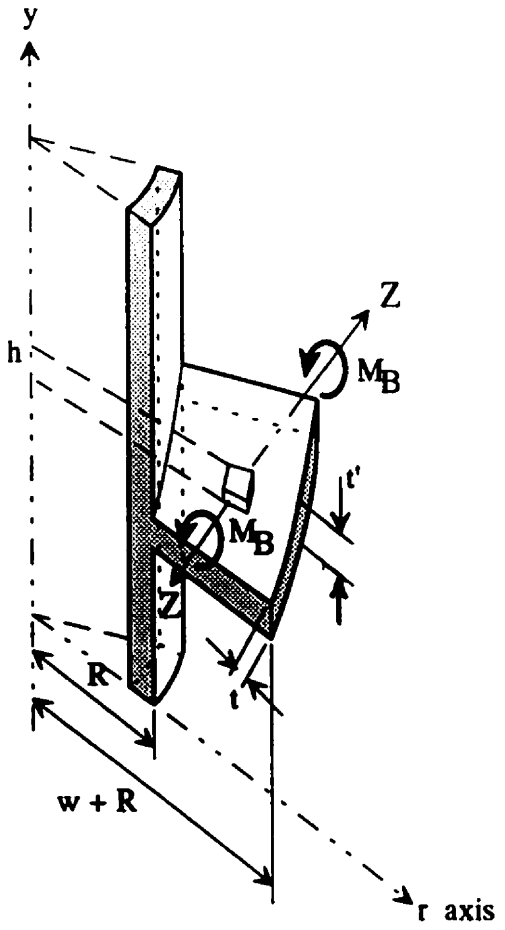

Figure 4-1: Axisymetric Flighting Element Nomenclature

The following equations are based on the geometry of an axisymetric element with a width of unity at the flighting tip:

$$I_{z\text{-}z} = \frac{bh^3}{12} - 2Ad^2 \qquad \text{...Eq. (2)}$$

Where: $I_{z\text{-}z}$ = Moment of Inertia about the Neutral Axis (mm^4/mm)

b = Element width at strain gage (mm/mm)

h = Height of element at strain gage (mm)

A = Area of excluded cross-section (mm^2/mm)

d = Distance from Z-Z Axis to excluded area centroid (mm)

And :

$$b = \frac{r}{w + R} \qquad \text{...Eq. (3)}$$

Where: r = Radius from centre of shaft to strain gage (mm)

w = Width of flighting at element (mm)

R = Radius of pile segment shaft (mm)

And :

$$h = y + t' \qquad \text{...Eq. (4)}$$

Where: y = Rise in Flighting at element (mm)

t' = Effective vertical thickness of flighting at element (mm)

And :

$$y = \frac{P\,b}{2\,\pi\,(r)} \qquad \text{... Eq. (5)}$$

Where: P = Pitch of flighting per revolution (mm)

And :

$$\phi_i = \frac{y}{b} = \frac{P}{2\pi r} \qquad \text{... Eq. (6)}$$

Where: ϕ_i = Slope of element (mm/mm)

And :

$$t' = \frac{t}{\cos(\arctan(\phi_i))} \qquad \text{...Eq. (7)}$$

Where: t = true thickness of flighting (mm)

And:

$$A = \frac{b\,y}{2} \qquad \text{...Eq. (8)}$$

Where: A = Area of excluded cross-section (mm^2/mm)

And:

$$d = \frac{h}{2} - \frac{y}{3} \qquad \text{...Eq. (9)}$$

The internal bending moment at yielding is calculated from the yield strain of 0.0015 mm/mm. The plastic internal bending moment is determined from the mobilization of yield stress (Assumed f_y = 300 MPa) across the entire element cross-section.

Table 3 : Flighting Properties at Strain Gages

Strain Gage	String "B"			
	Root	**FB1**	**FB2**	**FB3**
Position, r (mm)	87.45	101.45	111.45	121.45
Width, b (mm/mm)	0.7084	0.8218	0.9028	0.9838
Thickness, t' (mm)	4.9608	4.8562	4.8035	4.7628
Height, h (mm)	5.2728	5.1682	5.1155	5.0748
Moment of Inertia, I_{z-z} (mm^4/mm)	7.2367	7.8765	8.3749	8.8974
Yield Moment,M_y (Nmm/mm)	823.5	914.4	982.3	1051.9
Plastic Moment, M_p (Nmm/mm)	872.8	970.3	1043.0	1117.5

By solving the above equations for each of the strain gage locations, and using the recorded strains, the bending moment at three points on the flighting were calculated. The internal bending moment at the tip of the flighting was assumed to be zero by physical constraints. This fourth point and the three data points were then used to construct a "best fit" third-order or second-order polynomial equation describing the bending moment distribution across the flighting at discrete times or at applied axial loads.

4.3 Pressure Distribution on Flighting

In **Section 4.2**, "best fit" polynomial equations ($2^{nd.}$ and $3^{rd.}$ order) of the bending moment distributions were determined. From these equations, the pressure distribution was found by finding the second derivative of the bending moment equation in relation to the radial position, "r". The method is illustrated in **Figure 4-2**. The magnitudes of the pressure were based on the limited amount of data of the bending moment distributions, and are therefore only illustrative. It should be noted that the calculated pressures represent only net pressures applied to the flighting, and do not represent those pressures actually being applied to the top and bottom of the flighting simultaneously.

In both load applications, the initial strain condition was assumed to be zero as no information on strain was recorded before Load Application No. 1 nor between Load Application No. 1 and No. 2. Consequently, the initial pressure distribution on the flighting has been assumed to be zero as well. In reality, there may have existed pre-test pressures on the flighting caused by downdrag or uplift resulting from frost heave, or temperature changes.

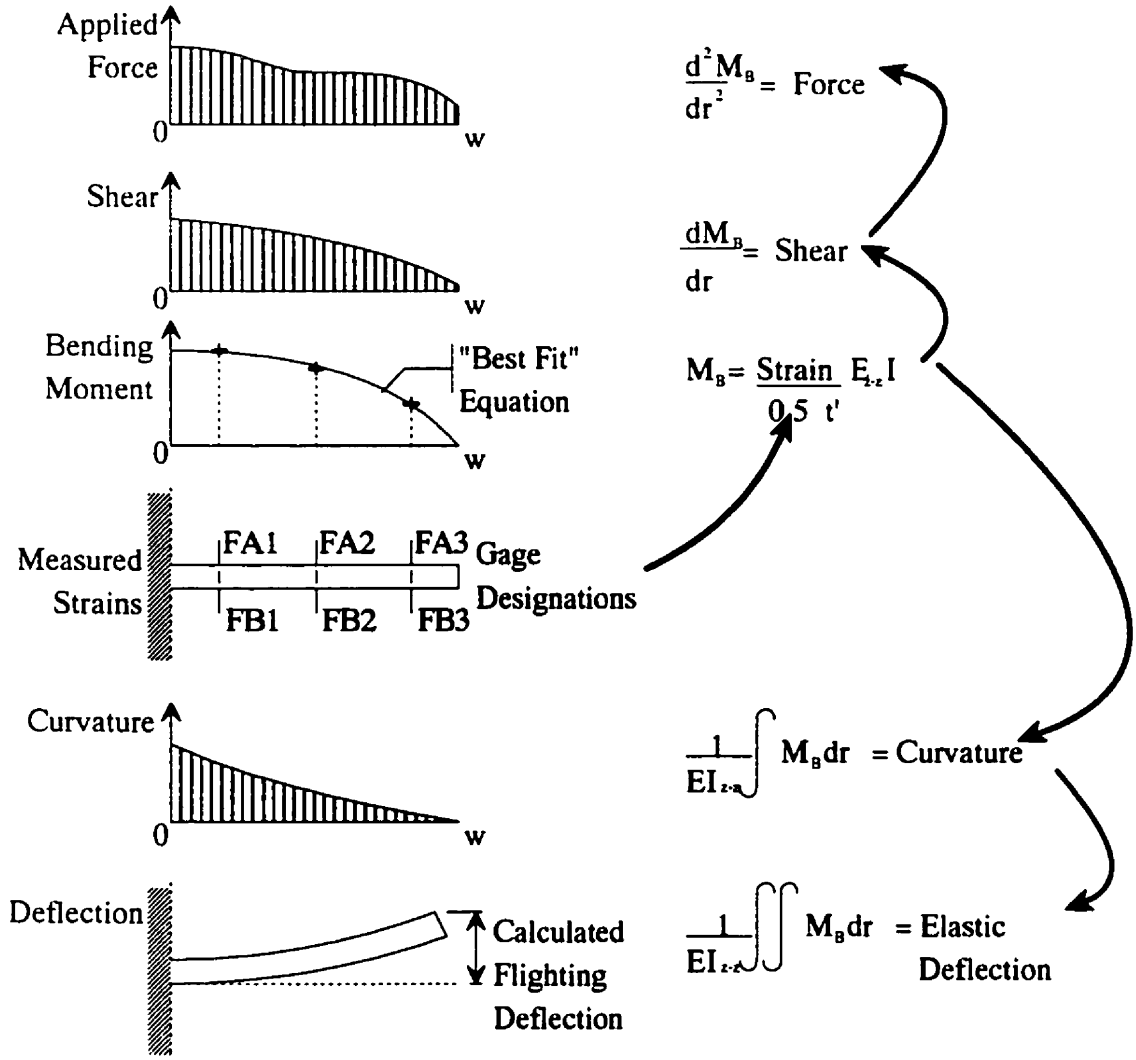

Figure 4-2: Determination of Flighting Behaviour from Strains

Using the methods described previously, the best fit equations for the internal moment at a given applied load were determined. From this internal moment distribution, an equation for net resisting pressure was determined at that given applied load. This was then used to determine the net pressure at each of the strain gage locations, the flighting root and tip. The product of the net pressure distribution and corresponding flighting area at each given applied

axial load was then used to determine the effective load transferred from the flighting to the soil.

Figure 4-3(a) illustrates the relationship between applied load and pile head displacement for Load Application No. 1. Initially, the relationship between applied load and displacement was approximately linear, but at an applied load of approximately 145 kN, a sudden displacement of five millimetres occurred after which an approximately linear relationship between applied load and displacement resumed at a slightly higher rate. There was no indication of a cause for the sudden five millimetres of displacement. A total applied load of 205 kN resulted in a total pile head displacement of thirteen (13) millimetres. The results indicated that neither the pile segment nor the soil failed. During decremental unloading, the pile segment rebounded approximately five (5) millimetres elastically, and there was approximately eight (8) millimetres of total permanent recovery. The recovery rate was fairly uniform without any sudden changes.

Figure 4-3(b) is a plot of the strains recorded across the flighting section as the load on the pile was increased. Gage FB1, located near the pile shaft recorded the largest strains, while gage FB3, located near the flighting tip, recorded the smallest strains. Decremental unloading of the pile segment, resulted in only a small amount of recovered strains indicating that the flighting remained in a stressed condition after unloading, especially in the vicinity of the pile segment shaft.

Using the strains determined in **Figure 4-3(b)** and an assumed boundary condition of zero strain at the flighting tip, a best-fit equation was determined for a given applied axial load. The moment equation is a function of radial distance from the pile segment centre for a discrete applied load. As described in Section 4-3, the first derivative of this equation is the internal shear force, while the second derivative is the applied net pressure in relation to radial distance from the pile centerline. Initial net pressures indicated a maximum upward pressure at the flighting root at Gage FB3 and a maximum downward pressure near the flighting tip at Gage FB1. **Figure 4-3(c)** shows an inversion of net pressure at an applied load of approximately 67 kN. After the inversion of net pressure, the net pressure declines towards a upwards pressure of 1.8 kN/mm^2/mm. During the decremental unloading of the pile segment, all net pressures declined relatively linearly to a negligible net value.

In **Figure 4-3(d)**, the initial total load transferred from the pile flighting to the soil shows an apparent maximum downdrag force of 50 kN, which after an applied load of about 60 kN, changed to an upward force. The upward force reached a maximum value of about 75 kN when the applied load was about 110 kN. Thereafter, increases in the applied load resulted in a reduction in the load transferred by the flighting. At the maximum applied load of 210 kN, the flighting carried a load of approximately 35 kN. Upon unloading of the pile, the load carried by the flighting declined to a small (10 kN) residual magnitude.

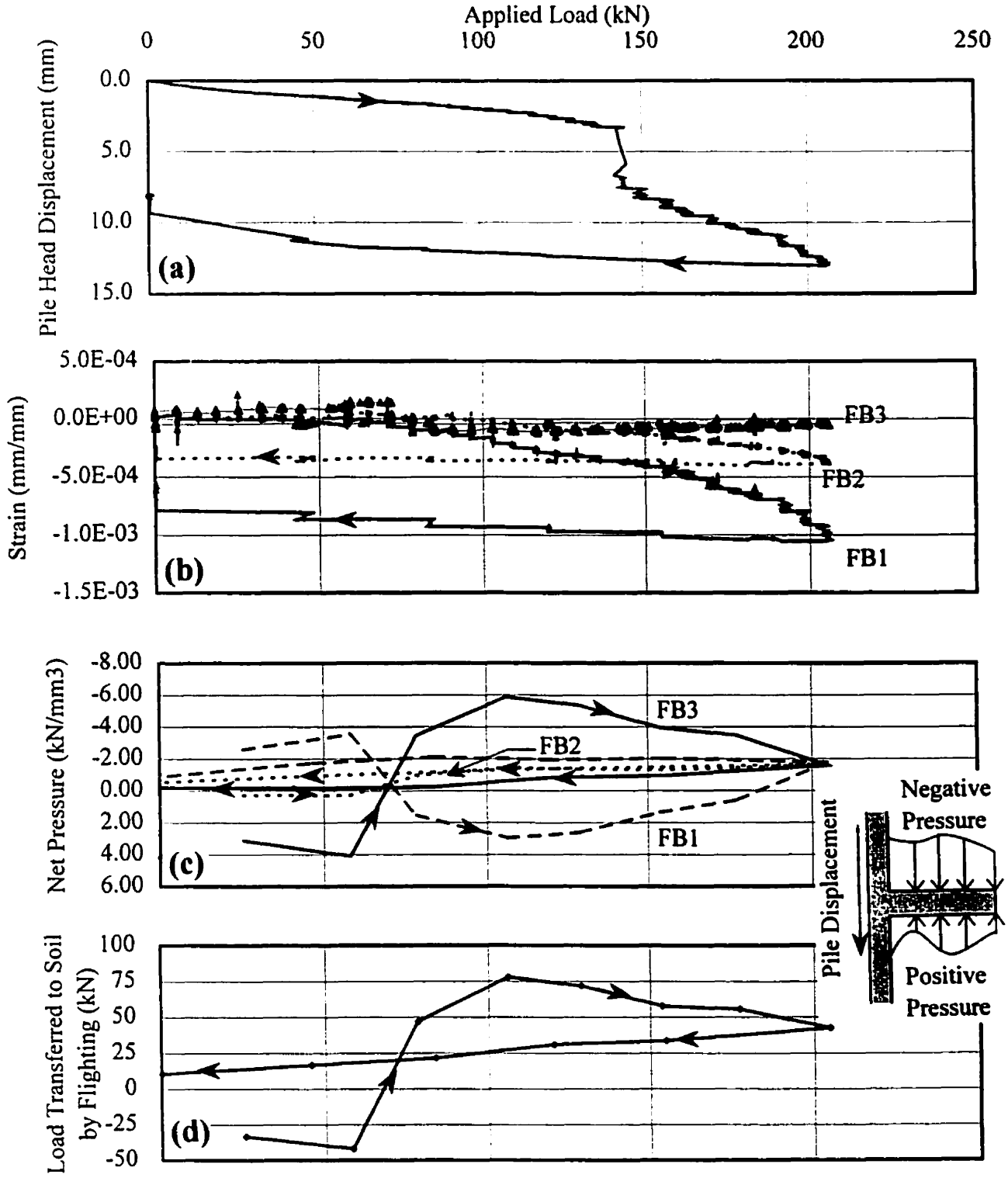

Figure 4-3 (a, b, c, d): Displacement, Strain, Net Pressure and Load Transferred versus Applied Load - Load Application No. 1

Figure 4-4(a) illustrates the pile head displacement versus applied load for Load Application No. 2. The relationship is essentially linear through the entire loading process with a change in rate of displacement at an applied load of 275 kN after which the rate of displacement increased. Pile head displacements during unloading were relatively linear with approximately five (5) millimetres of elastic recovery and a total of six (6) millimetres of total recovery.

The measured strains in the flighting in relation to the applied axial load are plotted in **Figure 4-4(b)**. The recorded strains are relative to the initial strain state of the pile segment. Therefore all subsequent analyses are also relative to the initial state at the beginning of Load Application No. 2. With increasing load, the strain in Strain Gage FB1 increased linearly once the applied load exceeded the previous maximum load application. A small increase in strain was recorded at strain gage FB2 and a negligible amount near the flighting tip at strain gage FB3. At an applied load of approximately 275 kN, the strains near the flighting root appear to be reaching an asymptotic value, while those at FB2 and FB3 show a decline in strain. During decremental unloading of the pile segment, the strains recovered linearly to approximately the initial strain state. Most recovery took place over an extended time period after all load was removed.

From the internal bending moment distribution, an equation for net resisting pressure was derived for several discreet applied loads. The results are plotted in **Figure 4-4(c)**. From the initial applied loads, the net pressure near the root of the flights (Gage FB3) increased steadily

upwards, while the net pressure near the flighting tips increased downwards. The net pressure near the mid-point of the flighting increased linearly slightly upwards. After the maximum applied load, the pile segment was unloaded decrementally. During unloading, the net pressure at Gage FB1 and FB3 fell slightly, and then increased midway through the unloading process. After this local maximum pressure, the net pressures at both Gages FB1 and FB3 declined further, but did not return to zero for an extended time period after complete unloading.

The net resisting pressure distribution determined for the flighting was used to determine an approximation of the relative total load transferred carried by the flighting to the soil as illustrated in **Figure 4-4(d)**. The figure suggests that initially there was a downdrag on the flighting.

The validity of the results depicted in **Figures 4-3 and 4-4** are somewhat questionable considering the assumptions inherent in the analyses and the scatter of the strain gage data. In particular, the existence of initial downdrag is difficult to account for.

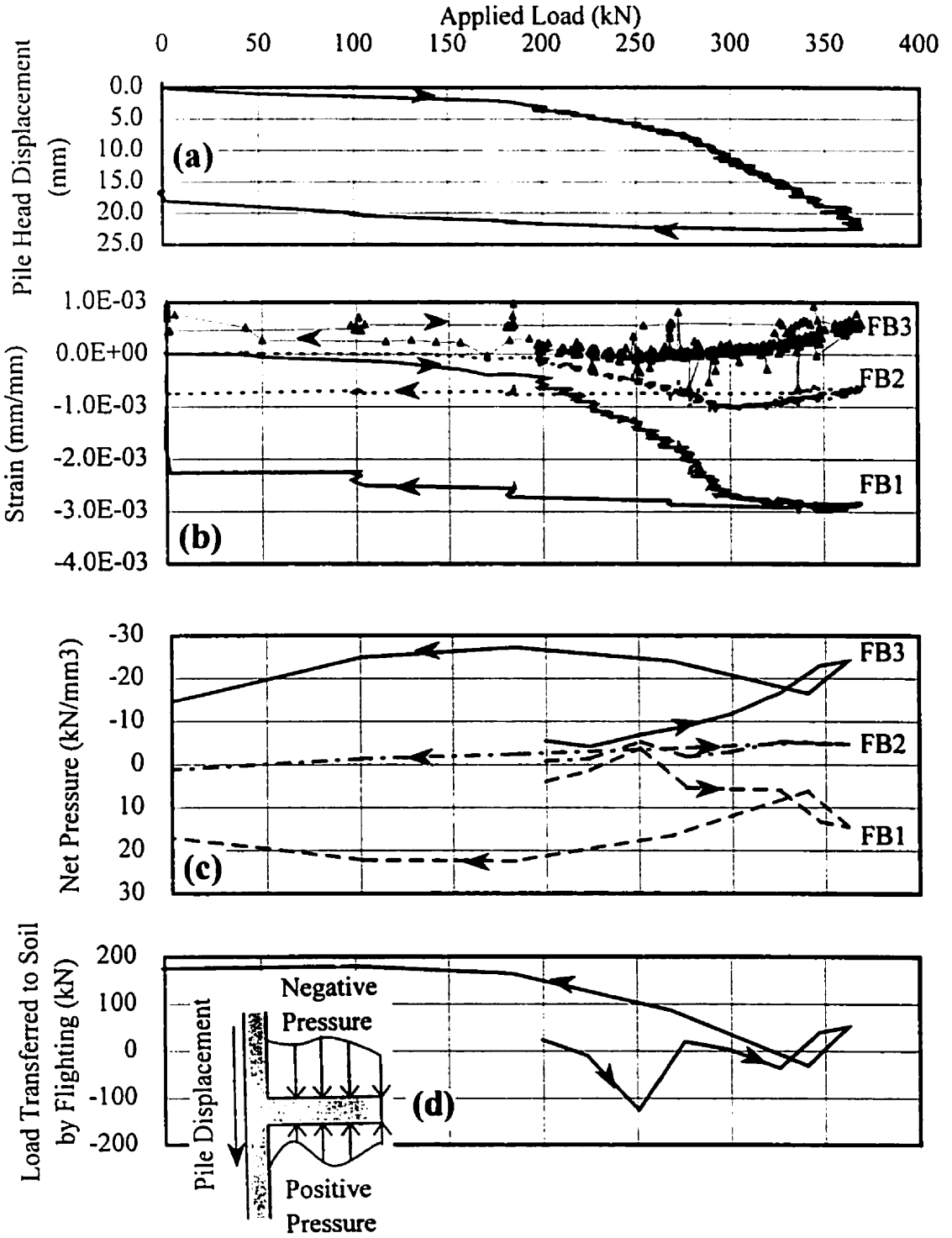

Figure 4-4 (a, b, c, d): Displacement, Strain, Net Pressure, and Load Transferred versus Applied Load - Load Application No. 2

4.4 Adfreeze/Friction

Adfreeze contributes to load transfer through a shear bond between the pile shaft surface and the soil mass. This bond reaches failure at small strains (Sayles, 1988), but may have significant strength until that failure. Following failure of adfreeze, the shaft carries load through friction. It has been assumed that the shaft of the pile segment transferred some of the applied axial load through adfreeze/shaft friction.

To determine the adfreeze/friction contribution, the force transferred from the pile shaft to the soil mass was calculated along each unit length of segment shaft. The recorded strains from the two strain gage strings ("A" & "B") were converted to axial stresses. By multiplying by the cross-sectional area of the shaft, the load within the pile segment shaft was calculated (Equation No. 10). The difference between internal axial forces at consecutive positions represents the load transferred over that length from the shaft to the surrounding soil. The load transferred over this shaft length was converted to shear stresses by dividing the force by the outside area of the shaft (Equation No. 11). This method is illustrated in **Figure 4-5**.

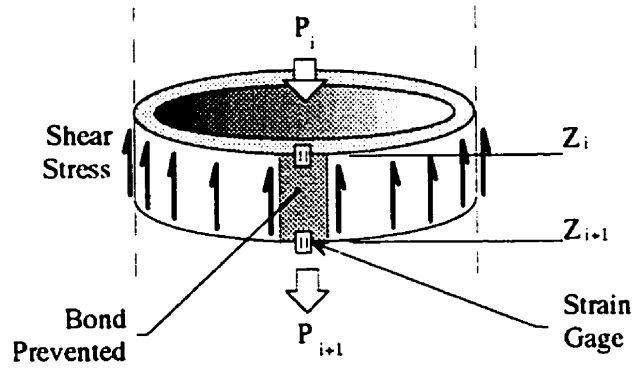

Figure 4-5: Method of Calculation of Adfreeze Shear Stress on Pile Segment Shaft

The following equations are used to develop the shear stress based on strain gage results :

$$P_i = \sigma_i A_P = (\epsilon_i - \epsilon_o) E_S A_P \quad \text{...Eq. (10)}$$

Where:

P_i = Force in pile shaft at gage i (kN)

σ_i = Stress in pile shaft at gage i (MPa)

A_P = Cross-sectional area of pile shaft (mm^2)

E_S = Young's Modulus of Steel (GPa)

ϵ_i = Measured strain at gage i (mm/mm)

ϵ_0 = Initial strain in gage i (mm/mm)

And :

$$\tau_{ADF} = \frac{dP}{dA_{ADF}} = \frac{(P_i - P_{i+1})}{(\pi D (Z_{i+1} - Z_i))} \quad \text{...Eq. (11)}$$

Where:

τ_{ADF} = Adfreeze shear stress (MPa)

D = Outside diameter of the pile shaft (mm)

Z_i = Positive depth from surface to gage i (mm)

Figure 4-6 illustrates a plot of the applied axial shaft load and the internal load in the pile segment versus strain gage position for Load Application No. 1. For the load increments plotted, the axial load in the pile shaft tends to decline to near zero over the length of the flighting, with a small force transferred to the balance of the pile shaft. A variety of polynomial and logarithmic equations were attempted to determine a "best-fit" equation to the data. It was found that a bi-linear equation provided the best-fit. Generally, the first equation corresponded to the flighted portion of the pile segment and the second linear equation corresponded to the straight shaft portion. The best-fit relationship indicated that for the particular range of loads applied to the pile, none of the applied load was carried through end-bearing.

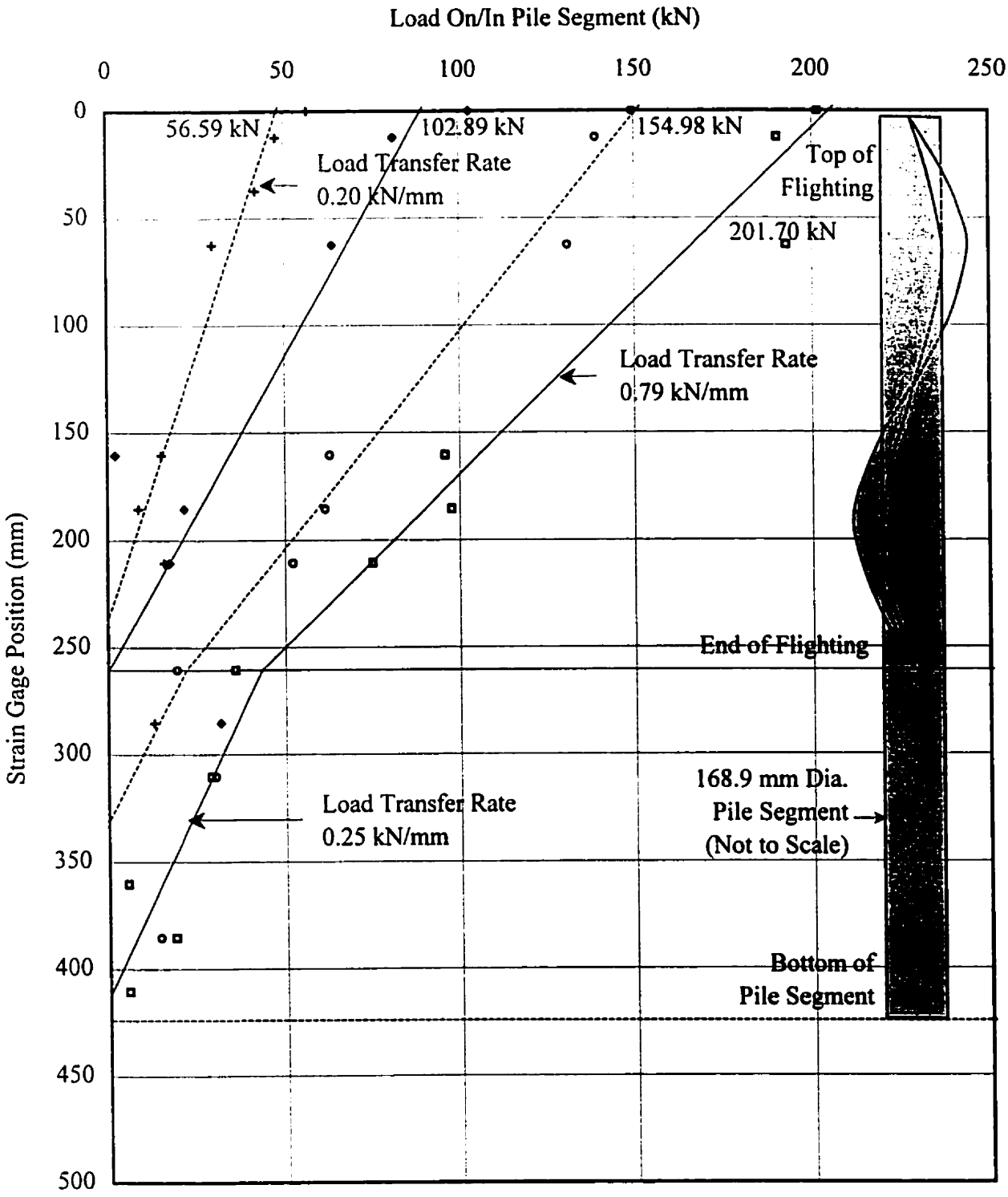

Figure 4-6: Force in Pile Segment Shaft versus Applied Load - Load Application No. 1

Figure 4-7 illustrates a plot of the applied axial shaft load and the internal load in the pile segment versus strain gage position for Load Application No. 2. Similarly to **Figure 4-6**, bi-linear equations were used to determine "best-fit" equations for the data. As with **Figure 4-6**, these bi-linear equations tended to correspond to the two distinct portions of the pile segment. However, unlike the results of the previous load test, the bi-linear equations for the second load test indicated that part of the applied load was carried through end-bearing. As mentioned in Chapter 2, the pile tip was placed on a polystyrene foam pad to prevent the pile end section from developing end-bearing. However, as noted in Section 3.3.3, during the initial setup of the test program, a plug of ice formed in the bottom of the pile, thereby providing it with the capability of developing end-bearing. The results of the two tests suggest that the ice plug came into play during the second load test.

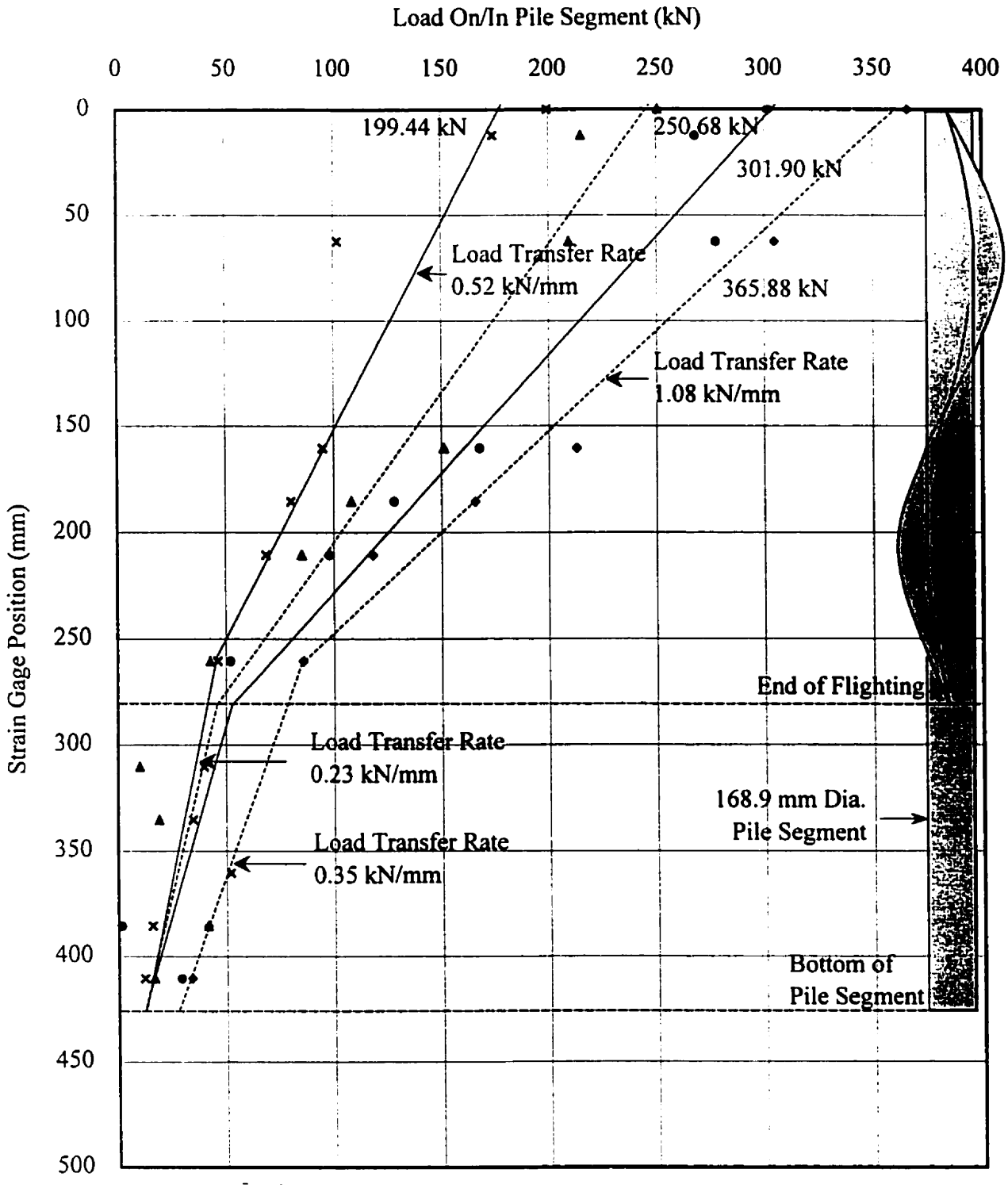

Figure 4-7: Force in Pile Segment Shaft versus Applied Load - Load Application No. 2

4.5 Separation of Transfer Mechanisms

The pressure distribution and the resulting equivalent loads transferred by the flight were previously determined in **Section 4.3** for selected applied loads. However, the data contain significant scatter and other irregularities. Consequently, these data were not used for further analysis. The separation of load transfer through the flighting and the straight shaft sections of the pile were determined by the rate of load transfer over the two sections of pile found in **Figures 4-6 and 4-7**. In **Figure 4-8**, total pile load resistance, flighting load transfer, and end-bearing load transfer are plotted against applied axial load for both load applications. The difference between total pile load and the sum of end-bearing and flighting transfer is the equivalent shaft load transfer.

Figure 4-8 illustrates that at loads below 100 kN, the load transfer is predominately by the flighting. As the applied load increases above 100 kN, the contribution by the pile shaft below the flighting increases gradually. At approximately 150 kN, end-bearing begins and increases gradually. At peak load (368 kN), 74.5% was transferred by the flighting, 17.8% by the straight shaft portion, and 7.7% through end-bearing.

Although approximately only one-half of the pile length had flighting, this section of the pile carried 75% of the total load.

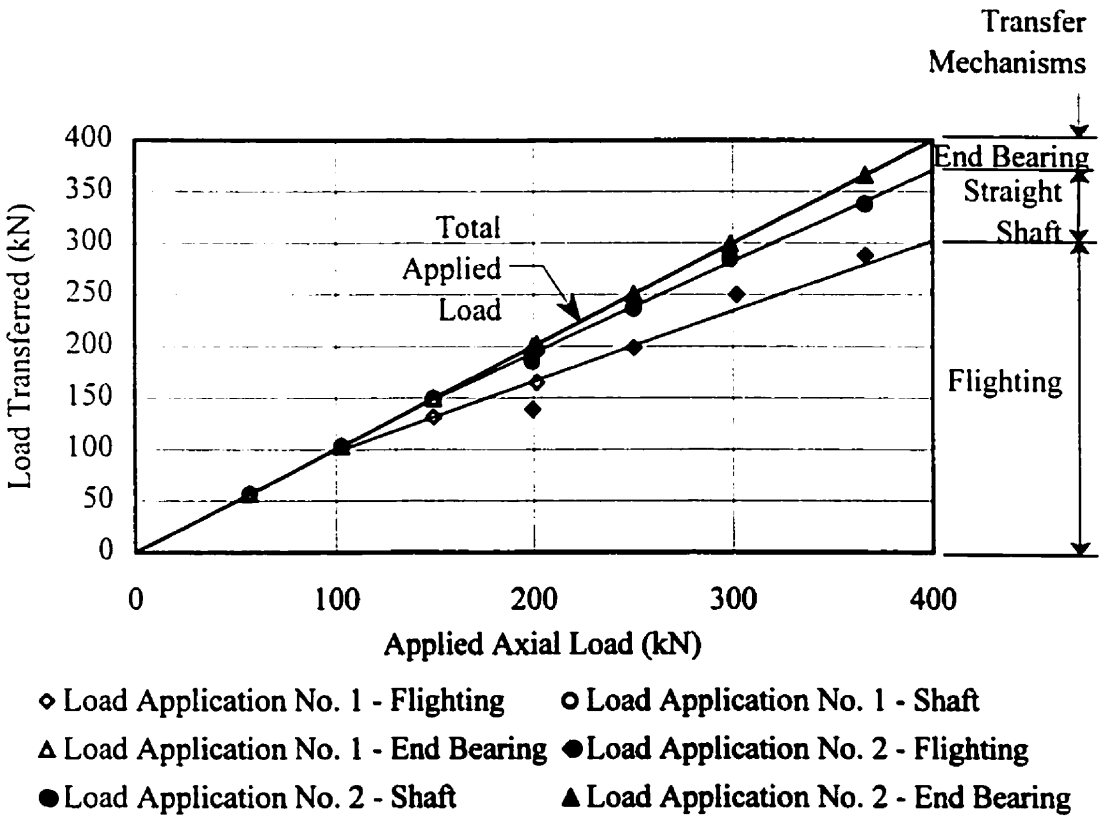

Figure 4-8: Load Transfer Components versus Applied Load

4.6 Discussion of Transfer of Load

The relatively rapidly applied axial load may have been transferred through several mechanisms to the surrounding frozen soil mass from the flighted steel pipe pile. There were several potential mechanisms available for the transfer. Briefly, they are :

- Adfreeze on the flighting surface
- Adfreeze on the shaft surface
- Soil compression below the flights
- Shear below the flights
- Static friction along the pile surface

- Kinetic friction along the pile surface

- End-bearing

The individual mechanisms could not be quantified and so the transfer was separated into three components; flighting, straight-shaft, and end-bearing as indicated in **Figure 4-8**. Interpretation of the data by use of bi-linear equations indicated that initially as the load on the pile was increased, the transfer was progressively through the flighting. When the load reached approximately 100 kN, the straight shaft section began to transfer some of the load. This continued progressively and at a later stage, end-bearing began to develop and continued to increase as the pile load was increased. By plotting total load transferred against the applied axial load (**Figure 4-8**) for both load applications, three distinct components of load transfer are apparent. These three components tend to be linear in relation to applied load.

Figure 4-9 illustrates applied load versus the measured pile head displacement. Initially, load transfer is through the flighting for the first two millimetres of displacement. Load transfer along the straight shaft segment began at 100 kN with a corresponding pile displacement of two millimetres. End bearing began at an applied load of 150 kN corresponding to a pile displacement of eight millimetres.

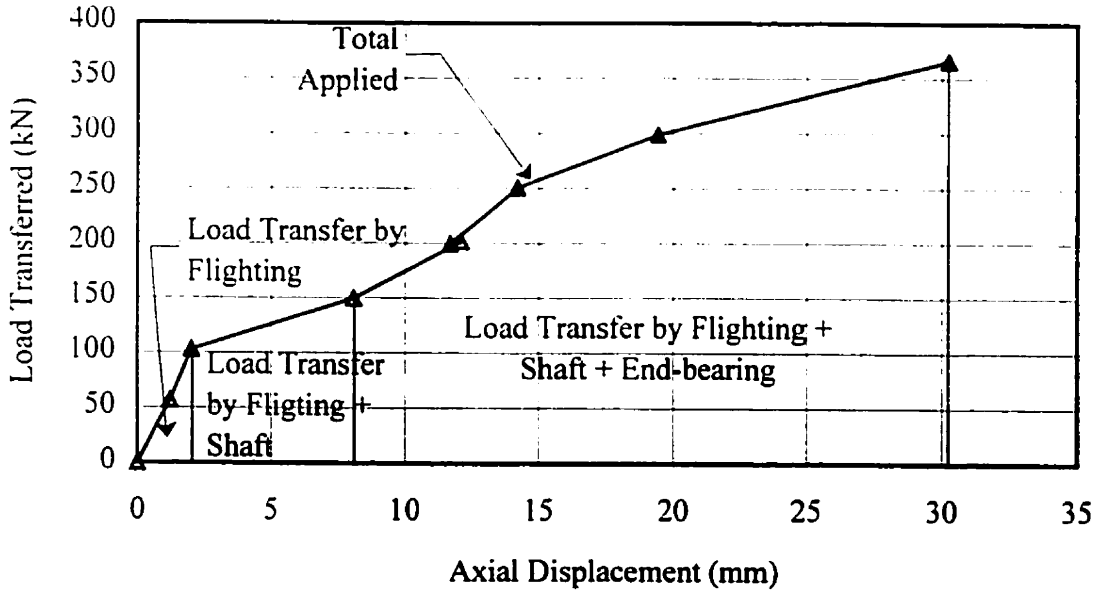

Figure 4-9: Load Transfer Components versus Axial Displacement

In **Figure 4-9**, the development of load transfer mechanisms is plotted as a function of pile head displacement. For the first two millimetres of displacement, the transfer was through the flighting only. For the next six millimetres, the transfer was through the flighting and through shaft adfreeze/friction. At displacements greater than eight millimetres, load transfer was through flighting, the straight-shaft section, and through end-bearing. The information indicates that the pile was stiff in relation to the frozen soil.

5. Conclusions and Recommendations

5.1 Conclusions

Several conclusions concerning the load transfer from a flighted steel pipe pile to the surrounding soil can be drawn from this investigation. Those conclusions are

1. Generally, as the pile load was increased, the transfer to the soil progressed through three phases; firstly through the flighting section, then secondly through the flighting section and the smooth-shaft section, and lastly through the combination of the flighting section, smooth shaft section, and through end-bearing.
2. At the maximum applied load, the flighted section, which made up approximately half of the pile segment length, transferred approximately 75 % of the applied load, while the smooth shaft section transferred 18 %, and 7 % was transferred through end-bearing. These results are valid for the specific test conditions, load application rate, and pile segment geometry and are not generalized to other conditions.
3. The rate of load transfer through the flighting section was higher than the rate of load transfer through the smooth shaft section. At the maximum applied load, the average rate of load transfer through the flighting section was 1080 kN/m. of flighted pile length, whereas the corresponding load transfer rate through the smooth shaft section was only 350 kN/m. of pile length.
4. Despite having instrumented the flighting itself, no conclusion could be reached regarding the distribution of load transfer across the flighting from the pile shaft to the

flighting tip. Also, no conclusion could be determined as to whether the load transfer by the flighting was through adfreeze, bearing, or a combination of both. The data were neither comprehensive enough nor reliable enough to reach any conclusion in this regard.

5. As the pile segment was not loaded to failure, the ultimate load carrying capacity of the flighting could not be established.

This investigation provided valuable insight into the mechanisms of load transfer of a flighted steel pipe pile segment. The relative contributions by various load transfer mechanisms is significant.

5.2 Recommendations for Further Study

The literature review and the investigation resulted in several potential improvements in the study of load transfer behaviour of flighted steel pipe piles. The recommendations may be considered applicable to other research on flighted steel pipe piles or related research.

1. Research should continue by performing similar pile load tests with additional instrumentation, which would be able to accurately define the normal pressure distribution and shear stress distributions. It is recommended that the following changes be applied to further research:

   a.) Small surface pressure transducing strain gages are available to measure the

applied normal pressure across small surface areas. This would confirm the pressure distributions determined in this investigation more directly.

b.) Install "tell-tales" at the tip of the flighting to determine the deflection of the flighting in relation to the pile segment displacement to better establish the flighting behaviour, and therefore load transfer.

c.) Install all strain gage wiring within the pile segment interior to minimize both the effects on strain gage performance and the effects on local load transfer.

d.) Formation of a verifiable void below the pile segment to ensure no end-bearing effects occur during pile segment testing.

e.) Testing should be performed to failure of the pile segment, either to a reasonable displacement criteria, or to the ultimate maximum load.

2. Also, additional pile segment load tests with controlled variation of soil temperature, flight geometry, and soil density would determine the sensitivity of pile load capacity to each of these parameters. This may be achieved by:

a.) Provision of some means of greater control over the soil temperature regime within the soil mass to ensure consistent frozen soil properties. This may be accomplished by the installation of a perimeter of small thermosyphons to ensure soil temperate coincides with air temperature, and also more uniform through the soil depth.

b.) Perform additional tests with variations of flight pitch, thickness, and the flighting projection from the segment shaft. These tests would provide some

indication of the sensitively of load transfer to changes in flight geometry.

c.) Consistent soil placement methods for the entire soil mass below and around the pile segment would improve the consistency of in-situ soil properties and reduce the potential influence of soil properties. As normal installation of flighted piles does not permit the compaction of soil, some evaluation of the impact of vibration during soil placement may be beneficial.

Bibliography

Alkire, B.D. & Andersland, O.B.
The Effect of Confining Pressure on the Mechanical Properties of Sand-ice Materials. Journal of Glaciology, Volume 12, Pgs. 469 - 481. 1973

Alwahhab, M.R.M. et al
Roughness Criteria for Steel Piles in Frozen Sand. Proceedings of the 5th. Engineering Mechanics Division of A.S.C.E. Specialty Conference, Laramie, Wyoming. Pgs. 1288 - 1291. 1984.

Alwahhab, M.R.M.
Bond and Slip of Steel Bars in Frozen Sand. Unpublished Ph.D. Thesis, Michigan State University, East Lansing, Michigan. 1983.

Amir, J.M.
Piling in Rock. A.A.Balkema, Boston. 1986.

Andersen, G.R.
Physical Mechanisms Controlling the Strength and Deformation Behaviour of Frozen Sand. Ph.D. Thesis, Massachusetts Institute of Technology, Cambridge. 2 Volumes, 560 Pages. 1991.

Andersland, O.B. et al
Load Capacity of Model Piles in Frozen Ground. Proceedings of the Fourth International Specialty Conference on Cold Regions Engineering, Edmonton, Alberta, Pgs. 29 - 39. 1984.

Andersland, O.B. & Anderson, D.M. (Editors)
Geotechnical Engineering in Cold Regions. McGraw-Hill Book Company, Toronto, Ontario. 1978.

Andersland, O.B., & Alwahhab, O.B.
Lug Behaviour of Model Steel Piles in Frozen Sand. Proceedings of the Fourth Intl. Conference on Permafrost, Fairbanks, Pgs. 16 - 21. 1981.

Anderson, D.M. & Morgenstern, N.R.
Physics, Chemistry, and Mechanics of Frozen Ground : A Review. Proceedings of the Second International Conference on Permafrost : North American Contribution, Pgs. 257 - 288. 1973.

Atkinson, J.H. & Bransby, P.L.
The Mechanics of Soils: An Introduction to Critical State Soil Mechanics. McGraw Hill Book Co. (UK) Ltd., 375 Pages. 1978.

Baker, T.H.W.
Preparation of Artificially Frozen Sand Specimens. National Research Council of Canada, DBR Paper No. 682. 1976.

Baker, T.H.W.
Strain Rate Effect on the Compressive Strength of Frozen Sand. Engineering Geology, Volume 13, Pgs. 223 - 231. 1979.

Bibliography (Continued)

Baker, R.W.
The Influence of Ice Grain Size on Creep. Journal of Glaciology, Volume 21, Pgs. 485 - 500. 1978.

Barnes, P., Tabor, D. & Walker, J.C.F.
The Friction and Creep of Polycrystalline Ice. Proceedings of the Royal Society, London, Volume 324A, Pgs. 127 - 155. 1971.

Biggar, K.W., & Sego, D.C.
Field Load Testing of Various Pile Configurations in Saline Permafrost and Seasonally Frozen Rock. Proceedings of the 42nd. Canadian Geotechnical Conference, Winnipeg, Manitoba, Pgs. 304 - 312. 1989.

Biggar, K.W., & Sego, D.C.
Field Pile Load Tests in Saline Permafrost. Part I : Test Procedures and Results. Canadian Geotechnical Journal, Volume 30, Pgs. 34 - 45. 1993a.

Biggar, K.W., & Sego, D.C.
Field Pile Load Tests in Saline Permafrost. Part II : Analysis of Results. Canadian Geotechnical Journal, Volume 30, Pgs. 46 - 59. 1993b.

Bishop, A.W.
Shear Strength Parameters for Undisturbed and Remoulded Specimens. Proceedings of the Roscoe Memorial Symposium, G.T. Foulis & Co., Ltd., Pgs. 3 - 58. 1971.

Bishop. A.W. & Eldin, A.K.G.
Undrained Triaxial Tests on Saturated Sands and Their Significance in the General Theory of Shear Strength. Geotechnique, Volume 2, Pgs. 13 - 32.

Bishop., A.W. & Henkel, D.J.
The Measurement of Soil Properties in the Triaxial Test. Edward Arnold Publishing, London, 227 Pages. 1962.

Black, R.S.
Load Transfer Mechanisms Between Flighted Steel Pipe Piles and Frozen Sand. B.Sc. Thesis, University of Manitoba, Winnipeg, Manitoba. 1994.

Black, W.T., & Thomas, H.P.
Prototype Pile Tests in Permafrost Soils. Pipelines in Adverse Environments : A State of the Art, Proceedings of the A.S.C.E. Pipeline Division Specialty Conference, New Orleans, Volume I, Pgs. 372 - 383. 1979.

Chamberlain, E.
Mechanical Properties of Frozen Ground Under High Pressure. The North American Contribution to the Second International Permafrost Conference, Yakutsk, National Academy of Sciences, Washington, D.C., Pgs. 273 - 305. 1973.

Crory, F.E.
Pile Foundations in Permafrost. Proceedings of the First International Conference on Permafrost, Pgs. 467 - 472. 1966.

Bibliography (Continued)

Dickin, E.A. & Leung, C.F.
Performance of Pile with Enlarged Bases Subject to Uplift Forces. Canadian Geotechnical Journal, Volume 27, Pgs. 546-556. 1990.

Dickin, E.A. & Leung, C.F.
The Influence of Foundation Geometry on the Uplift Behaviour of Piles with Enlarged Bases. Canadian Geotechnical Journal, Volume 29, Pgs. 498-505. 1992.

Dostovalov, B.N.
Structures, Phase Transitions, and Properties of Free and Bound Water. Proceedings of the Second International Conference on Permafrost: USSR Contribution, Pgs. 287 - 292. 1973.

Dubois, D.P.
Load Transfer From Thermopiles With and Without Continuous Flighting. M.Eng. (C.E.) Report, University of Manitoba, Winnipeg, Manitoba, May 1994.

Farmer, I.W.
Stress Distribution along a Resin Grouted Rock Anchor. International Journal of Rock Mechanics & Mining Science, Volume 12, No. 11, Pgs. 347 - 351. 1975.

Fedorovich, D.I., Targulyan, Y.O. et al
Improved Types of Piles for Construction on Permafrost Soils in the North of West Siberia. Soil Mechanics and Foundation Engineering. Sept./Oct. 1987. Volume 24(5), Pgs. 171-176. 1988.

Fedorovich, D.I. et al.
Pile Foundation Construction Characteristics in the Alaska Oil Pipeline. Soil Mechanics and Foundation Engineering, Volume 28, No. 5, Russian Government Publication, Pgs. 204 - 207. Mar. 1992.

Frederking, R. at al.
Effects of Pile Material and Loading State on Adhesive Strength of Piles in Ice. Canadian Geotechnical Journal, Volume 20, Pgs. 673 - 680. 1983.

Foster, M.L.
Adfreeze Strength of Ice to Steel Pipe Piles as a Function of Temperature. Proceedings of Fourth International Conference on Cold Regions Engineering, Anchorage, Alaska, A.S.C.E., Pgs. 11 - 20. 1986.

Glos III, G.H. and Briggs Jr., O.H.
Rock Sockets in Soft Rock. Journal of Geotechnical Engineering, Volume 109, No. 4, Pgs. 525-535, Paper No. 17922. April 1983.

Gold, L.W.
Ice Pressures and Bearing Capacity. Geotechnical Engineering for Cold Regions (O.B. Andersland and D.M. Anderson, Editors). McGraw Hill Book Co., New York, Pgs. 505 - 551. 1978.

Goodman, M.A. & Wood, D.B.
A Mechanical Model for Permafrost Freezeback Pressure Behaviour. Paper SPE 4589, Presented at the SPE Fall Meeting, Las Vegas. 1973.

Bibliography (Continued)

Goughnour, R.R., & Andersland, O.B.
Mechanical Properties of a Sand-Ice System. Journal of the Soil Mechanics and Foundations Division, A.S.C.E., Pgs. 923-950. July 1968.

Hammer, T.A. at al.
Design and Installation of a Pile Foundation in a Remote Area of Alaska. Fifth International Cold Regions Specialty Conference, A.S.C.E., St. Paul, Minnesota, Pgs. 215 - 225. 1989.

Haynes, F.D. & Zarling, J.P.
Thermosyphon Devices and Slab-on-grade Foundation Design. Final Report : AK-RD-86-16, Dept. of Transportation and Public Facilities, Anchorage, Alaska. June 1985.

Haynes, F.D. et al.
Laboratory Tests with a 37 metre Thermosyphon in Soil. Proceedings of the Eleventh International Conference on Offshore Mechanics and Arctic Engineering, A.S.M.E., Calgary, Alberta, Pgs. 139 - 143. June 1992.

Haynes, F.D. & Karalius, J.A.
Effect of Temperature on the Strength of a Frozen Silt. U.S. Army CRREL Report No. 77 - 3, 27 Pages. 1978.

Haynes, F.D., Karalius, J.A. & Kalafut, J.
Strain Rate Effect on the Strength of a Frozen Silt. U.S. Army CREEL Report No. 350. 1975.

Heydinger, A.G.
Piles in Permafrost. Journal of Cold Regions Engineering, Pgs. 57 - 75. 1987.

Hivon, E.G.
Behaviour of Saline Frozen Soils. Ph.D. Thesis, University of Alberta, Edmonton, Alberta, 435 Pages. 1991.

Hobbs, Peter V.
Ice Physics. Oxford University Press (Clarendon Press), Oxford. 1974.

Holubec, I.
Thread Bar Pile for Permafrost. Proceedings of the 5th. Canadian Permafrost Conference, Pgs. 341 - 348. 1990.

Hryciw, R.D. and Irsyam, M.
Behaviour of Sand Particles Around Rigid Ribbed Inclusions During Shear. Soils and Foundations, Volume 33, No. 3, Pgs. 1-13. September 1993.

Inoue, M. et al.
Adhesion Strength of Pile in Saline Ice. Proceedings of the Eighth IAHR Symposium on Ice, Iowa City, Iowa, Pgs. 89 - 104. Aug. 1986.

Irsyam, M. and Hryciw, R.D.
Friction and Passive Resistance in Soil Reinforced by Plane Ribbed Inclusions. Geotechnique, Volume 41, No. 4, Pgs. 485-498. 1991.

Bibliography (Continued)

Jellinek, H.H.G.
Adhesive Properties of Ice. Journal of Colloid Science, Volume 14, Pgs. 268 - 280. 1959.

Jellinek, H.H.G.
Liquid-like Layer on Ice. Journal of Applied Physics, Volume 32, No. 9, Page 1793 September 1961.

Jellinek, H.H.G.
Liquid-like (Transition) Layer on Ice. Journal of Colloid and Interface Science. Volume 25, Pgs. 192 - 205. 1967.

Jellinek, H.H.G.
Adhesion of Ice Frozen From Dilute Electrolyte Solutions. CRREL Research Report 317. 1974.

Ji, J.Z. & Domaschuk, L.
An Effective Stress Creep Model for Frozen Sand Under Shear. Proceedings of the Canadian Society of Civil Engineering, Winnipeg, Manitoba. 1994.

Johnson, J.B. et al.
Measurement of Frost Heave Forces on H-Piles and Pipe Piles. U.S. Army CRREL Report 88 - 21, 49 Pages. Dec. 1988.

Johnston, G.H. & Ladanyi, B.
Field Tests of Grouted Rod Anchors in Permafrost. Canadian Geotechical Journal, Volume 9, No. 2, Pgs. 176 - 194. 1972.

Johnston, G.H.
Permafrost : Engineering Design and Construction. John Wiley & Sons, Toronto. 1981.

Kast, G., & Skermer, N.
DEW Line Anchors in Permafrost. Geotechnical News, Volume 4, No.4, Pgs. 30 - 34. 1986.

Laba. J.T.
Adfreezing of Sands to Concrete. U.S. National Research Council, Transportation Research Board, Record No. 497, Pgs. 31 - 39. 1974.

Ladanyi, B.
Design and Construction of Deep Foundations in Permafrost : North American Practise. Proceedings of the Fourth International Conference on Permafrost. Pgs. 43 - 50. 1983.

Ladanyi, B. et al.
Study of Some Factors Affecting the Adfreeze Bond of Piles in Permafrost. Permafrost Canada : Proceedings of the Fifth Canadian Permafrost Conference, Quebec City, Quebec, Pgs. 327 - 334. 1989.

Bibliography (Continued)

Ladanyi, B.

Some Thoughts on Piles in Permafrost. The Northern Engineer, Volume 23, No. 1., University of Alaska School of Engineering, Fairbanks, Alaska. Pgs. 7 - 13 Feb 1991.

Ladanyi, B.

Etude des Relations Entre les Contraintes et le Deformations Lors du Cisaillement des Sols Pulverulents. Annales des Travaux Publics de Belgique, Vol. 3, Pgs. 241 - 270. 1960.

Ladanyi, B.

Bearing Capacity of Frozen Soils. Preprints Volume, 27th Canadian Geotechnical Conference, Edmonton, Alberta, Pgs. 97 - 107. 1974.

Ladanyi, B.

Mechanical Behaviour of Frozen Soils. Proc. Int. Symp. on the Mechanical Behaviour of Structured Media, (A.P.V. Selvadurai, Editor), Ottawa, Ontario, Part B., Pgs. 205 - 245. 1981a

Ladanyi, B.

Shear-induced Stresses in the Pore Ice in Frozen Particulate Materials. Proceedings from the Symposium on Free Boundary Problems, Montecatini, Research Notes in Mathematics, No. 78, Pitman Books Ltd., Vol. II, Pgs. 549 - 560. 1981b.

Ladanyi, B.

Stress Transfer Mechanism in Frozen Soils. Special Lecture, 10th CANCAM, University of Western Ontario, Pgs. 11 - 23. 1985.

Ladanyi, B.

Stress Transfer Mechanism in Frozen Soils under Deviatoric Loading. Proceedings of the International Colloquim on Free Boundary Problems, Iree, Germany. 1987.

Ladanyi, B.

Short- and Long-term Behaviour of Axially Loaded Piles in Permafrost. Proceed. of the International Symposium on Deep Foundations on Bored and Auger Piles, Ghent, Belgium, Pgs. 121 - 131. 1988.

Ladanyi, B.

An Engineering Theory of Creep of Frozen Soils. Canadian Geotechnical Journal, Volume 9, Pgs. 63 - 80. 1972.

Ladanyi, B.

Bearing Capacity of Deep Footings in Sensitive Clays. Proceedings of the 8th International Conference of S.M.F.E., Moscow, Volume 2.1, Pgs. 159 - 166. 1973.

Ladanyi, B. & Eckardt, H.

Dilatometer Testing in Thick Cylinders of Frozen Sand. Proceedings of the Fourth International Conference on Permafrost, Fairbanks, Alaska, Pgs. 667 - 682. 1983

Bibliography (Continued)

Ladanyi, B. & Johnston, G.H.
Evaluation of In-situ Creep Properties of Frozen Soils with the Pressurometer. Proceeding of the 2nd International Permafrost Conference · North American Contribution, Yakutsk, Volume 2, Pgs. 310 - 318. 1973.

Ladanyi, B. & Johnston, G.H.
Behaviour of Circular Footings and Plate Anchors Embedded in Permafrost. Canadian Geotechnical Journal, Volume 11, 1974.

Ladanyi, B. & Guichaoua, A.
Bearing Capacity and Settlement of Shaped Piles in Permafrost. Proceedings of the XII CSMFE. San Francisco, California. Pgs. 1421 - 1427. 1985.

Ladanyi, B. & Paquin, J.
Creep Behaviour of Frozen Sand Under A Deep Circular Load. Proceedings of the Third International Conference on Permafrost, Edmonton, Alberta, Volume I, Pgs. 679 - 686. 1978.

Linell, K.A. & Kaplar, C.W.
Description and Classification of Frozen Soils. Proceedings of the First International Conference on Permafrost, Pgs. 481 - 487. 1963.

Lock, G.S.H. et al.
Performance of a Right Angled, Evaporative Thermosyphon. Proceedings of the Eleventh International Conference on Offshore Mechanics and Arctic Engineering, A.S.M.E., Calgary, Alberta, Pgs. 145 - 148. June 1992.

Lock, G.S.H. et al.
Performance of an Offset Evaporative Thermosyphon. Proceedings of the Eleventh International Conference on Offshore Mechanics and Arctic Engineering, A.S.M.E, Calgary, Alberta, Pgs. 149 - 153. June 1992.

Lock, G.S.H. et al.
Effect of Orientation on the Cranked, Tubular Thermosyphon. Proceedings of the Eleventh International Conference on Offshore Mechanics and Arctic Engineering, A.S.M.E., Calgary, Alberta, Pgs. 155 - 158. June 1992.

Long, E.L.
Designing Friction Piles for Increased Stability at Lower Installed Cost in Permafrost. Proceedings of Second International Conference on Permafrost, Pgs. 693 - 699. 1973.

Long, E.L. & Yarmak, E. Jr.
Permafrost Foundations Maintained by Passive Refrigeration. Proceedings of the Energy-Sources Technology Conference & Exhibition, Ocean Engineering Division of A.S.M.E., New Orleans, Louisiana. 1982.

Bibliography (Continued)

Luscher, U., Black, W.T., & McPhail, J.F.
Results of Load Tests on Temperature-Controlled Piles in Permafrost. Proceedings of the Fourth International Conference on Permafrost, Fairbanks, Alaska, Pgs. 756 - 761. 1983.

Mattes, N.S. & Poulos, H.G.
Settlement of Single Compressible Pile. Journal of Soil Mechanics & Foundation Engineering Division of A.S.C.E., Volume 95, SM1, Pgs. 189 - 207. 1969.

Meyerhof, G.G.
The Ultimate Bearing Capacity of Foundations. Geotechnique, Volume 1, Pgs. 301 - 332. 1951.

Michel, B.
Ice Mechanics. Les Presses De L'Universite Laval, Montreal, Quebec. 1978.

Mirenburg, Y.S.
Optimization of Pile Load Test Duration in Permafrost Soils. All-Union Conference on Experience with Construction of Bases and Foundations on Permafrost Soils, Abstracts of Proceedings, Moscow, Pgs. 131 - 132. 1981.

Mirenburg, Y.S.
Method of Reduction of Static Pile Test Duration in Frozen Soils. Transcripts from NIIOSPa, No. 70, Moscow, Pgs. 98 - 106. 1978.

Mitchell, R.J. & O'Connor, M.J.
The Energy Surface : A New Concept to Describe the Behaviour of Frozen Soils. Proceedings of the Third International Conference on Permafrost. Pgs. 119 - 126. 1978.

Morel, J.F.
Etude des Contraintes Intergranulaires Lors du Cisaillement d'un Sable Gele. M.Sc.A. Thesis, Ecole Polytechnique, Montreal, 98 Pages. 1987.

Morgenstern, N.R., Roggensack, W.D., & Weaver, J.S.
The Behaviour of Friction Piles in Ice and Ice-rich Soils. Canadian Geotechnical Journal, Volume 17, No. 3, Pgs. 405 - 415. 1980.

Murff, J.D.
Response of Axially Loaded Piles. Journal of the Geotechnical Engineering Division of A.S.C.E., Volume 101, GT3, Pgs. 356 - 360. 1975.

Nelson, W.G. & Phukan, A.
Adfreeze Strength of Fresh and Sea Ice Bonded to Steel Piles. The Northern Engineer, Volume 20, No. 2, Pgs. 19 - 23.

Bibliography (Continued)

Nerseova, Z. A. & Tsytovich, N.A.
Unfrozen Water in Frozen Soils. Proceedings of First International Conference on Permafrost, Pgs. 230 - 234. 1963.

Neukirchner, R.J.
Standard Method for Pile Load Tests in Permafrost. Proceedings of the Fifth International Conference on Permafrost, Trondheim, Norway, Pgs. 1147 - 1151. August 1988.

Nixon, J.F.
Foundation Design Approaches in Permafrost Areas. Canadian Geotechnical Journal, Volume 15, Pgs. 96 - 112. 1978.

Nixon, J.F. & McRoberts, E.E.
A Design Approach for Pile Foundations in Permafrost. Canadian Geotechnical Journal, Volume 13, No. 1, Pgs. 40 - 57. 1976.

Nottingham, D. & Christopherson, A.B.
Driven Piles in Permafrost : State of the Art. Proceedings of the Fourth International Conference on Permafrost, Fairbanks, Alaska, Pgs. 928 - 933. 1983.

Parameswaran, V.R.
Adfreeze Strength of Frozen Sand to Model Piles. Canadian Geotechnical Journal, Volume 15, Pgs. 494 - 500. 1978.

Parameswaran, V.R.
Adfreeze Strength of Model Piles in Ice. Canadian Geotechnical Journal, Volume 18, Pgs. 8 - 16. 1980.

Parameswaran, V.R.
Bearing Capacity Calculations for Piles in Permafrost. Proceedings of Fourth International Conference on Cold Regions Engineering, Anchorage, Alaska, A.S.C.E., Pgs. 751 - 759. 1986.

Parameswaran, V.R.
Adfreeze Strength of Ice to Model Piles. Canadian Geotechnical Journal, Volume 24, Pgs. 446 - 452. 1987.

Parameswaran, V.R.
Laboratory Studies of the Adfreeze Bond Between Small-Scale Model Piles and Frozen Sand. Proceedings of the Third International Conference on Permafrost, Pgs. 714 - 720. 1978.

Pekarskaya, N.K.
The Strain-Hardening of Frozen Ground During the Creep Process. Proceedings of the Second Intl. Conf. on Permafrost : USSR Contribution, Pgs. 841 - 842. 1973.

Pells, P.J.N. and Turner, R.M.
Elastic Solutions for the Design and Analysis of Rock-Socketed Piles. Canadian Geotechnical Journal, Volume 16, Pgs. 481-487. 1979.

Bibliography (Continued)

Penner, E. & Goodrich, L.E.

Adfreezing Stresses on Steel Pipe Piles, Thompson, Manitoba. Proceedings of the Fourth International Conference on Permafrost, Fairbanks, Alaska. Pgs. 979 - 983 July 1983.

Phukan, A.

Design of Deep Foundations in Discontinuous Permafrost. Proceedings of the A.S.C.E. Convention and Exposition, Portland, Oregon, Pgs. 80 - 122. 1980.

Phukan, A.

Frozen Ground Engineering. Prentice-Hall, Inc. Englewood Cliffs, New Jersey, 07632, 1985.

Phukan, A.

Foundations in Cold Regions. Foundation Engineering Handbook, Edited by H.Y. Fang. Van Nostrand Reinhold, New York, Pgs. 735 - 749. 1991.

Poules, H.G.

Analysis of the Settlement of Pile Groups. Geotechnique, Volume 18. 1968.

Poulos, H.G. & Davis, E.H.

The Settlement Behaviour of Single Axially Loaded Incompressible Piles and Piers. Geotechnique, Volume 18, Pgs. 351 - 371. 1968.

Puswewala, U.G.A

Computational Modelling of Structure-Frozen Soil/Ice Interaction. Ph.D. Thesis, University of Manitoba, Winnipeg, Manitoba. 1991.

Roggensack, W.D. & Morgenstern, N.R.

Direct Shear Tests on Natural Fine-grained Permafrost Soils. Proceedings of the Third International Conference on Permafrost, Edmonton, Alberta, Volume 1, Pgs. 728 - 735. 1978.

Rowley, K.R., Watson, G.H. & Ladanyi, B.

Vertical and Lateral Pile Load Tests in Permafrost. Proceedings of the 2nd International Permafrost Conference, Yakutsk: North American Contribution, Volume 1, Pgs. 712 - 721. 1973.

Sackinger, W.M. & Sackinger, P.A.

Shear Strength of the Adfreeze Bond of Sea Ice to Structures. Proceedings of the Fourth International Conference on Port and Ocean Engineering under Arctic Conditions (POAC 77). Memorial University of Newfoundland, St. Johns. Volume II, Pgs. 607 - 614. 1977.

Bibliography (Continued)

Sadovskiy, A.V.
Adfreeze Between Ground and Foundation Materials. Proceedings of the First Intl. Conf. on Permafrost : USSR Contribution, Pgs. 650 - 653. 1973.

Saeki, H. et al.
Mechanical Properties of Adhesion Strength to Pile Structures. Proceedings of IAHR Ice Symposium, Volume III, Quebec City, Quebec, Pgs. 641 - 649. 1981.

Sanger, F.J.
Foundations of Structures in Cold Regions. CRREL, Hanover, New Hampshire, Monograph III-C4. 1969.

Sanger, F.J. & Kaplar, C.W.
Plastic Deformation of Frozen Soils. Proceedings of the First International Conference on Permafrost, Pgs. 305 - 315. 1963.

Sayles, F.H.
Triaxial and Creep Tests on Frozen Ottawa Sand. The North American Contribution to the Second International Permafrost Conference, Yakutsk, Pgs. 384 - 391. 1973.

Sayles, F.H.
Triaxial Constant Strain Rate Tests and Triaxial Creep Tests on Frozen Ottawa Sand. U.S. Army CRREL, Technical Report No. 253. 1974.

Savel'ev, B.A. et al.
Artificial Freezing-on of Engineering Ice-Soil Structures. Proceedings of the Fifth International Symposium on Ground Freezing, Pgs. 497 - 503. 1989.

Schneebeli, G.
Une Analogie Four L'etude de la Stabilite des Ouvrages en Terre a Deux Dimensions. Proceedings of the Fourth International Conference on Soil Mechanics and Foundation Engineering, London, Vol. II, Pgs. 228 - 232. 1957.

Schofield, A.N. & Wroth, C.P.
Critical State Soil Mechanics. McGraw-Hill Book Co., New York, 310 Pages. 1968.

Searle, I.W. & Bartholomew, R.F.
The Behaviour of Driven Cast-in-Situ and Bored Piles in Weathered Chalk. Piles in Weak Rock, Pgs. 21 - 32. The Institution of Civil Engineers, London, 1977.

Seed, H.B. & Lee, K.L.
Drained Strength Characteristics of Sands. Proceedings of the A.S.C.E. Conference, Volume 93, SM6, Pgs. 117 - 141. 1967a.

Seed, H.B. & Lee, K.L.
Undrained Strength Characteristics of Cohesionless Soils. Proceedings of the A.S.C.E. Conference, Volume 93, SM6, Pgs. 333 - 360. 1967b.

Sego, D.C.
Deformation of Ice under Low Stresses. Unpublished Ph.D. Thesis, University of Alberta, Edmonton, Alberta, 500 Pages. 1980.

Bibliography (Continued)

Sego, D.C., & Chernenko, D.
Confining Pressure Influence on the Behaviour of Frozen Saline Sand. Proceed. of Third International Cold Regions Engineering Specialty Conference, Edmonton, Alberta, Volume 2, Pgs. 565 - 578. 1984.

Sego, D.C., & Morgenstern, N.R.
Deformation of Ice under Low Stresses. Canadian Geotechnical Journal, Volume 20, Pgs. 587 - 602. 1983.

Sego, D.C., Schultz, T., & Banasch, R.
Strength and Deformation Behaviour of Frozen Saline Sand. Proceedings of the Third International Symposium on Ground Freezing, Hanover, New Hampshire, Volume 1, Pgs. 11 - 19. 1982.

Sego, D.C., & Smith, L.B.
Effect of Backfill Properties and Surface Treatment on the Capacity of Adfreeze Pipe Piles. Canadian Geotechnical Journal, Volume 26, Pgs. 718 - 725. 1989.

Soo, S., Wen, R.K., & Anderland, O.B.
Flexural Behaviour of Frozen Sand. Canadian Geotechnical Journal, Volume 23, Pgs. 355 - 361. 1986.

Stehle, N.S.
Adfreeze Strength of Ice. Proceedings of the International Association for Hydraulic Research (IAHR) Ice Symposium, Session 5-3. Reykjavik, Iceland. Pgs. 12. 1970.

Stelzer, D.L.
Cyclic Load Effects on Model Pile Behaviour in Frozen Sand. Unpublished Ph.D. Thesis, Michigan State University, East Lansing, Michigan. 1989.

Stelzer, D.L., & Andersland, O.B.
Dynamic Load Effect on Settlement of Model Piles in Frozen Sand. PERMAFROST : Proceedings of the 5th. International Conference, Tapir Publications, Trondheim, Norway, Volume 2, Pgs. 1165 - 1170. 1988.

Stelzer, D.L., & Andersland, O.B.
Pile Roughness and Load Capacity in Frozen Soils. Proceedings of Fourth International Conference on Cold Regions Engineering, Anchorage, Alaska, A.S.C.E. 1986.

Stelzer, D.L., & Andersland, O.B.
Pile Roughness and Load Capacity in Frozen Soils. Fifth International Cold Regions Specialty Conference, A.S.C.E., St. Paul, Minnesota, Pgs. 226 - 235. Feb. 1989.

Stelzer, D.L., & Andersland, O.B.
Model Pile Settlement Behaviour in Frozen Sand. The Journal of Cold Regions Engineering, Volume 5, No.1, Pgs. 1 - 13. March 1991.

Bibliography (Continued)

Theriault, A. et al.
Behaviour of Long Piles in Permafrost. Proceedings of the Fifth International Conference on Permafrost, Trondheim, Norway, Pgs. 1175 - 1180. August 1988.

Thomas, H.P. & U. Luscher.
Improvement of Bearing Capacity of Pipe Piles by Corrugations. Proc. Joint US-USSR Seminar. Leningrad. 1979. CRREL Special Report, Pgs. 229 - 234. 1980.

Thompson, E.G. & Sayles, F.H.
In-situ Creep of Room in Frozen Soil. Proceedings of the ASCE Conference, No. 98, SM9, Pgs. 899 - 915. 1972.

Ting, J.M.
The Creep of Frozen Sands : Qualitative and Quantitative Models. D.Sc Thesis, Massachusetts Institute of Technology. 1981.

Tsytovich, N.A.
The Mechanics of Frozen Ground. Scripta Book Company, Washington. 1975.

Vialov, S.S. ‡
Rheological Properties and Bearing Capacity of Frozen Soils. Translation No. 74, CRREL, Hanover, New Hampshire. 1959.

Vialov, S.S.
The Strength and the Creep of Frozen Soils and Calculations for Ice-Soil Retaining Structures. Translation No. 76, CRREL, Hanover, New Hampshire. 1962.

Vialov, S.S.
Rheology of Frozen Soils. Proceedings of the First Intl. Conf. on Permafrost. Pgs. 332 - 337. 1963.

Vialov, S.S.
Rheological Fundamentals of Soil Mechanics. Developments in Geotechnical Engineering, Volume 36, Elsevier Publishing, New York, New York. 1986.

Vialov, S.S., & Lunev, M.V.
Experimental Investigation of Behaviour of Pile Clusters in Permafrost Soil. Soil Mechanics and Foundation Engineering, Volume 25, No. 2, Pgs. 51 - 57. September 1988.

Vialov, S.S. et al.
Improved Methods of Testing Piles in Frozen Soils. Soil Mechanics and Foundation Engineering, Volume 27 No. 4, Soviet Government Publication, Pgs. 155 - 161. Jan. 1991.

Vialov, S.S. et al.
Single Pile and Pile Group in Permafrost. Proceedings of the Sixth International Cold Regions Specialty Conference, A.S.C.E., West Lebanon, New Hampshire, Pgs. 44 - 53. Feb. 1991.

Bibliography (Continued)

Vialov, S.S. et al.
Testing and Design of Single Piles with Allowances for Creep. Soil Mechanics and Foundation Engineering, Volume 28, No. 3, Soviet Government Publication, Pgs. 104 - 110. June 1991.

Vologdina, I.S.
Force of Adfreeze of Frozen Soils with Wood and Concrete. Moscow, Izd-vo AN SSSR. 1936.

Weaver, J.S.
Pile Foundations in Permafrost. Unpublished Ph. D. Thesis, University of Alberta, Edmonton, Alberta. 1979.

Weaver, J.S. & Morgenstern, N.R.
Simple Shear Creep Tests on Frozen Soils. Canadian Geotechnical Journal, Volume 18, Pgs. 217 - 229. 1981a.

Weaver, J.S. & Morgenstern, N.R.
Pile Design in Permafrost. Canadian Geotechnical Journal. Volume 18, Pgs. 357 - 370. 1981b.

Zarling, J.P. et al.
Design and Performance Experience of Foundations Stabilized with Thermosyphons. Permafrost Canada : Proceedings of the Fifth Canadian Permafrost Conference, Quebec City, Quebec, Pgs. 365 - 370. 1989.

Notes :
‡ Vialov, S. S. is also published as Vyalov, S. S. by some authors.
† Reference Article or Publication
CRREL U.S. Army Corps of Engineering Cold Regions Research and Engineering Laboratory, Hanover, New Hampshire, 03755-1290 maintain an extensive library of published material relating to Cold Regions Engineering, and has an concise annual bibliography of all material held by their Library.

Appendix A

Experimental Test Results

Load Application No. 1

Load Application No. 2

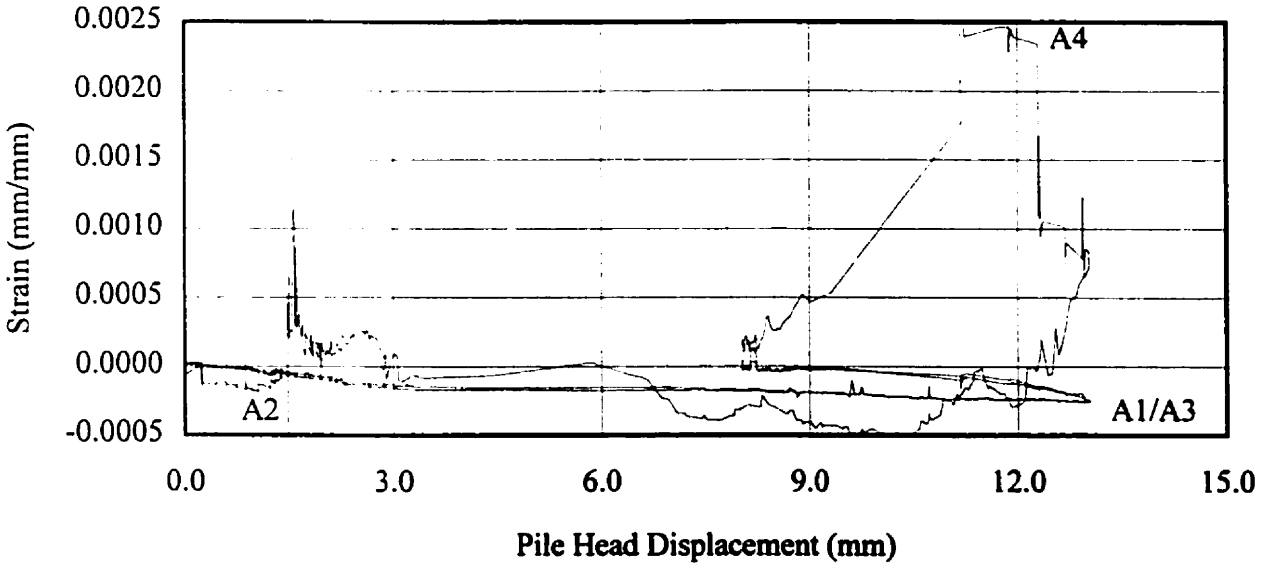

Figure A-1: Pile Head Displacement versus Strain Gage A1 through A4 Load Application No. 1

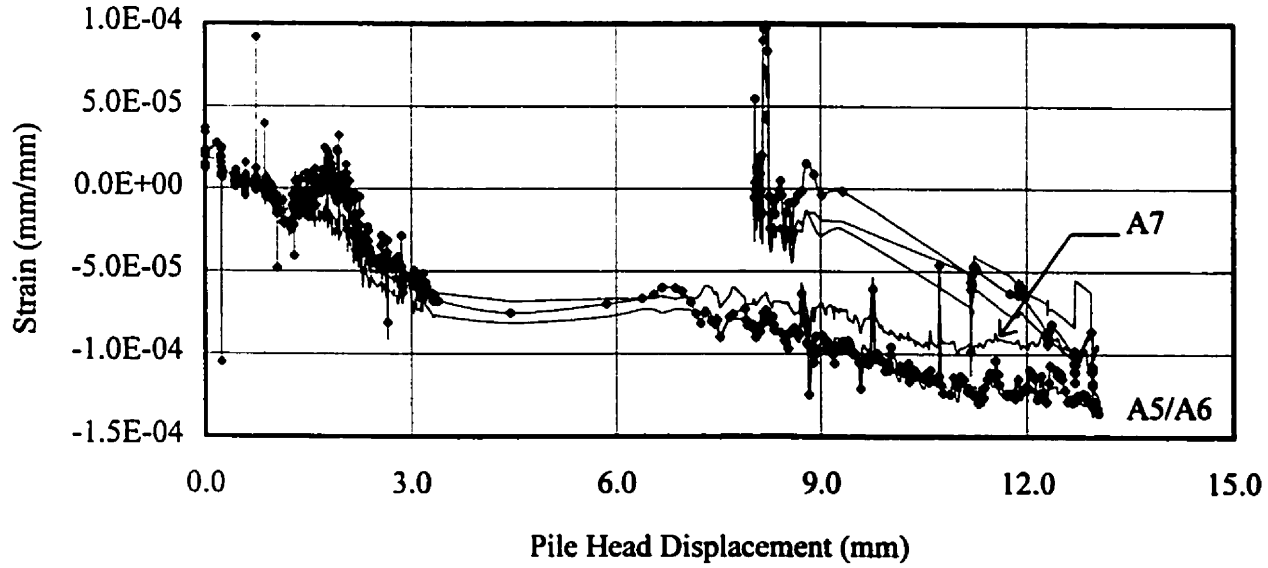

Figure A-2: Pile Head Displacement versus Strain Gage A5 through A8 Load Application No. 1

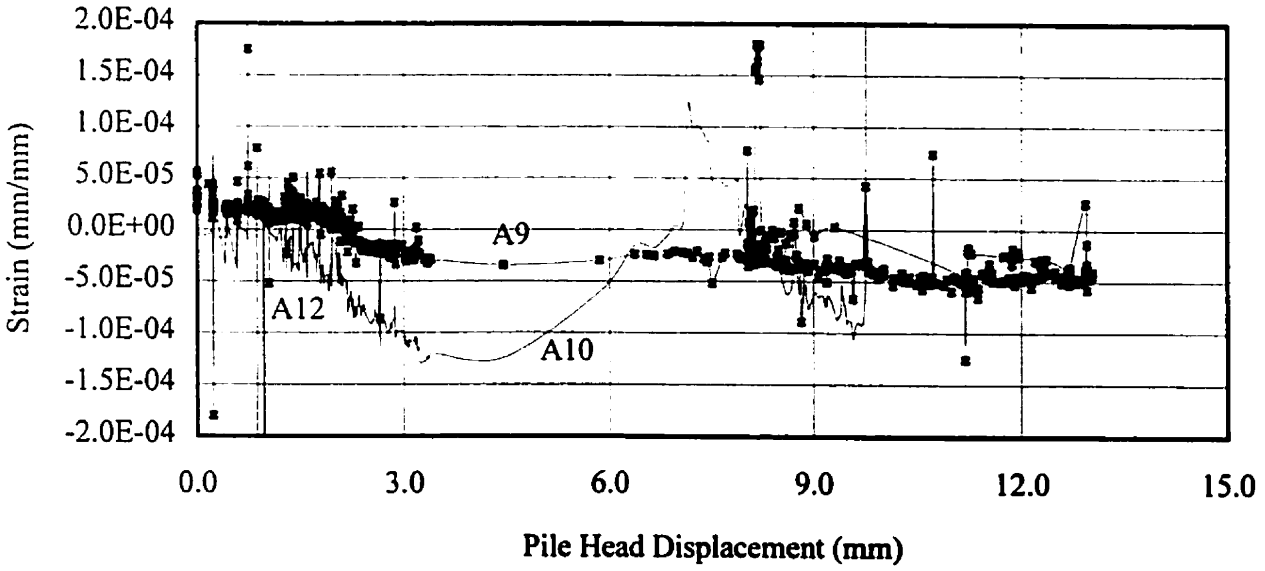

Figure A-3: Pile Head Displacement versus Strain Gage A9 through A12 Load Application No. 1

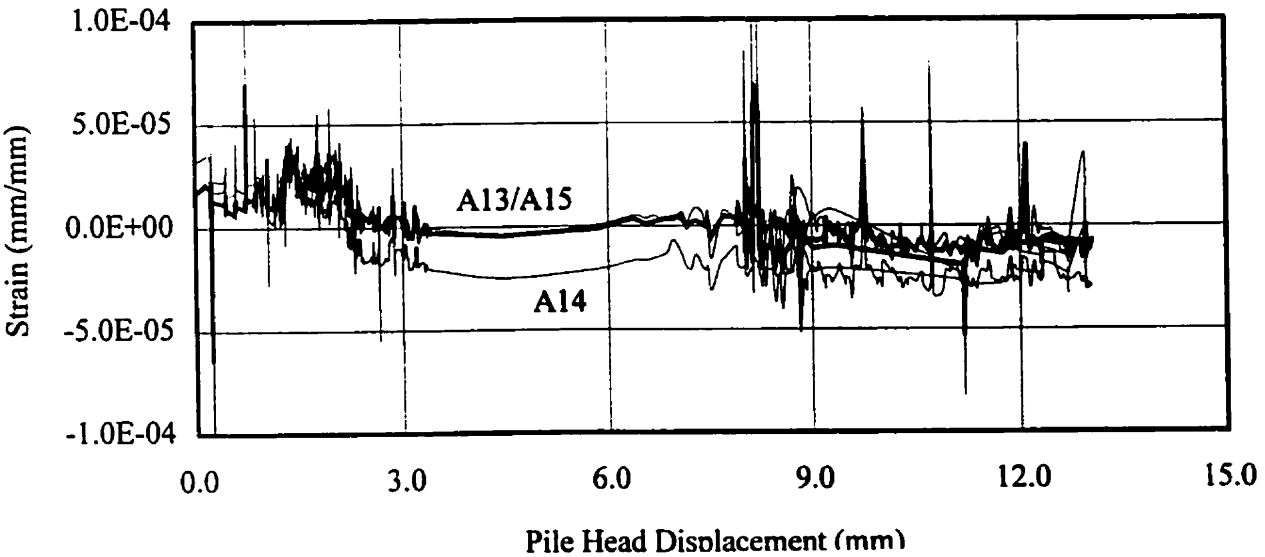

Figure A-4: Pile Head Displacement versus Strain Gage A13 through A15 Load Application No. 1

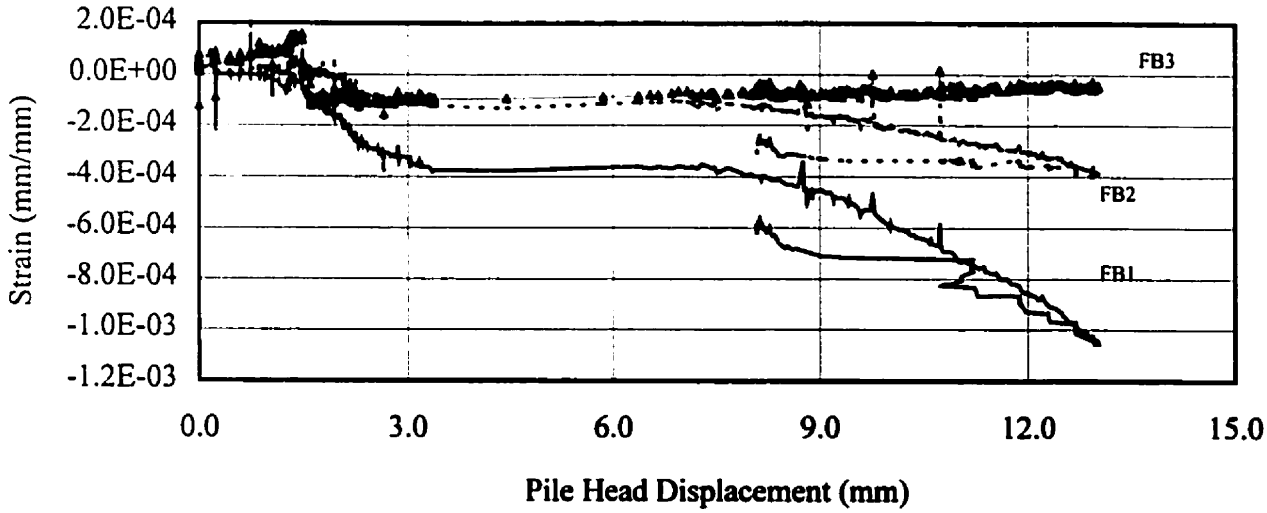

Figure A-5: Pile Head Displacement versus Strain Gage FB1 through FB3 Load Application No. 1

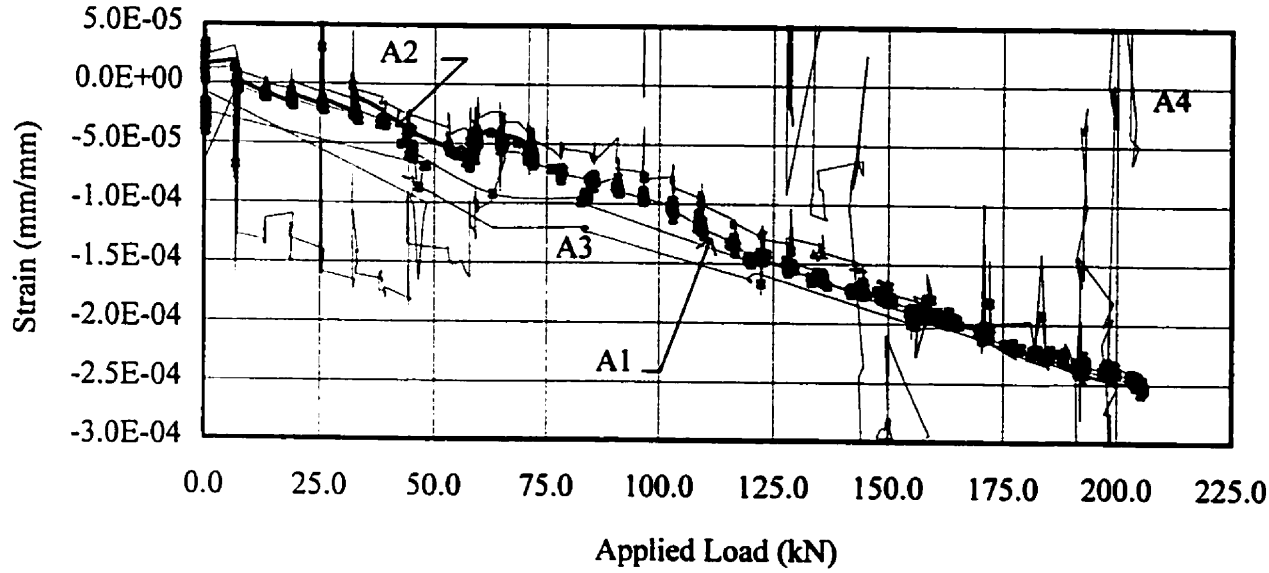

Figure A-6: Applied Load versus Strain Gage A1 through A4 Load Application No. 1

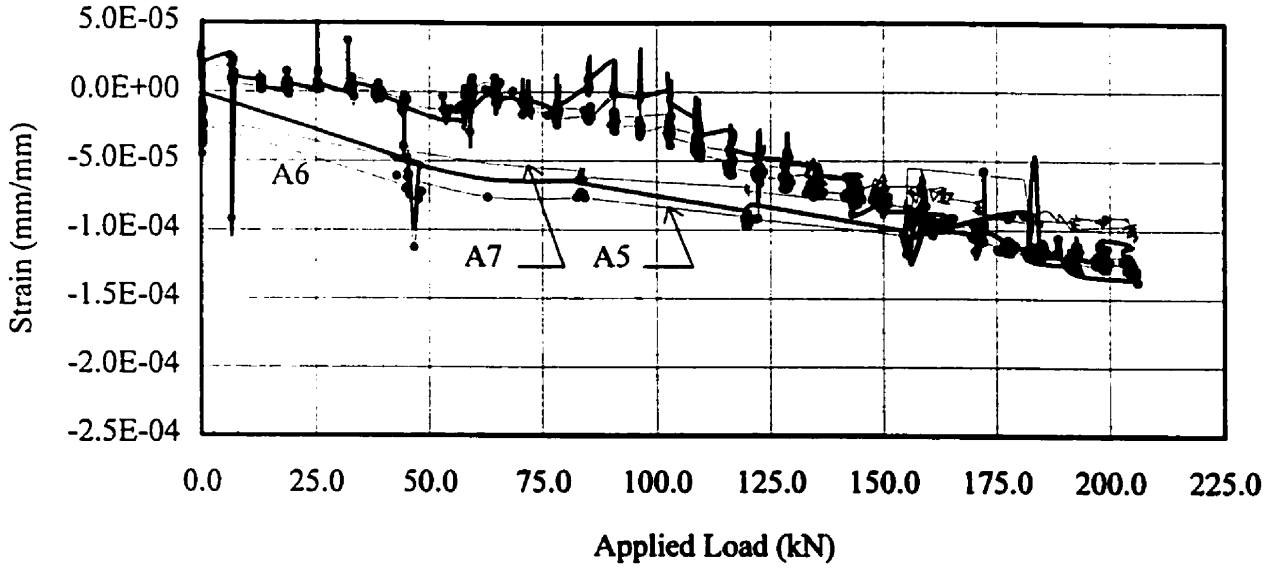

Figure A-7: Applied Load versus Strain Gage A5 through A8
Load Application No. 1

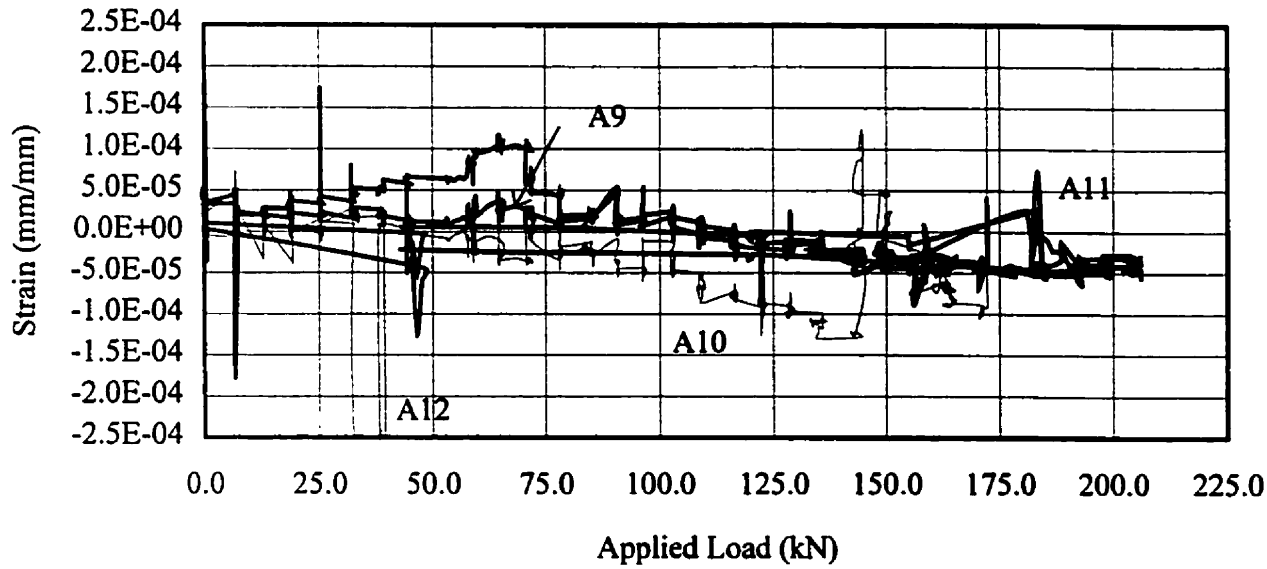

Figure A-8: Applied Load versus Strain Gage A9 through A12
Load Application No. 1

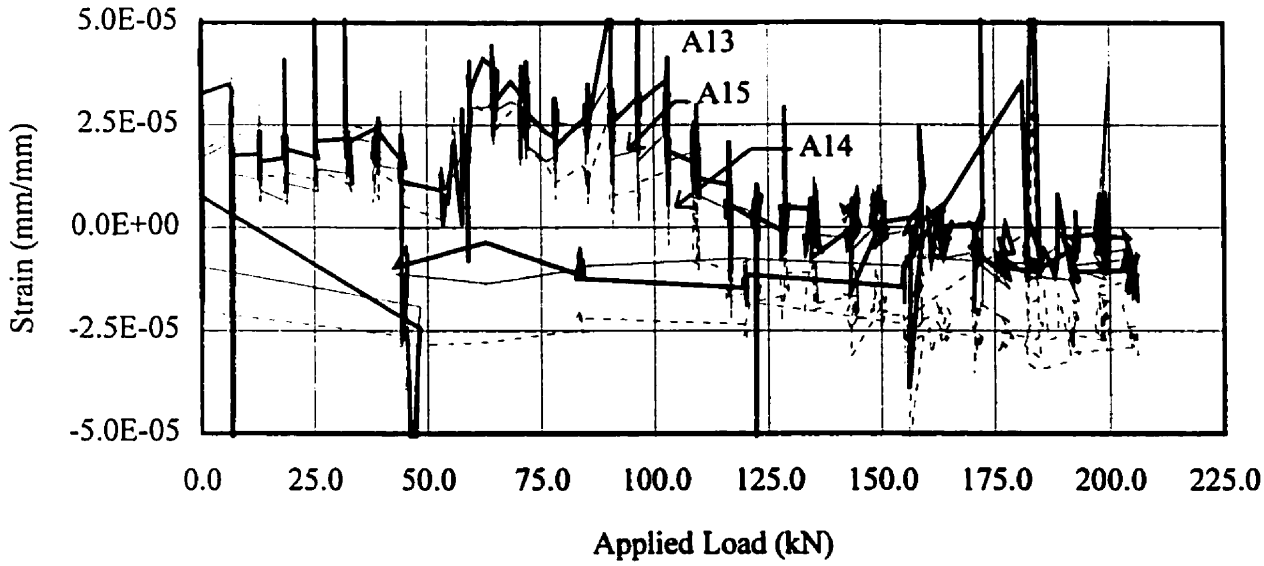

Figure A-9: Applied Load versus Strain Gage A13 through A15
Load Application No. 1

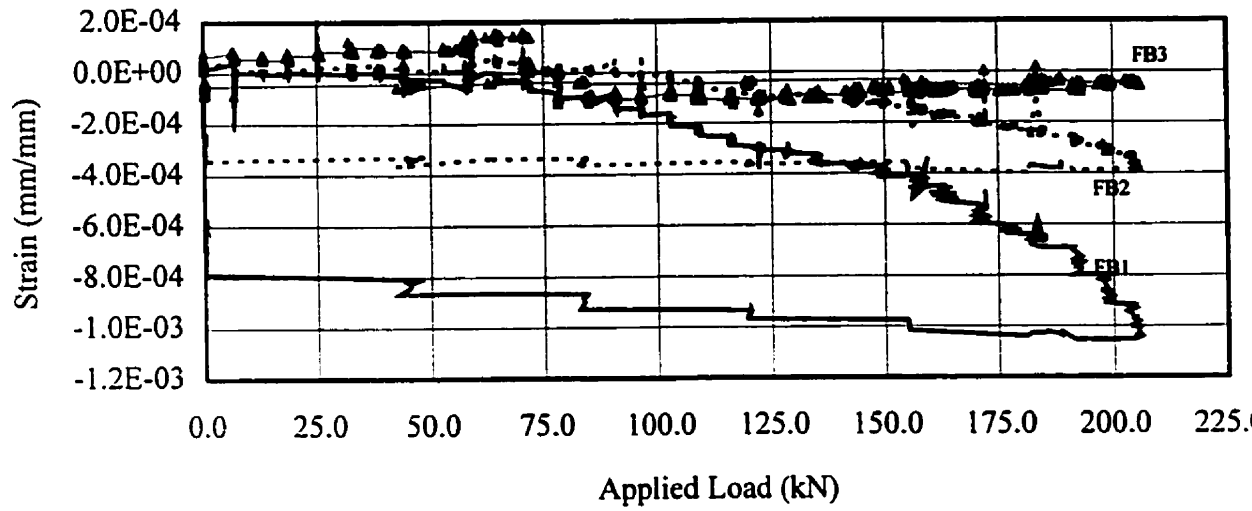

Figure A-10: Applied Load versus Strain Gage FB1 through FB3
Load Application No. 1

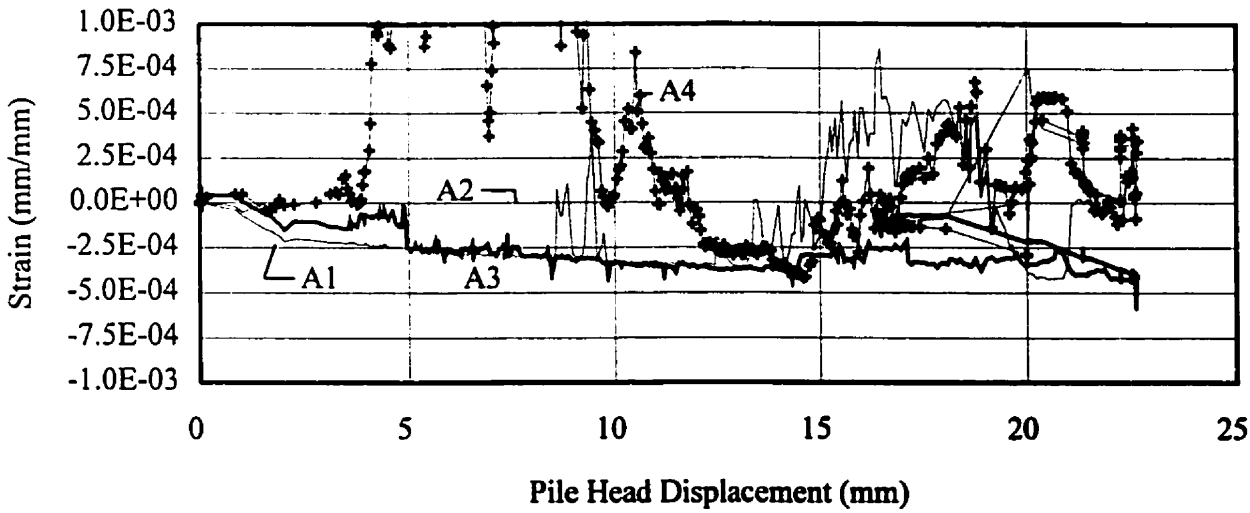

Figure A-11: Pile Head Displacement versus Strain Gage A1 through A4 Load Application No. 2

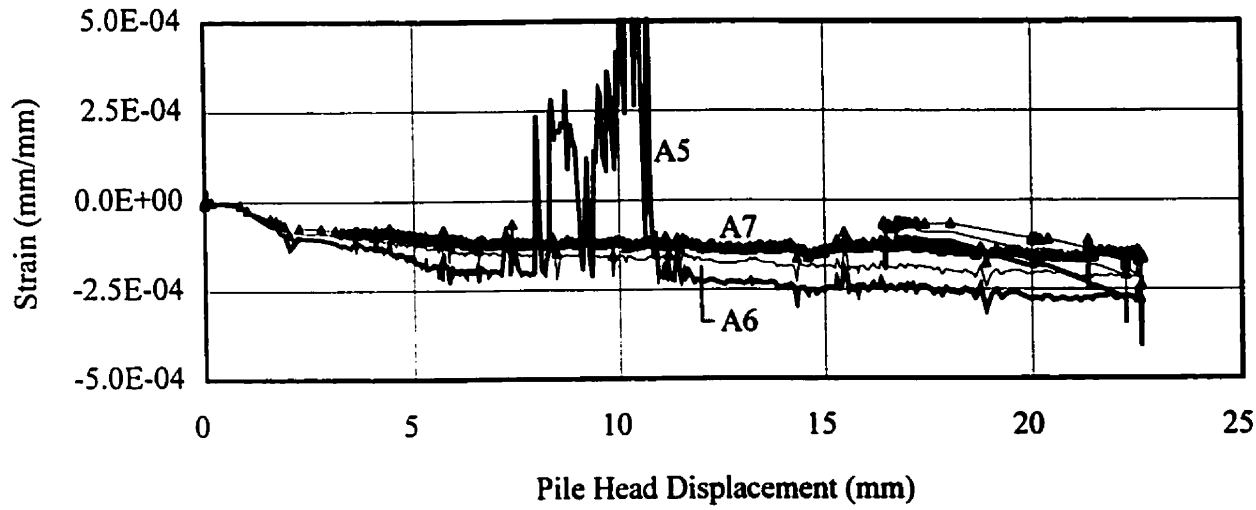

Figure A-12: Pile Head Displacement versus Strain Gage A5 through A8 Load Application No. 2

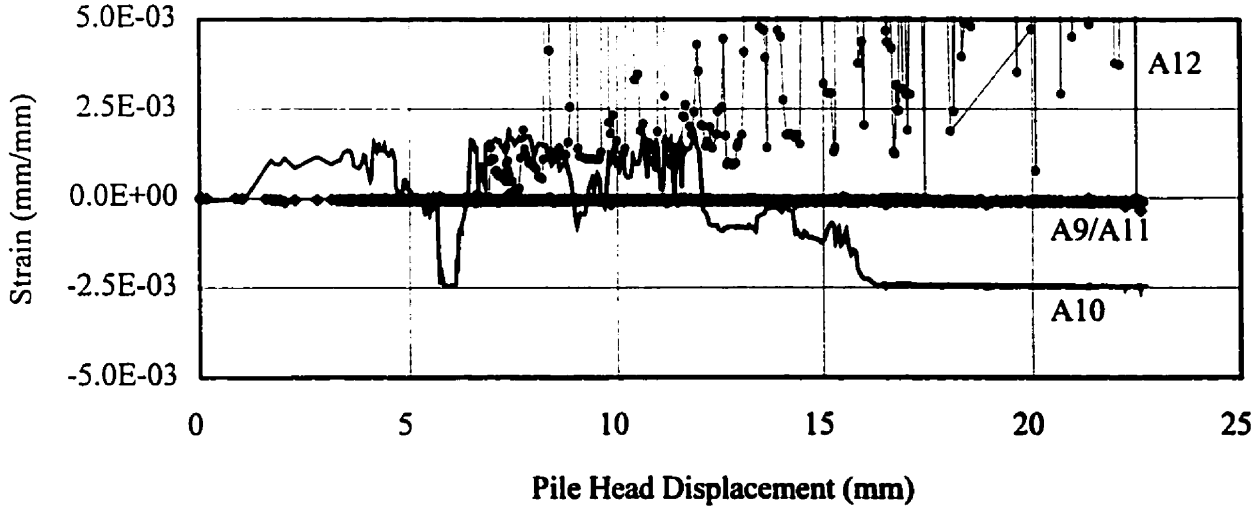

Figure A-13: Pile Head Displacement versus Strain Gage A9 through A12 Load Application No. 2

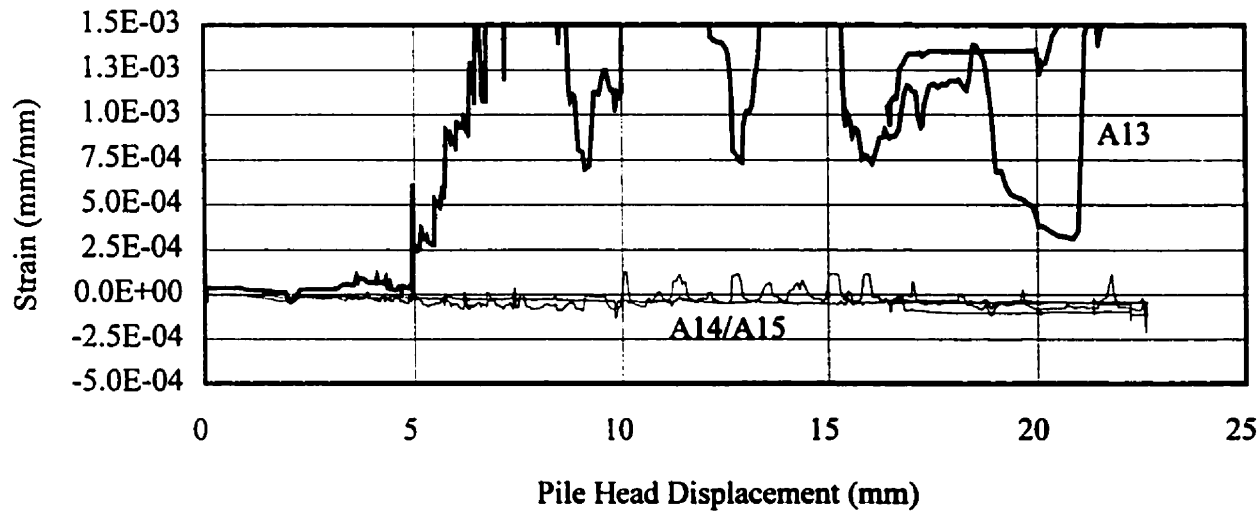

Figure A-14: Pile Head Displacement versus Strain Gage A13 through A15 Load Application No. 2

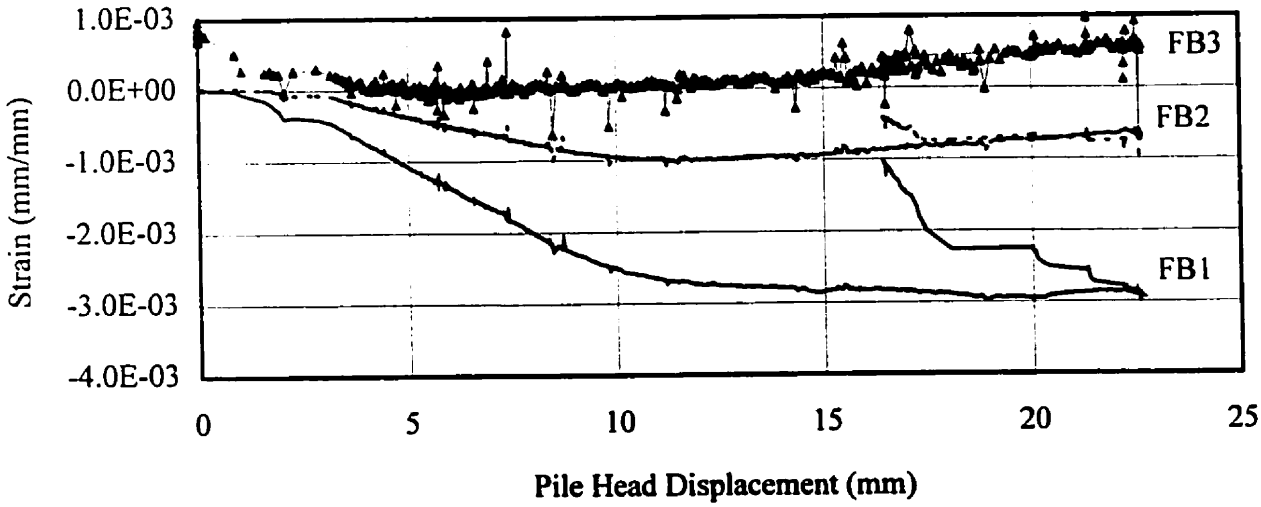

Figure A-15: Pile Head Displacement versus Strain Gage FB1 through FB3 Load Application No. 2

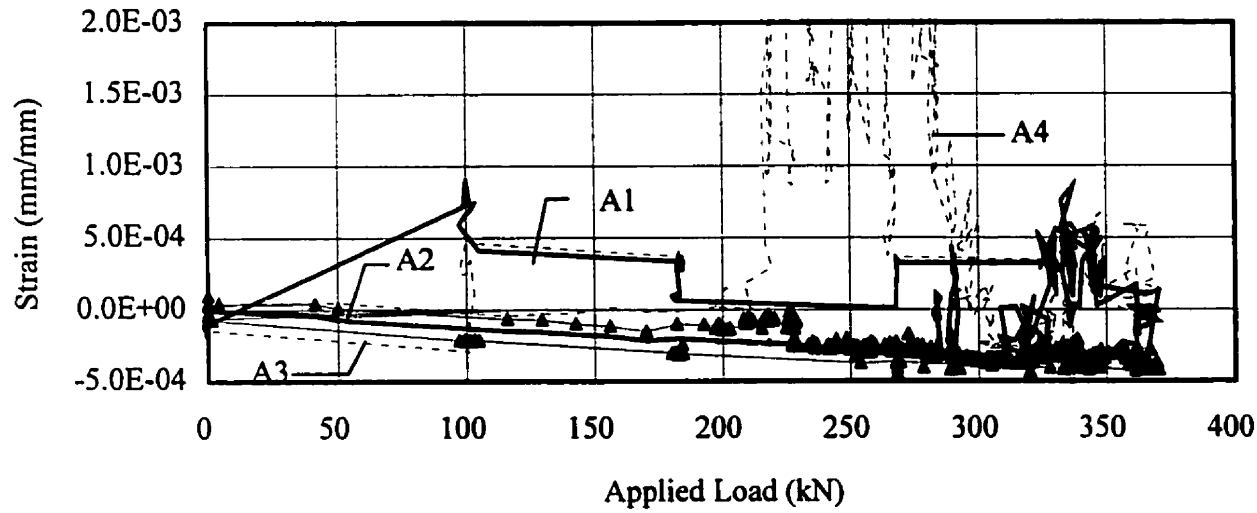

Figure A-16: Applied Load versus Strain Gage A1 through A4 Load Application No. 2

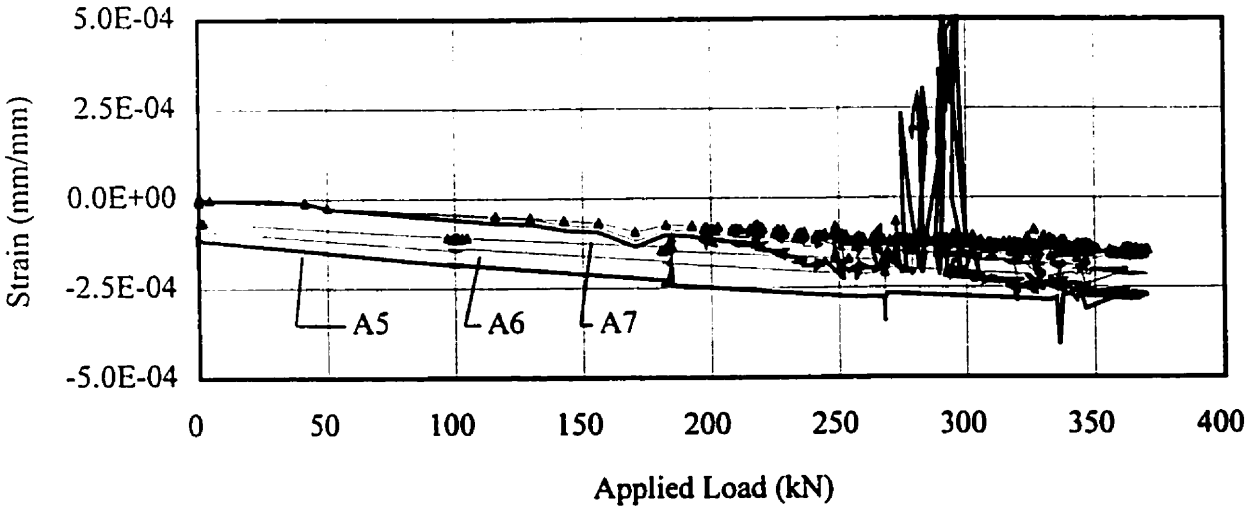

Figure A-17: Applied Load versus Strain Gage A5 through A8 Load Application No. 2

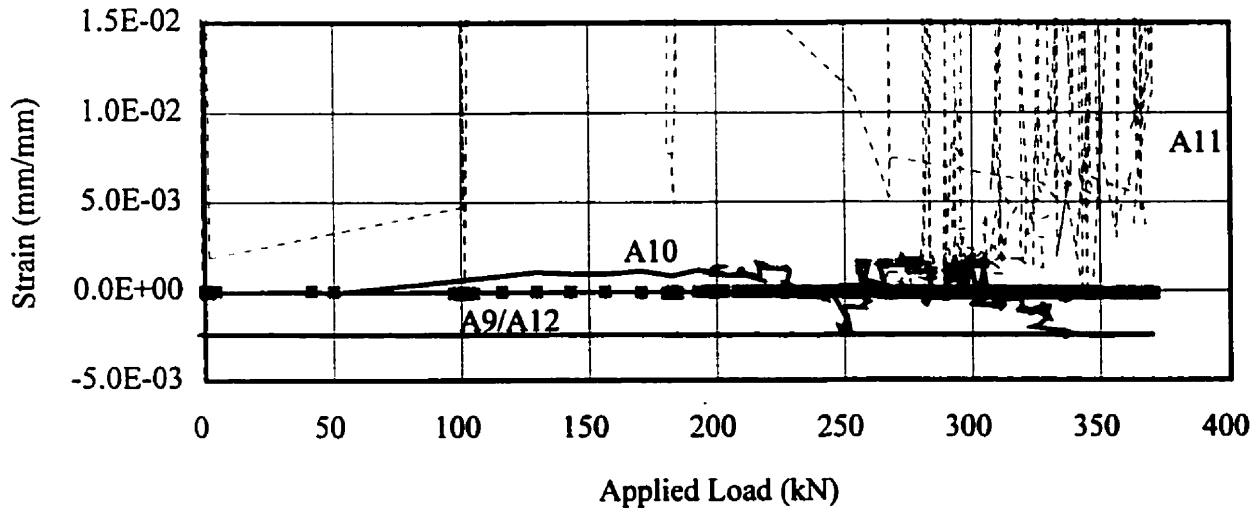

Figure A-18: Applied Load versus Strain Gage A9 through A12 Load Application No. 2

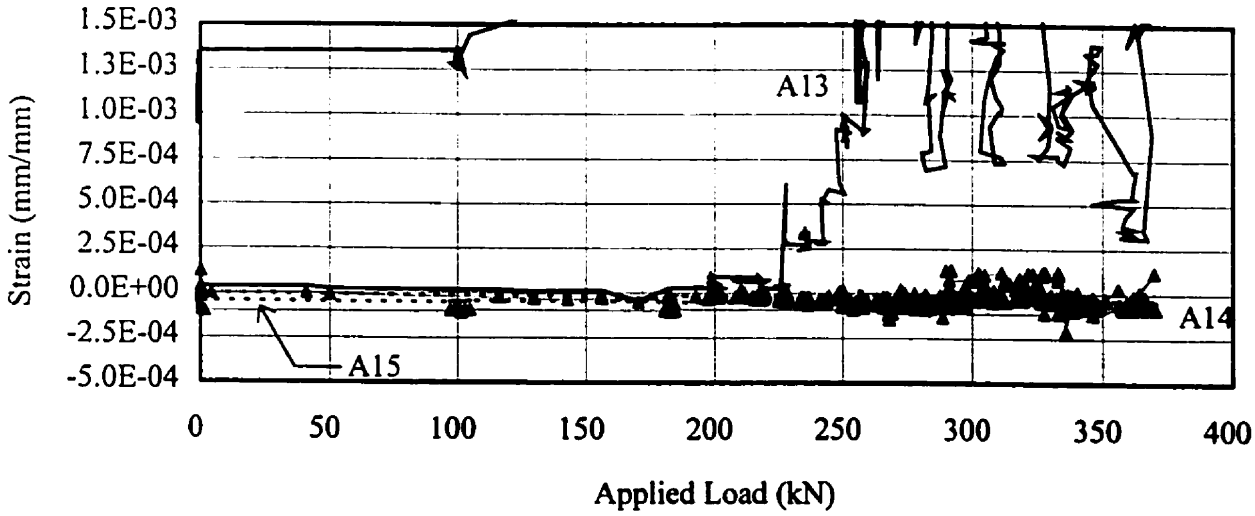

Figure A-19: Applied Load versus Strain Gage A13 through A15 Load Application No. 2

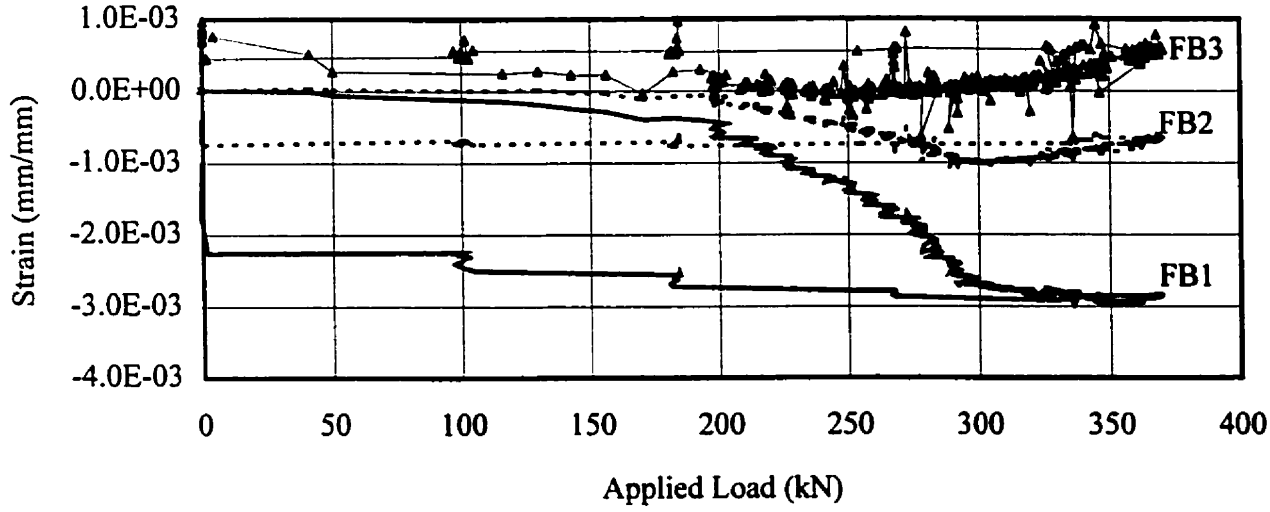

Figure A-20: Applied Load versus Strain Gage FB1 through FB3 Load Application No. 2

Appendix B

Calculations for Analysis

For Selected Absolute Displacements of the Pile Segment, listed below are :

- Best Fit Equations for Flighting Bending Moments using String "B" Strain Gage Data.
- First derivative of the Moment Equations (Shear Force)
- Second derivative of the Moment Equations (Pressure)

<u>D = 0</u>

$M = 0$

$\delta M/\delta R = V = 0$

$\delta V/\delta R = P = 0$

<u>D = 5 mm</u>

$M = -54708.6 + 1458.9\,R - 12.99\,R^2 + 0.0386\,R^3$

$\delta M/\delta R = V = 1458 - 26\,R + 0.1158\,R^2$

$\delta V/\delta R = P = -26 + 0.2316\,R$

<u>D = 10 mm</u>

$M = -37846.4 + 968.9\,R - 8.337\,R^2 + 0.024\,R^3$

$\delta M/\delta R = V = 968.9 - 16.674\,R + 0.072\,R^2$

$\delta V/\delta R = P = -16.674 + 0.144\,R$

D = 15 mm

$M = -17856.57 + 282.38\ R - 1.1152\ R^2$

$\delta M/\delta R = V = 282.38 - 2.23\ R$

$\delta V/\delta R = P = -2.23$ MPa

D = 20 mm

$M = 116354 - 3546.64\ R + 34.80\ R^2 - 0.1109\ R^3$

$\delta M/\delta R = V = -3546.64 + 69.60\ R - 0.3327\ R^2$

$\delta V/\delta R = P = 69.60 - 0.6654\ R$

D = 25 mm

$M = 147662.5 - 4498.6\ R + 44.28\ R^2 - 0.14195\ R^3$

$\delta M/\delta R = V = -4498.6 + 88.56\ R - 0.4258\ R^2$

$\delta V/\delta R = P = 88.56 - 0.8517\ R$

D = 30 mm

$M = 259\,062.7 - 7649.08\ R + 73.81\ R^2 - 0.2336\ R^3$

$\delta M/\delta R = V = -7649.08 + 147.62\ R - 0.7008\ R^2$

$\delta V/\delta R = P = 147.62 - 1.4016\ R$

Note : R is in millimetres, and the pressure is in MPa.

Appendix C

Additional Analyses

Figure C-1 illustrates the internal bending moment at FB1 which increases exponentially with time until the point of unloading, at which approximately one-third of the internal bending moment recovers. Location FB2 developed approximately 40% of the bending moment at FB1. Location FB3 developed a negligible increase in internal bending moment.

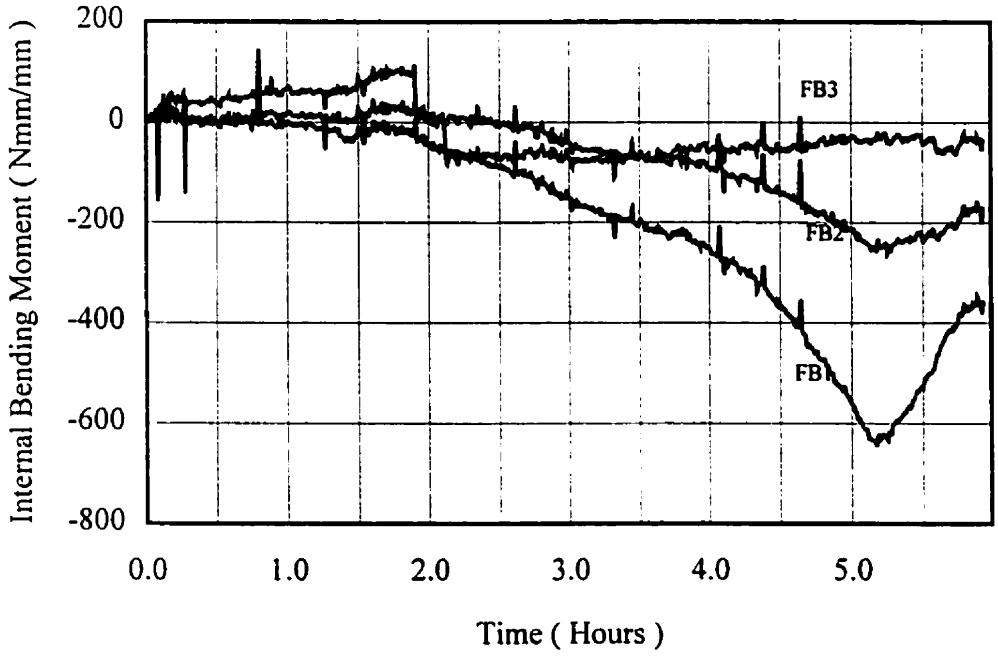

Figure C-1: Internal Bending Moments versus Time - Load Application No. 1

Similar to **Figure C-1**, **Figure C-2** illustrates the internal bending moment at FB1 increases non-uniformly with time until the point of unloading, at which approximately one-half of the internal bending moment recovers. Location FB2 developed approximately 35% of the bending moment at FB1. Location FB3 developed a negligible increase in internal bending moment. Internal bending moments determined for Load Application No. 2 are relative

because of the need to reset the strain gage initial reading prior to starting Load Application No. 2.

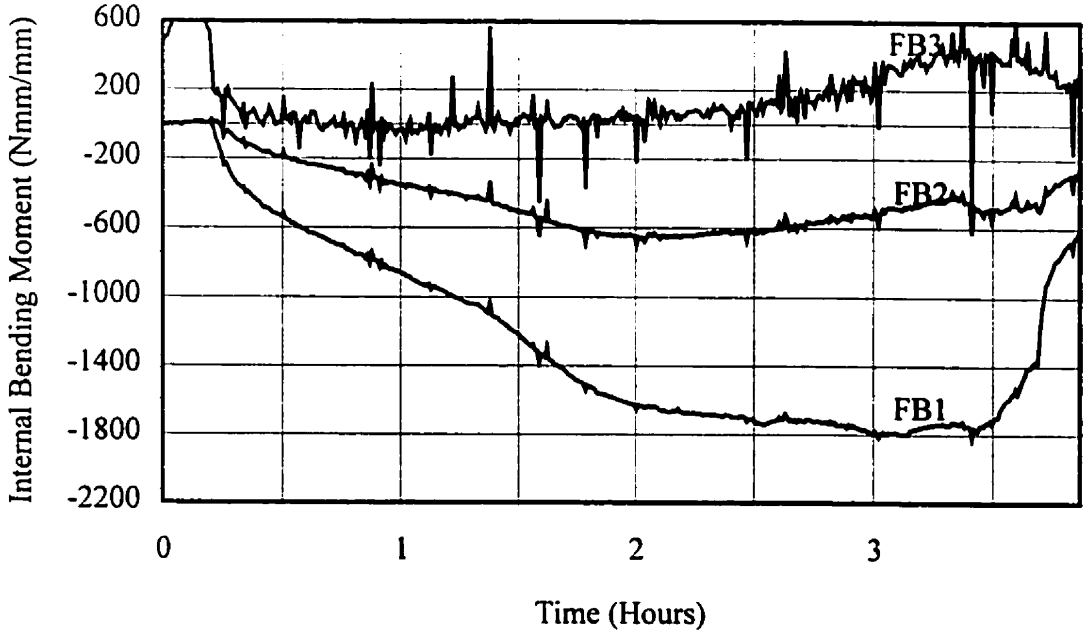

Figure C-2: Internal Bending Moments versus Displacement-Load Application No. 1